AUTOREGRESSIVE CONDITIONAL NEURAL PROCESSES

Anonymous authors
Paper under double-blind review

ABSTRACT

Conditional neural processes (CNPs; Garnelo et al., 2018a) are attractive meta-learning models which produce well-calibrated predictions and are trainable via a simple maximum likelihood procedure. Although CNPs have many advantages, they are unable to model dependencies in their predictions. Various works propose solutions to this, but these come at the cost of either requiring approximations or being limited to Gaussian predictions. In this work, we instead propose to change how CNPs are deployed at test time, *without any modifications to the model or training procedure*. Instead of making predictions independently for every target point, we autoregressively define a joint predictive distribution using the chain rule of probability, taking inspiration from the neural autoregressive density estimator (NADE) literature. We show that this simple procedure allows factorised Gaussian CNPs to model highly dependent, non-Gaussian predictive distributions. Perhaps surprisingly, in an extensive range of tasks with synthetic and real data, we show that CNPs in autoregressive (AR) mode not only significantly outperform non-AR CNPs, but are also competitive with more sophisticated models that are significantly more expensive and challenging to train. This performance is remarkable since AR CNPs are not trained to model joint dependencies. Our work provides an example of how ideas from neural distribution estimation can benefit neural processes, motivating research into the AR deployment of other neural process models.

1 INTRODUCTION

Conditional neural processes (CNPs; Garnelo et al., 2018a) are a family of meta-learning models which combine the flexibility of deep learning with the uncertainty awareness of probabilistic models. They are trained to produce well-calibrated predictions via a simple maximum-likelihood procedure, and naturally handle off-the-grid and missing data, making them ideally suited for tasks in climate science and healthcare. Since their introduction, attentive (ACNP; Kim et al., 2019) and convolutional (ConvCNP; Gordon et al., 2020) variants have also been proposed. Unfortunately, existing CNPs do not model statistical dependencies (Figure 1; left). This harms their predictive performance and makes it impossible to draw coherent function samples, which are necessary in downstream estimation tasks (Markou et al., 2022). Various approaches have been proposed to address this. Garnelo et al. (2018b) introduced the latent neural process (LNP), which uses a latent variable to induce dependencies and model non-Gaussianity. However, this renders the likelihood intractable, necessitating approximate inference. Another approach, which maintains tractability at the cost of only allowing Gaussian

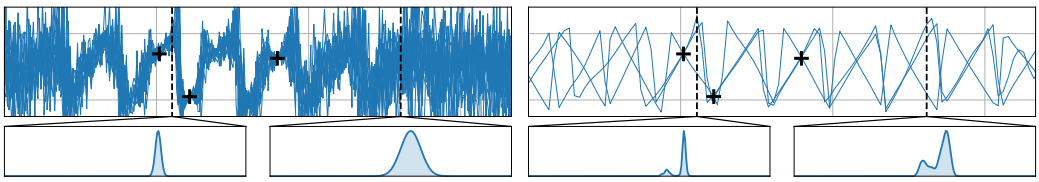

Figure 1: A ConvCNP trained on random sawtooth functions and applied in standard mode (*left*) and in our proposed autoregressive (AR) mode (*right*). The black crosses denote observed data points, the blue lines show model samples, and the bottom plots show the marginal predictive distributions at the locations marked by the dashed vertical lines. In standard mode, the CNP models each output with an independent Gaussian (*left*). However, the *same* CNP, when run in AR mode, can produce coherent samples and model multimodality (*right*).

Class	Consistent	Dependencies	Non-Gaussian	Exact Training
AR CNPs (this work)	✗	✓	✓	✓
CNPs (Garnelo et al., 2018a)	✓	✗	✓	✓
GNPs (Markou et al., 2022)	✓	✓	✗	✓
LNPs (Garnelo et al., 2018b)	✓	✓	✓	✗

Table 1: Comparison of various classes of neural processes. Shows whether a class produces consistent predictions, models dependencies, can produce non-Gaussian predictions, and can be trained without approximating the objective function. For CNPs, even though the presentation by Garnelo et al. (2018a) assumes Gaussian predictions, it is simple to relax this Gaussianity assumption; this is not the case for GNPs.

predictions, is the fully convolutional Gaussian neural process (FullConvGNP; Bruinsma et al., 2021). It uses a neural network to define the mean and covariance function of a predictive Gaussian process (GP) which models dependencies. However, it uses a much more complex architecture and is only practically applicable to problems with one-dimensional inputs, limiting its adoption compared to the more lightweight CNP. Recently, Markou et al. (2022) proposed the Gaussian neural process (GNP), which is considerably simpler but sacrifices performance relative to the FullConvGNP.

In this paper we propose a much simpler method for modelling dependencies with neural processes that has been largely overlooked: autoregressive (AR) sampling. AR sampling requires *no changes* to the architecture *or* training procedure. Instead, we *change how the CNP is deployed at test time*, extracting predictive information that would ordinarily be ignored. Instead of making predictions at all target points simultaneously, we autoregressively feed samples back into the model. AR CNPs trade the fundamental property of *consistency under marginalisation and permutation*, which is foundational to many neural process models, for non-Gaussian and correlated predictions. In Table 1 we place AR CNPs within the framework of other neural process models. Our key contributions are:

- We show that CNPs used in AR mode capture rich, non-Gaussian predictive distributions and produce coherent samples (Figure 1). This is remarkable as the CNPs used have Gaussian likelihoods, are not trained to model joint dependencies or non-Gaussianity, and are significantly cheaper to train than LNPs and FullConvGNPs (Figure 2).
- We prove that given sufficient data and model capacity, the performance of AR CNPs is at least as good as that of GNPs, which explicitly model correlations in their predictions.
- Viewing AR CNPs as a type of neural density estimator (Uria et al., 2016), we highlight their connections to a range of existing methods in the deep generative modelling literature.
- In an extensive range of Gaussian and non-Gaussian regression tasks, we show that AR CNPs are consistently competitive with, and often significantly outperform, all other neural process models in terms of predictive log-likelihood.
- We deploy AR CNPs on a range of tasks involving real-world climate data. To handle the high-resolution data in a computationally tractable manner, we introduce a novel multi-scale architecture for ConvCNPs. We also combine AR ConvCNPs with a beta-categorical mixture likelihood, producing strong results compared to other neural processes.

Our work represents a promising first application of this procedure to the simplest class of neural processes, and motivates future work on applications of AR sampling to other neural process models.

2 Autoregressive Conditional Neural Processes

Meta-learning. We first define the problem set-up. Let $\mathcal{X}$ be a compact input space and let $\mathcal{Y}$ be the output space. Let $\mathcal{D}_N = (\mathcal{X} \times \mathcal{Y})^N$ be the collection of all sets of N input–output pairs, and let $\mathcal{D} = \bigcup_{N=0}^{\infty} \mathcal{D}_N$. We call elements $D \in \mathcal{D}$ *data sets* and denote $D = (\mathbf{x}, \mathbf{y})$ where $\mathbf{x} \in \mathcal{X}^N$, $\mathbf{y} \in \mathcal{Y}^N$ are the inputs and outputs respectively. In meta-learning we are given a collection of data sets $(D_m)_{m=1}^M$, called a *meta–data set*, with the individual data sets D_m called *tasks* (Vinyals et al., 2016). Every task D_m is split up $D_m = D_m^{(\mathrm{c})} \cup D_m^{(\mathrm{t})}$ into a *context set* $D_m^{(\mathrm{c})} = (\mathbf{x}_m^{(\mathrm{c})}, \mathbf{y}_m^{(\mathrm{c})})$ and a *target set* $D_m^{(\mathrm{t})} = (\mathbf{x}_m^{(\mathrm{t})}, \mathbf{y}_m^{(\mathrm{t})})$. Here $\mathbf{x}_m^{(\mathrm{c})}$ are called the *context inputs*, $\mathbf{y}_m^{(\mathrm{c})}$ the *context outputs*, $\mathbf{x}_m^{(\mathrm{t})}$ the *target inputs*, and $\mathbf{y}_m^{(\mathrm{t})}$ the *target outputs*. Our goal is to devise an algorithm which takes in a context set $D_m^{(\mathrm{c})}$ and produces the best possible prediction for the target outputs $\mathbf{y}_m^{(\mathrm{t})}$ given target inputs $\mathbf{x}_m^{(\mathrm{t})}$.

Neural processes. Let $\mathcal{P}$ be the set of all $\mathcal{Y}$-valued stochastic processes on $\mathcal{X}$. Neural processes (NPs) directly and flexibly parametrise a map $\pi_\theta \colon \mathcal{D} \to \mathcal{Q}$ where $\mathcal{Q} \subseteq \mathcal{P}$ and where θ are learnable parameters. CNPs set $\mathcal{Q}$ to be the collection of GPs f such that $\mathrm{cov}(f(x), f(y)) = 0$ for $x \neq y$. GNPs let $\mathcal{Q}$ be the collection of continuous GPs. Latent NPs (LNPs; Garnelo et al., 2018b) let $\mathcal{Q}$ be a collection of non-Gaussian processes by making use of a latent variable. Let $P_{\mathbf{x}_m^{(\mathrm{t})}} \pi(D_m^{(\mathrm{c})})$ denote the finite-dimensional distribution of the process $\pi(D_m^{(\mathrm{c})})$ evaluated at inputs $\mathbf{x}_m^{(\mathrm{t})}$, and denote its density

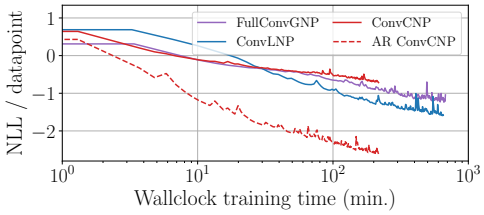

Figure 2: Negative log-likelihoods on non-Gaussian sawtooth data. Deploying the ConvCNP in AR mode dramatically improves performance, and outperforms state-of-the-art NPs with Gaussian (FullConvGNP) and non-Gaussian (ConvLNP) predictive distributions, at a fraction of the training cost.

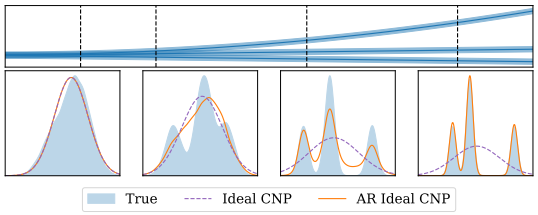

Figure 3: *Top:* generative process: mixture model of three deterministic functions with additive Gaussian noise. *Bottom:* at the four target locations indicated by dashed lines, the panes show the true distribution and predictions by the ideal CNP and the ideal CNP applied autoregressively at the targets from left to right. See Appendices D.3 and E.

by $q_\theta(\bullet \mid \mathbf{x}_m^{(t)}, D_m^{(c)})$. To learn the parameters θ, NPs seek to maximise:

$$\mathcal{L}_M(\pi) = \tfrac{1}{M} \textstyle\sum_{m=1}^{M} \log q_\theta(\mathbf{y}_m^{(t)} \mid \mathbf{x}_m^{(t)}, D_m^{(c)}). \tag{1}$$

For CNPs and GNPs, $\mathcal{L}_M$ can be computed exactly since q_θ is Gaussian.[1]. However, for LNPs, $\mathcal{L}_M$ must be approximated (Garnelo et al., 2018b; Foong et al., 2020), typically impacting performance.

Autoregressive CNPs. Our proposal is to take an existing CNP and run it in an autoregressive fashion, feeding predictions for earlier outputs back into the model. Inspired by the product rule, we define the joint predictive as a product of conditionals, modelling each conditional with a CNP. For example, in the case of three target points, $q_\theta(y_3^{(t)} \mid \mathbf{y}_{1:2}^{(t)}, D_m^{(c)}) q_\theta(y_2^{(t)} \mid y_1^{(t)}, D_m^{(c)}) q_\theta(y_1^{(t)} \mid D_m^{(c)})$. To enable a theoretical analysis of this procedure, we now proceed to set up more formal notation. Suppose that $\pi_\theta \colon \mathcal{D} \to \mathcal{Q}$ is an NP, and we wish to predict at some target inputs $\mathbf{x}^{(t)}$ given a context set $D^{(c)}$. Standard NPs would output the predictive $P_{\mathbf{x}^{(t)}} \pi_\theta(D^{(c)})$ which, for CNPs, would be a factorised Gaussian. We propose to instead roll out the NP autoregressively, as described in Proc. 2.1.

Procedure 2.1 (Autoregressive application of neural process)**.** For a neural process π_θ, context set $D^{(c)} = (\mathbf{x}^{(c)}, \mathbf{y}^{(c)})$, and target inputs $\mathbf{x}^{(t)}$, let $\mathrm{AR}_{\mathbf{x}^{(t)}}(\pi_\theta, D^{(c)})$ be the distribution defined as follows:

$$\text{for } i = 1, \ldots, N, \quad y_i^{(t)} \sim P_{x_i^{(t)}} \pi_\theta(\mathbf{x}^{(c)} \oplus \mathbf{x}_{1:(i-1)}^{(t)}, \mathbf{y}^{(c)} \oplus \mathbf{y}_{1:(i-1)}^{(t)}), \tag{2}$$

where $\mathbf{a} \oplus \mathbf{b}$ concatenates two vectors $\mathbf{a}$ and $\mathbf{b}$. See Figure 7 in Appendix C for an illustration.

Since earlier samples $y_i^{(t)}$ feed back into later applications of π_θ, the whole sample $\mathbf{y}^{(t)}$ is correlated, *even if π_θ does not model dependencies between target outputs*, as with CNPs. At test time, when evaluating the corresponding the density $q_\theta^{(\mathrm{AR})}$ of $\mathrm{AR}_{\mathbf{x}^{(t)}}(\pi_\theta, D^{(c)})$ at $\mathbf{y}^{(t)}$, we use the formula

$$\log q_\theta^{(\mathrm{AR})}(\mathbf{y}^{(t)} \mid \mathbf{x}^{(t)}, D^{(c)}) = \textstyle\sum_{i=1}^{N} \log q_\theta(y_i^{(t)} \mid x_i^{(t)}, D^{(c)} \oplus (\mathbf{x}_{1:(i-1)}^{(t)}, \mathbf{y}_{1:(i-1)}^{(t)})). \tag{3}$$

Whilst any NP can be used in AR, we focus on CNPs as they are the computationally cheapest class.

Understanding the infinite data limit. To better understand why AR CNPs successfully model dependencies, we analyse the idealised case of infinite data and model capacity. Let $p(f)$ be the law of the data-generating stochastic process, and let $p(\varepsilon)$ be the law of a stochastic process representing observation noise, defined by letting $\varepsilon(\mathbf{x})$ be a vector of i.i.d. noise variables for all $\mathbf{x}$. We assume

$$\mathbf{y}_m^{(c)} = y_m(\mathbf{x}_m^{(c)}) \quad \text{and} \quad \mathbf{y}_m^{(t)} = y_m(\mathbf{x}_m^{(t)}) \quad \text{where} \quad y_m(\bullet) = f_m(\bullet) + \varepsilon_m(\bullet), \tag{4}$$

$(f_m)_{m=1}^M$ are i.i.d. draws from $p(f)$, and $(\varepsilon_m)_{m=1}^M$ are i.i.d. draws from $p(\varepsilon)$. Define the *prediction map* $\pi_y \colon \mathcal{D} \to \mathcal{P}$ as the mapping from a data set to the posterior over y, $\pi_y(D) = p(y \mid D)$. Then $\mathcal{L}_M$ is a Monte Carlo approximation of the following infinite-sample objective (Foong et al., 2020):

$$\mathcal{L}_\infty(\pi) = -\mathbb{E}_{p(D^{(c)}) p(\mathbf{x}^{(t)})}[\mathrm{KL}(P_{\mathbf{x}^{(t)}} \pi_y(D^{(c)}), P_{\mathbf{x}^{(t)}} \pi(D^{(c)}))] + \text{const}. \tag{5}$$

Under appropriate regularity assumptions, $\mathcal{L}_\infty(\pi)$ is maximised over all π when the expected KL divergence term is zero, which occurs if and only if $\pi = \pi_y$. In practice, NPs do not maximise $\mathcal{L}_\infty(\pi)$ over all π, but (i) use a finite-sized meta–data set and (ii) restrict $\mathcal{Q} \subseteq \mathcal{P}$.

$$\overbrace{\pi_M \in \underset{\text{all } \pi \colon \mathcal{D} \to \mathcal{Q}}{\arg\max}\, \mathcal{L}_M(\pi)}^{\text{what we compute in practice}} \xrightarrow[M \to \infty]{} \overbrace{\pi_\infty \in \underset{\text{all } \pi \colon \mathcal{D} \to \mathcal{Q}}{\arg\max}\, \mathcal{L}_\infty(\pi)}^{\text{ideal NP}} \xrightarrow[\mathcal{Q} \to \mathcal{P}]{} \overbrace{\pi_y = \underset{\text{all } \pi \colon \mathcal{D} \to \mathcal{P}}{\arg\max}\, \mathcal{L}_\infty(\pi)}^{\text{exact prediction map}} \tag{6}$$

[1]Unless otherwise specified, we assume CNPs use Gaussian likelihoods, as in Garnelo et al. (2018a). However, it is straightforward to modify them to use non-Gaussian likelihoods, as we do in Section 4.4.

Here π_M is an NP trained on the practical objective (1), which, in the limit of infinite data, approximates the so-called *ideal NP* π_∞. The ideal NP depends on the choice of $\mathcal{Q}$, *i.e.* the class of NPs under consideration, and, in turn, approximates π_y. For CNPs and GNPs, using the fact that minimising $\mathrm{KL}(p, q)$ over q matches moments (Minka, 2001), we can readily determine and even practically compute the ideal NP for these two classes of NPs. The *ideal CNP* predicts a diagonal-covariance GP whose mean function and *marginal variance function* match π_y: $\pi_\infty(D) = \mathcal{GP}(m, k)$ where $m(x) = \mathbb{E}[y(x) \mid D]$, and $k(x, x') = \mathbb{V}[y(x) \mid D]$ if $x = x'$ and $k(x, x') = 0$ otherwise. On the other hand, the *ideal GNP* predicts a GP whose mean function and *full covariance function* match π_y: $\pi_\infty(D) = \mathcal{GP}(m, k)$ where $m(x) = \mathbb{E}[y(x) \mid D]$, $k(x, x') = \mathrm{cov}(y(x), y(x') \mid D)$. The main result of this subsection is that the ideal CNP, despite not modelling correlations, becomes superior to the ideal GNP *when deployed in AR mode*:

Proposition 2.1 (Advantage of AR CNPs over GNPs)**.** Assume appropriate regularity conditions on y. Let π_{C} be the ideal CNP and let π_{G} be the ideal GNP. Then, for all inputs $\mathbf{x}$ and data sets $D \in \mathcal{D}$,

$$\mathrm{KL}(P_{\mathbf{x}}\pi_y(D), \mathrm{AR}_{\mathbf{x}}(\pi_{\mathrm{C}}, D)) \leq \mathrm{KL}(P_{\mathbf{x}}\pi_y(D), P_{\mathbf{x}}\pi_{\mathrm{G}}(D)). \tag{7}$$

We provide a proof in Appendix A. Intuitively, the advantage of AR CNPs comes from their ability to model non-Gaussian dependencies. Proposition 2.1 shows that to outperform the GNP, it suffices to train a CNP to model the *marginals* of π_y, and rely on the AR procedure to induce dependencies. A visualisation of the ideal CNP and the ideal CNP applied autoregressively can be seen in Figure 3.

Consistency and the AR design space. As shown in Table 1, AR CNPs give up the fundamental property of *consistency*, as the distributions $\{\mathrm{AR}_{\mathbf{x}}(\pi_\theta, D_m^{(\mathrm{c})}) : \mathbf{x} \in \mathcal{X}^N,\ N \in \mathbb{N}\}$ are not consistent under permutation or marginalisation: permuting $\mathbf{x}$ can change the distribution, as can introducing and marginalising new target points. This violates the conditions of the Kolmogorov extension theorem (Oksendal, 2013), preventing the distributions from defining a consistent stochastic process. There is thus a large design space involved when deploying AR CNPs, where choices that have no effect on the predictions of other NPs can now significantly affect performance.

One such choice is how many points to sample at a time. Sampling one at a time induces dependencies between all points, but requires N forward passes. Alternatively, we could divide the N inputs in $\mathbf{x}^{(\mathrm{t})}$ into blocks of K points each, and sample each block with a single CNP forward pass. This requires N/K forward passes, with points in the same block conditionally independent. If $K = N$, this is the standard CNP prediction, and if $K = 1$, we recover Procedure 2.1. This provides a knob for practitioners to trade off between faster, consistent, but less expressive standard CNP predictions, and slower, less consistent, but more expressive AR predictions. In this paper, we use full AR mode with $K = 1$, and leave an investigation of block AR sampling to future work.

Obtaining smooth samples. Due to the lack of consistency in AR mode, the spacing chosen between target points can significantly affect performance. For example, care must be taken so the number of target points is not much greater than the size of the context sets seen during train time, to avoid confronting the model with an out-of-distribution context set size at test time. This raises the question of how to sample functions on a very fine grid. Furthermore, since CNPs do not differentiate between epistemic and aleatoric uncertainty, it is not clear how to obtain smooth, noiseless samples, that is, samples for f uncorrupted by the i.i.d. noise ε in (4). The following proposition shows that, for a smooth sample corrupted by additive noise, the smooth component can be approximated with the predictive mean conditioned on noisy observations:

Proposition 2.2 (Recovery of smooth samples)**.** Let $\mathcal{X} \subseteq \mathbb{R}$ be compact, and let f be a stochastic process with surely continuous sample paths and $\sup_{x \in \mathcal{X}} \|f(x)\|_{L^2} < \infty$. Let $(\varepsilon_n)_{n \geq 0}$ be i.i.d. (potentially non-Gaussian) random variables such that $\mathbb{E}[\varepsilon_0] = 0$ and $\mathbb{V}[\varepsilon_0] < \infty$. Consider any sequence $(x_n)_{n \geq 1} \subseteq \mathcal{X}$, and let $x^* \in \mathcal{X}$ be a limit point of $(x_n)_{n \geq 1}$. If $y(x^*) = f(x^*) + \varepsilon_0$ and $y_n = f(x_n) + \varepsilon_n$ are noisy observations of f, then

$$\lim_{n \to \infty} \mathbb{E}[y(x^*) \mid y_1, \ldots, y_n] = f(x^*) \quad \text{almost surely.} \tag{8}$$

We provide a proof in Appendix B. Equation (8) suggests the following two-step procedure for obtaining smooth samples from AR CNPs. **Step 1:** Let $\mathbf{x}_{1:n}$ be a number target inputs that does not exceed the number of points seen during training. Sample $\mathbf{y}_{1:n} \sim \mathrm{AR}_{\mathbf{x}_{1:n}}(\pi_\theta, D_m^{(\mathrm{c})})$. This sample includes observation noise. **Step 2:** Remove the noise from the sample by passing it through the model once more: $\mathcal{N}(\boldsymbol{\mu}_{1:n}, \mathbf{D}) = P_{\mathbf{x}_{1:n}}\pi_\theta(D_m^{(\mathrm{c})} \oplus (\mathbf{x}_{1:n}, \mathbf{y}_{1:n}))$. Here the predictive mean $\boldsymbol{\mu}_{1:n}$ forms the noiseless sample. To produce a sample at arbitrarily many inputs, one may also evaluate $\mathcal{N}(\boldsymbol{\mu}'_{1:n}, \mathbf{D}) = P_{\mathbf{x}'_{1:n}}\pi_\theta(D_m^{(\mathrm{c})} \oplus (\mathbf{x}_{1:n}, \mathbf{y}_{1:n}))$ where $\mathbf{x}'_{1:n}$ is arbitrary. This result of this procedure is illustrated in Figure 4, and was used to generate the noiseless samples shown in Figure 1 (right). Figure 7 in Appendix C also illustrates this two-step procedure in a pictorial step-by-step fashion.

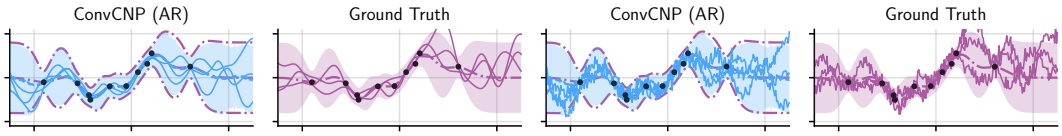

Figure 4: Comparison of noiseless (*left*) and noisy (*right*) samples from an AR ConvCNP trained on data sampled from a GP with an exponentiated-quadratic kernel, and the ground truth GP. The noiseless AR samples were generated from the noisy AR samples using the procedure suggested by Proposition 2.2.

3 Connections to Other Neural Distribution Estimators

Various paradigms have been developed for neural distribution estimators, including normalising flows (Dinh et al., 2014), generative adversarial networks (GANs; Goodfellow et al., 2014), variational autoencoders (VAEs; Kingma & Welling, 2013), autoregressive models (Uria et al., 2016), and diffusion models (Sohl-Dickstein et al., 2015; Ho et al., 2020). We argue that NPs should be viewed as neural distribution estimators alongside these models, revealing interesting connections between them. Figure 5 visualises the landscape of neural distribution estimators, highlighting the dimensionality of the target distribution, and the use of attention or convolution.

Our proposed AR CNPs can be viewed both as a kind of NP, and as an instance of autoregressive models. As such, they inherit the strengths of AR models, such as their ability to model complex dependencies with a tractable likelihood, but also some of their weaknesses, most notably slow test-time sampling. Slow sampling is the main drawback of applying AR CNPs to large target sets, though it may be possible to adapt techniques for speeding up other AR models to AR CNPs (Ramachandran et al., 2017a). One major difference between AR CNPs and existing AR models is that AR CNPs model an uncountably infinite set of variables, which allows querying arbitrary input locations but leads to the consistency issues discussed in Section 2.

Another distinguishing feature of the AR CNP is that it is trained to be order agnostic with respect to the product rule decomposition of the joint distribution: there is no preferred ordering of the input values during train time. DEformer (Alcorn & Nguyen, 2021), EoNADE (Uria et al., 2014), and

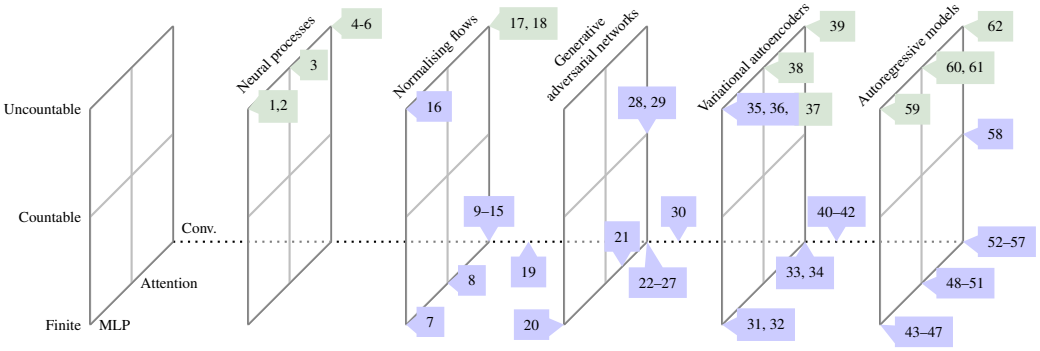

Neural processes

1. CNP (Garnelo et al., 2018a)
2. GNP (Markou et al., 2022)
3. ACNP (Kim et al., 2019)
4. ConvCNP Gordon et al. (2020)
5. ConvGNP (Markou et al., 2022)
6. FullConvGNP (Bruinsma et al., 2021)

Normalising flows

7. NICE (Dinh et al., 2014)
8. Flow++ (Ho et al., 2019)
9. RealNVP (Dinh et al., 2016)
10. FFJORD (Grathwohl et al., 2018)
11. Glow (Kingma & Dhariwal, 2018)
12. i-ResNets (Behrmann et al., 2018)
13. Res. Flows (Chen et al., 2019)
14. IAF (Kingma et al., 2016)
15. NAF (Huang et al., 2018)
16. TGP (Maroñas et al., 2021)
17. BRUNO (Korshunova et al., 2020)
18. Copula GNP (Markou et al., 2022)
19. FlowGAN (Grover et al., 2018)

GANs

20. GAN (Goodfellow et al., 2014)
21. SAGAN (Zhang et al., 2019)
22. DCGAN (Radford et al., 2015)
23. WGAN (Arjovsky et al., 2017)
24. InfoGAN (Chen et al., 2016a)
25. SNGAN (Miyato et al., 2018)
26. BigGAN (Brock et al., 2018)
27. StyleGAN (Karras et al., 2019)
28. Spatial GAN (Jetchev et al., 2016)
29. ∞-GAN (Lu et al., 2020)
30. PresGAN (Dieng et al., 2019)

Variational autoencoders

31. VAEs (Kingma & Welling, 2013)
32. IWAE (Burda et al., 2015)
33. Conv. VAE (Salimans et al., 2015)
34. VDVAE (Child, 2020)
35. GP-VAE (Fortuin et al., 2020)
36. SGP-VAE (Ashman et al., 2020)
37. LNP (Garnelo et al., 2018b)
38. ALNP (Kim et al., 2019)
39. ConvLNP (Foong et al., 2020)
40. VQ-VAE (Oord et al., 2017)
41. PixelVAE (Gulrajani et al., 2016)
42. VLAE (Chen et al., 2016b)

Autoregressive models

43. RNADE (Uria et al., 2013)
44. NADE (Uria et al., 2016)
45. DeepNADE (Uria et al., 2014)
46. EoNADE (Uria et al., 2014)
47. MADE (Germain et al., 2015)
48. PixelSNAIL (Chen et al., 2018)
49. Sparse Transformer (Child et al., 2019)
50. DEformer (Alcorn & Nguyen, 2021)
51. XLNet (Yang et al., 2019)
52. ConvNADE (Uria et al., 2016)
53. WaveNet (Oord et al., 2016a)
54. PixelCNN (Oord et al., 2016b)
55. PixelCNN++ (Salimans et al., 2017)
56. Fast PixelCNN++ (Ramachandran et al., 2017b)
57. Scalable Pixel Net (Menick & Kalchbrenner, 2018)
58. ARDMs (Hoogeboom et al., 2021)
59. AR CNP (this work)
60. AR ACNP (this work)
61. Transformer NP (Nguyen & Grover, 2022)
62. AR ConvCNP (this work)

Figure 5: Conceptual diagram showing the relationships between AR CNPs and various neural distribution estimators. The vertical axis denotes whether the model learns a distribution over a finite number of random variables, a countably infinite number, or an uncountably infinite number. The axis into the page denotes whether the architecture is MLP-based, or uses attention or convolutions. From left to right, we show different modelling paradigms. Fruitful exchanges occur when NPs (highlighted in green) are introduced into other modelling paradigms. Our proposed AR CNPs can be viewed as introducing NPs to the AR modelling paradigm.

XLnet (Yang et al., 2019) are other examples of AR models designed for order agnosticism. The AR CNP shares design choices with other AR models to achieve this goal: (i) a shared architecture is used to produce each conditional distribution, similar to WaveNet (Oord et al., 2016a) and PixelCNN (Oord et al., 2016b); (ii) the datapoint index is given as input to the network as in the DEformer model (Alcorn & Nguyen, 2021); and (iii) training maximises a log-likelihood including all decompositions of the joint distribution, similar to EoNADE (Uria et al., 2014) and XLnet (Yang et al., 2019).

In recent work, Nguyen & Grover (2022) proposed the Transformer NP (TNPs), which uses a causally-masked transformer architecture with an autoregressive likelihood. In contrast, rather than proposing a new AR architecture, our work focuses on running *existing CNPs* in AR mode to obtain coherent samples and improved likelihoods, without modifying the architecture or training procedure. In prior work, Volpp et al. (2021) used AR sampling in order to visualise samples from CNPs. However, their work focuses on proposing a novel context aggregation mechanism for NPs, and they do not evaluate the likelihood of CNPs autoregressively or investigate any performance gains.

Figure 5 also shows the connections betweeen NPs and VAEs and normalising flows. Just as VAEs typically use decoders that parametrise a factorised distribution, and rely on the latent variable to induce dependencies, the same is true for LNPs. Again, the key difference with standard VAEs is that LNPs model a distribution over an uncountable number of variables. In addition, models like conditional BRUNO (Korshunova et al., 2020) and copula GNPs (Markou et al., 2022) combine ideas from NPs and normalising flows, by transforming a stochastic process with an invertible transformation. Finally, GAN models such as Spatial GAN (Jetchev et al., 2016) and $\infty-$GAN (Lu et al., 2020) model countable numbers of variables, such as images of arbitrary size. Inspecting Figure 5, we see that GANs are the only class of models depicted that do not currently have an NP version, or a version that models an uncountable number of variables. This suggests adversarial training of NPs as an interesting avenue for future investigation.

4 The Performance of Autoregressive Neural Processes

In this section we investigate the performance of AR CNPs on synthetic and real data. Across a wide range of tasks, the AR CNP is competitive with much more sophisticated approaches. Throughout, we train LNPs with both the ELBO (Garnelo et al., 2018b) and ML objective (Foong et al., 2020). Code for reproducing our experiments can be found at `https://github.com/user/repo`. For all experiments, we use a random ordering of the target points in Proc. 2.1; see App. D for a justification.

4.1 Synthetically Generated Gaussian and Non-Gaussian Data

Synthetic experiment setup. We evaluate an extensive collection of NP models on a wide range of Gaussian and non-Gaussian synthetic regression tasks. We consider tasks with functions drawn from (i) different GPs; (ii) a non-Gaussian sawtooth process (as in Figure 1); (iii) a non-Gaussian mixture task, where, with equal probability, we sample the function from one of three possible GPs or the sawtooth process. We also consider various versions of the tasks for different input and output dimension d_x, d_y, with dependencies across the output channels. To ensure a fair comparison, we choose architectural details to make the parameter counts comparable between all models.

Results. Table 2 highlights the best performing models on some representative tasks; for further results across all twenty synthetic tasks and further experimental details, see Appendix H. The AR procedure dramatically improves the performance of the ConvCNP, with the AR ConvCNP being the best performing model for most tasks, except on the Gaussian EQ task where it performs marginally worse than the FullConvGNP. In particular, the AR ConvCNP outperforms the FullConvGNP and ConvGNP on non-Gaussian tasks, in agreement with Proposition 2.1, while having a faster training time than the other convolutional models (Figure 2). For the sawtooth task, Figure 10 in Appendix H.2 illustrates that predictions by the AR ConvCNP can be multi-modal and non-Gaussian, even when using a Gaussian likelihood. Finally, we note that in tasks with $d_x = 2$, where the FullConvGNP cannot be used (as discussed in Section 1), the AR ConvCNP far outperforms all competing approaches.

4.2 Sim-to-Real Transfer with the Lotka–Volterra Equations

Predator-prey data. We next investigate sim-to-real transfer, where the models are trained on simulated data and tested on real data. NPs are well-suited to this setting, since a large meta-data set can be easily generated to train them. We consider the hare–lynx data set, which is a population time series of Snowshoe hares and Canadian lynx (MacLulich, 1937). To generate simulated data, we use a stochastic version of the Lotka–Volterra equations (Lotka, 1910; Volterra, 1926):

$$\mathrm{d}X_t = \alpha X_t \,\mathrm{d}t - \beta Y_t X_t \,\mathrm{d}t + \sigma X_t^{\nu} \,\mathrm{d}W_t^{(1)}, \quad \mathrm{d}Y_t = -\gamma X_t \,\mathrm{d}t + \delta Y_t X_t \,\mathrm{d}t + \sigma Y_t^{\nu} \,\mathrm{d}W_t^{(2)}. \tag{9}$$

	EQ		Sawtooth		Mixture	
	KL to ground truth (↓ better)		Pred. log-likelihood (↑ better)		Pred. log-likelihood (↑ better)	
	$d_x, d_y = 1$	$d_x, d_y = 2$	$d_x, d_y = 1$	$d_x, d_y = 2$	$d_x, d_y = 1$	$d_x, d_y = 2$
ConvCNP	0.41 ±0.01	0.41 ±0.00	2.38±0.04	0.12 ±0.01	−0.23±0.04	−0.85 ±0.01
ConvCNP (AR)	0.01 ±0.00	**0.03** ±0.00	**3.60**±0.01	**0.38** ±0.00	**0.45**±0.04	**−0.62** ±0.01
ConvGNP	0.01 ±0.00	0.19 ±0.00	2.62±0.05	0.26 ±0.01	−0.24±0.02	−0.74 ±0.01
FullConvGNP	**0.00** ±0.00		2.16±0.04		−0.05±0.03	
ConvLNP (ML)	0.25 ±0.01	0.39 ±0.00	3.06±0.04	0.31 ±0.01	−0.06±0.03	−0.78 ±0.02
ConvLNP (ELBO)	0.06 ±0.00	0.79 ±0.00	3.51±0.02	0.04 ±0.00	0.12±0.04	−0.92 ±0.01
Diagonal GP	0.40 ±0.01	0.40 ±0.00				
Trivial	1.19 ±0.00	0.79 ±0.00	−0.18±0.00	−0.32 ±0.00	−1.32±0.00	−1.46 ±0.00

Table 2: Performance of NPs training on the GP EQ task, sawtooth task, and mixture task. *Diagonal GP* denotes the exact GP predictive, but with correlations removed. *Trivial* denotes a model that predicts a Gaussian distribution with the empirical means and standard deviation of the context outputs. Significantly best models in bold. Note that the FullConvGNP cannot be run on tasks where $d_x > 1$.

MODEL	INT. (S)	FOR. (S)	REC. (S)	INT. (R)	FOR. (R)	REC. (R)
ConvCNP	−3.47 ±0.02	−4.06 ±0.02	−4.85 ±0.02	−4.17 ±0.04	−4.70 ±0.06	−4.97 ±0.01
ConvCNP (AR)	**−3.30** ±0.02	**−3.47** ±0.02	**−3.60** ±0.02	**−4.10** ±0.03	**−4.27** ±0.03	**−4.32** ±0.01
ConvGNP	−3.47 ±0.02	−3.65 ±0.02	−4.15 ±0.02	−4.21 ±0.05	−4.82 ±0.13	−4.61 ±0.01
FullConvGNP	**−3.29** ±0.02	**−3.46** ±0.02	−3.79 ±0.02	−4.16 ±0.04	**−4.28** ±0.04	−4.45 ±0.00
ConvLNP (ML)	−3.41 ±0.02	−3.84 ±0.02	−4.44 ±0.02	**−4.13** ±0.04	−4.45 ±0.05	−4.54 ±0.01
ConvLNP (ELBO)	−3.77 ±0.02	−3.83 ±0.02	−4.12 ±0.02	−5.45 ±0.05	−5.47 ±0.07	−6.39 ±0.05

Table 3: Normalised log-likelihoods in the predator–prey experiments, showing interpolation (int.), forecasting (for.), and reconstruction (rec.) on simulated (S) and real (R) data. Significantly best results in bold.

	ConvCNP	ConvCNP (AR)	ConvGNP	FullConvGNP	ConvLNP (ML)	ConvLNP (ELBO)
INT.	−1.02±0.01	**−0.34**±0.01	−0.93±0.01	**−0.35**±0.01	−1.04±0.01	−1.20±0.01
REC.	−2.07±0.03	−0.63±0.01	−1.45±0.03	**−0.57**±0.01	−1.53±0.02	−2.00±0.06

Table 4: Per-datapoint predictive log-likelihoods on the EEG experiments. Significantly best results in bold.

Under these equations, the prey population X_t grows exponentially with rate α, the predator population Y_t decays exponentially with rate γ, and the predators hunt the prey. $W^{(1)}$ and $W^{(2)}$ are independent Brownian motions introducing noisy behaviour. These equations generate non-Gaussian data with both within-channel as well as cross-channel dependencies. We simulate the Lotka-Volterra equations on a dense grid, and use them to generate meta–data sets in three different ways. *Interpolation*: we randomly subsample the data into context and target sets. *Forecasting*: we choose a random time, before which all data are contexts, and all future data are targets. *Reconstruction:* we randomly choose between the X_t or Y_t, split the chosen series as in forecasting, and append the other series to the context. In training, for every batch, we choose one of these tasks uniformly at random.

Results. Table 3 shows the results of the best performing models. The AR ConvCNP performs best both on the simulated as well as the real data, again demonstrating that running CNPs in AR mode improves performance and can even outperform strong GNP and LNP baselines. For full experimental details and additional results see Appendix I.

4.3 ELECTROENCEPHALOGRAM EXPERIMENTS

Electroencephalogram data. We next trained various NPs on real time series data consisting of electroencephalogram (EEG) measurements (Zhang et al., 1995b), following Markou et al. (2022). Each time series consists of 256 regularly spaced measurements across 7 correlated channels. For each channel, we randomly select a number of the 256 points uniformly at random to be target points, and use the remaining ones as context points, independently across the channels.

Results. After training, we test the models on this interpolation task and also on a reconstruction task, where we set a part of a channel as target and the remainder as context. In Table 4, we observe that the AR ConvCNP is competitive with the FullConvGNP, despite having significantly shorter training times and fewer parameters. Both the AR ConvCNP and the FullConvGNP outperform the ConvCNP and the ConvLNP. Full experimental detail are in Appendix J.

4.4 ENVIRONMENTAL MODELLING

Data fusion. A ubiquitous challenge in environmental sciences is fusing spatio-temporal data from disparate sources (Chang & Bai, 2018; Lahat et al., 2015). This challenge, which we refer to as

	GAUSSIAN				BETA-CATEGORICAL		
	ConvGNP	ConvLNP (ML)	ConvCNP	ConvCNP (AR)	ConvLNP (ML)	ConvCNP	ConvCNP (AR)
Log-lik.	$0.60_{\pm 0.02}$	$0.62_{\pm 0.02}$	$0.58_{\pm 0.02}$	$\mathbf{0.88}_{\pm 0.02}$	$1.06_{\pm 0.02}$	$1.03_{\pm 0.02}$	$\mathbf{1.27}_{\pm 0.02}$
MAE (%)	$13.05_{\pm 0.17}$	$12.98_{\pm 0.16}$	$13.01_{\pm 0.16}$	$13.01_{\pm 0.16}$	$12.99_{\pm 0.16}$	$13.13_{\pm 0.16}$	$13.13_{\pm 0.16}$

Table 5: Log-likelihoods (log-lik.) and mean absolute errors (MAE, in units of cloud cover %), over the 2019-2019 test period for the cloud cover task. Note that log-likelihoods cannot be compared directly across the Gaussian and beta-categorical models. Errors indicate standard errors. Significantly best results in bold.

data fusion, arises in diverse applications including climate monitoring (Gettelman et al., 2022), air quality estimation (Ferrer-Cid et al., 2020), land cover mapping (Robinson et al., 2021), population estimation (Lu et al., 2010), and hydrology (Hosseini & Kerachian, 2017). NPs naturally handle multiple sources of both on-grid and off-grid data, and can make predictions at arbitrary locations (Vaughan et al., 2022; Markou et al., 2022), making them particularly well suited to data fusion.

Joint and non-Gaussian statistics. Another challenge in environmental sciences is estimating the joint probability of events that span space and time. For example, a renewable energy provider may want to know the compound risk of *both* low wind speeds at their offshore wind farm *and* high cloud coverage over their solar panel farm, possibly at different locations. For such tasks, it is essential to model statistical dependencies to obtain well-calibrated uncertainty estimates. Furthermore, many environmental variables, such as cloud cover, are bounded in output space and are poorly modelled by Gaussian predictives. CNPs are most commonly applied with Gaussian likelihoods, but can be easily used with arbitrary likelihood functions. While GAN-based approaches (Ravuri et al., 2021) can capture both joint as well as non-Gaussian statistics, they are unsuitable for integrating off-grid with on-grid data, as may be required for data fusion. The AR ConvCNP thus fills a gap in the environmental modelling toolbox by enabling data fusion while capturing statistical dependencies and working with non-Gaussian likelihoods. Here, we assess the AR ConvCNP on two common environmental modelling tasks, namely *data assimilation* and *statistical downscaling*.

Data assimilation. Data assimilation is the task of combining observations of the Earth system to produce predictions on a regular grid, called a *reanalysis*. Reanalyses are typically generated by fitting the trajectories of physics-based climate models to observations (Hersbach et al., 2020; Gettelman et al., 2022). AR ConvCNPs can not only provide a substantial speedup over conventional data assimilation systems, but also permit rigorous uncertainty estimation. To explore the ability of the AR ConvCNP to emulate a data assimilation system for a non-Gaussian variable, we train convolutional NP models to predict simulated daily-average cloud cover fraction over Antarctica.

We use reanalysis data from ECMWF ERA5 (Hersbach et al., 2020) as ground truth. Cloud cover ranges in $[0, 1]$, with observations frequently taking values of 0 or 1 (Figure 13). We evaluate the performance of NPs using either a Gaussian likelihood or a more appropriate beta-categorical mixture model with three components. Two of these are discrete components that capture values of exactly 0 or 1, while the last is a beta distribution which captures continuous values in $(0, 1)$. This provides a robust way of handling 0 and 1 values, unlike the existing Copula GNP model (Markou et al., 2022) which can have its output constrained in $(0, 1)$ but places zero density at the endpoints.

Results. In Table 5 we see that the AR ConvCNP significantly outperforms competing NPs for both the Gaussian and beta-categorical likelihoods. Figure 6 shows samples drawn from the models, after observing context points on half of the space. The AR ConvCNP displays remarkable ability to extrapolate rich, non-stationary, multi-scale structure, such as sudden changes in cloud cover over the Ross Ice Shelf coastline at the bottom of the figure. By comparison, the ConvLNP and ConvGNP produce blurry, lower frequency samples. Unlike GPs, convolutional NP models have a fixed receptive field induced by the CNN architecture used for the encoder, which is computationally expensive to increase. Away from the context points on the left, samples from the non-AR models will be independent of the observations, reverting to some mean representation of the data (Fig. 6c-e). This highlights a further benefit of AR CNPs: successive AR applications increase the receptive field, enabling rich, conditional sample structure to extrapolate far away from observed data. Further commentary and model samples are provided in Appendix K.3. See Appendix K for full details.

Environmental downscaling. The spatial resolutions of physics-based reanalyses are limited by their vast computational demands, making them unsuitable for capturing local and extreme events (Stocker et al., 2013; Maraun et al., 2017). *Statistical downscaling* addresses this issue by leveraging additional information to produce fine-grained predictions (Maraun & Widmann, 2018). Recently, NPs have been shown to outperform a large ensemble of existing climate downscaling approaches

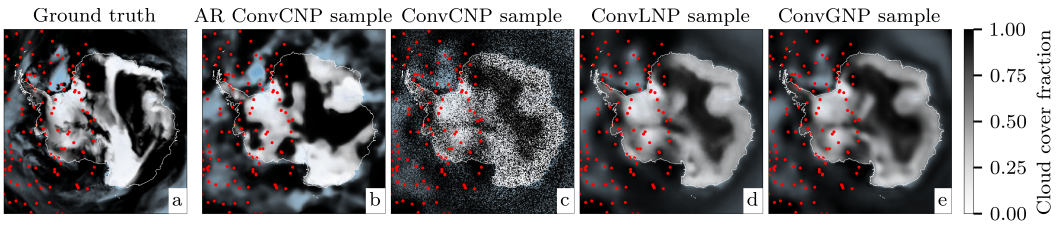

Figure 6: (a) Ground truth simulated cloud cover fraction on 25/06/2018. (b-e), Sample draws from the AR ConvCNP, ConvCNP, ConvLNP and ConvGNP with context points denoted by red dots. Context points were removed from the right hand side of the 2D space to test the models' abilities to extrapolate coherent function samples far away from observations. The ConvCNP and ConvLNP models used a beta-categorical likelihood while the ConvGNP uses a low-rank Gaussian likelihood.

(Vaughan et al., 2022). We compare the AR ConvCNP to the MLP ConvCNP of Vaughan et al. and the MLP ConvGNP of (Markou et al., 2022) in a temperature downscaling task over Germany. In this task, the context data consist of low-resolution ERA-Interim reanalysis data and high-resolution topography, and the target data consist of weather station observations from the ECA&D dataset. We also consider a second setup where we reveal some station observations to aid the downscaling process. As Appendix L.2 explains, the MLP ConvCNP and MLP ConvGNP cannot be naively extended to include these station observations. We therefore introduce a novel multiscale architecture, which we use to run the ConvCNP in AR mode. See Appendix L for full experimental details.

Results. In Table 6 we observe that the AR ConvCNP matches the performance of the ConvGNP, which is remarkable as the latter has been previously demonstrated to outperform a range of state-of-the-art downscaling approaches (Markou et al., 2022; Vaughan et al., 2022). When additional observations from weather stations are revealed, the AR ConvCNP significantly outperforms the MLP ConvGNP in both metrics.

Downscaling	Log-lik.	MAE (°C)	Down. + stations	Log-lik.	MAE (°C)
ConvCNP (MLP)	−1.55 ±0.01	**0.94** ±0.03	ConvCNP* (MLP)	−1.55 ±0.01	0.94 ±0.03
ConvGNP (MLP)	**−1.36** ±0.01	1.09 ±0.09	ConvGNP* (MLP)	−1.38 ±0.01	1.09 ±0.09
ConvCNP (AR)	**−1.36** ±0.01	1.04 ±0.04	ConvCNP (AR)	**−1.31** ±0.01	**0.85** ±0.05

Table 6: Log-likelihoods and mean absolute errors (MAEs) in the downscaling experiments, without (*left*) and with (*right*) assisting weather station observations. Significantly best results in bold. *Cannot use extra weather station observations.

5 Limitations and Conclusion

We have shown that the AR procedure can be readily applied to improve the performance of CNPs, producing coherent samples and dramatically improved likelihoods. Surprisingly, in an extensive range of experiments, this simple approach often outperforms more complicated methods which rely on latent variables or that explicitly model correlations. We demonstrate the effectiveness of our approach on data sets of real-world interest by applying AR CNPs on climate data fusion tasks, modelling $[0, 1]$-constrained data with a beta-categorical likelihood and introducing a novel multiscale architecture. Notably, AR CNPs fill a gap in the climate modelling toolbox by enabling joint, non-Gaussian predictives, which could be used to better estimate the magnitude of compound risks. We also position AR CNPs within the larger neural density estimator literature, showing the fruitfulness of combining NPs with other modelling paradigms.

More generally, AR CNPs equip the NP framework with a new knob where modelling complexity and computational expense at training time can be traded for computational expense at test time. In particular, the higher quality samples and better likelihoods obtained by applying NPs autoregressively come with the additional cost of performing a forward pass for every element in the target set. This can be prohibitively expensive for large target sets, and constitutes the primary practical drawback of using AR CNPs. In addition, since AR CNPs do not define a consistent stochastic process, design choices for the AR procedure may affect the quality of the results. Thus practitioners need to avoid choosing target sets that lead to pathological behaviour, such as when the spatial density of the target inputs is too high. However, the flexibility of this design space also presents an opportunity: as an example, in Appendix M we show that auxiliary target points can be used to further improve predictions. Finally, promising avenues for future work include applying the AR procedure to other NPs besides CNPs, and investigating the efficacy of the block sampling scheme presented in Section 2.

6 Reproducibility Statement

All our experiments are carried out using either synthetic or publicly available datasets. The EEG data set is available through the UCI database,[2] and the environmental data are also publicly available through the European Climate Data Service.[3]

We make the code necessary to reproduce our experiments[4] as well as instructions for obtaining, preprocessing and modelling the Antarctica data[5] publicly available. Proofs for Propositions 2.1 and 2.2 are given in Appendix A and Appendix B respectively. Details on the model architectures and the experimental setup can be found in Appendices F to H for the synthetic datasets, Appendix I the sim-to-real transfer experiments, Appendix J for the EEG experiments, Appendix K for the data assimilation experiment, and Appendix L for the downscaling experiment.

7 Ethics Statement

Training CNPs autoregressively improves their performance dramatically, but we do not foresee adverse societal impacts as a result of this work. That being said, the problem of capturing the statistical trends present in a dataset must be performed with care, especially in safety critical applications, where the stakes of making incorrect and confident predictions can have severe consequences. We view the AR procedure as a useful tool, rather than a panacea, for capturing such behaviours, and hope this work encourages further research into building effective but reliable models to this end.

We also note that while training CNPs is computationally cheaper than alternative NP models, AR sampling itself incurs a substantial computational cost, and thus energy cost, at test time. Running AR sampling on a large scale could lead to greater power demands for these models, resulting in larger carbon footprints which are undesirable. However, we believe the potential benefits for environmental modelling could outweigh this cost, while leveraging methods to make AR CNPs more computationally efficient should help alleviate this issue.

References

Michael A Alcorn and Anh Nguyen. The deformer: An order-agnostic distribution estimating transformer. *arXiv preprint arXiv:2106.06989*, 2021.

Martin Arjovsky, Soumith Chintala, and Leon Bottou. Wasserstein generative adversarial networks. In *Proceedings of the 34th International Conference on Machine Learning*, volume 70 of *Proceedings of Machine Learning Research*, pp. 214–223. PMLR, 2017.

Matthew Ashman, Jonathan So, Will Tebbutt, Vincent Fortuin, Michael Pearce, and Richard E Turner. Sparse gaussian process variational autoencoders. *arXiv preprint arXiv:2010.10177*, 2020.

Jimmy Lei Ba, Jamie Ryan Kiros, and Geoffrey E. Hinton. Layer normalization. *arXiv preprint arXiv:1607.06450*, 2016.

Henri Begleiter. EEG database data set, 2022. URL `https://archive.ics.uci.edu/ml/datasets/eeg+database`.

Jens Behrmann, Will Grathwohl, Ricky T. Q. Chen, David Duvenaud, and Jörn-Henrik Jacobsen. Invertible residual networks. *arXiv preprint arXiv:1811.00995*, 2018.

Andrew Brock, Jeff Donahue, and Karen Simonyan. Large scale gan training for high fidelity natural image synthesis. *arXiv preprint arXiv:1809.11096*, 2018.

Wessel P. Bruinsma, James Requeima, Andrew Y. K. Foong, Jonathan Gordon, and Richard E. Turner. The Gaussian neural process. In *Proceedings of the 3rd Symposium on Advances in Approximate Bayesian Inference*, 2021.

[2] `https://kdd.ics.uci.edu/databases/eeg/eeg.data.html`.

[3] `https://cds.climate.copernicus.eu/#!/home`.

[4] `https://github.com/user/repo1`.

[5] `https://github.com/user/repo2`.

Y. Burda, R. Grosse, and R. Salakhutdinov. Importance weighted autoencoders. *arXiv preprint arXiv:1509.00519*, 2015.

Ni-Bin Chang and Kaixu Bai. *Multisensor data fusion and machine learning for environmental remote sensing*. CRC Press, 2018.

Ricky TQ Chen, Jens Behrmann, David K Duvenaud, and Jörn-Henrik Jacobsen. Residual flows for invertible generative modeling. *Advances in Neural Information Processing Systems*, 32, 2019.

X. Chen, Y. Duan, R. Houthooft, J. Schulman, I. Sutskever, and P. Abbeel. Infogan: Interpretable representation learning by information maximizing generative adversarial nets. *arXiv preprint arXiv:1606.03657*, 2016a.

X. Chen, D. P. Kingma, T. Salimans, Y. Duan, P. Dhariwal, J. Schulman, I. Sutskever, and P. Abbeel. Variational lossy autoencoder. *arXiv preprint arXiv:1611.02731*, 2016b.

Xi Chen, Nikhil Mishra, Mostafa Rohaninejad, and Pieter Abbeel. Pixelsnail: An improved autoregressive generative model. In *International Conference on Machine Learning*, pp. 864–872. PMLR, 2018.

Rewon Child. Very deep vaes generalize autoregressive models and can outperform them on images. *arXiv preprint arXiv:2011.10650*, 2020.

Rewon Child, Scott Gray, Alec Radford, and Ilya Sutskever. Generating long sequences with sparse transformers. *arXiv preprint arXiv:1904.10509*, 2019.

Franccois Chollet. Xception: Deep learning with depthwise separable convolutions. In *Proceedings of the IEEE/CVF Conference on Computer Vision and Pattern Recognition*, 2017.

D. P. Dee, S. M. Uppala, A. J. Simmons, P. Berrisford, P. Poli, S. Kobayashi, U. Andrae, M. A. Balmaseda, G. Balsamo, P. Bauer, P. Bechtold, A. C. M. Beljaars, L. van de Berg, J. Bidlot, N. Bormann, C. Delsol, R. Dragani, M. Fuentes, A. J. Geer, L. Haimberger, S. B. Healy, H. Hersbach, E. V. Holm, L. Isaksen, P. Kållberg, M. Kohler, M. Matricardi, A. P. McNally, B. M. Monge-Sanz, J.-J. Morcrette, B.-K. Park, C. Peubey, P. de Rosnay, C. Tavolato, J.-N. Thepaut, and F. Vitart. The ERA-interim reanalysis: Configuration and performance of the data assimilation system. *Quarterly Journal of the Royal Meteorological Society*, 137(656):553–597, 2011. doi: 10.1002/qj.828.

Adji B Dieng, Francisco JR Ruiz, David M Blei, and Michalis K Titsias. Prescribed generative adversarial networks. *arXiv preprint arXiv:1910.04302*, 2019.

L. Dinh, J. Sohl-Dickstein, and S. Bengio. Density estimation using real NVP. *arXiv preprint arXiv:1605.08803*, 2016.

Laurent Dinh, David Krueger, and Yoshua Bengio. Nice: Non-linear independent components estimation, 2014.

Richard Durrett. *Probability: Theory and Examples*. Cambridge University Press, 4 edition, 2010.

Earth Resources Observation and Science Center, U.S. Geological Survey, U.S. Department of the Interior. USGS 30 arc-second global elevation data, GTOPO30, 1997. URL `https://doi.org/10.5065/A1Z4-EE71`.

Pau Ferrer-Cid, Jose M Barcelo-Ordinas, Jorge Garcia-Vidal, Anna Ripoll, and Mar Viana. Multisensor data fusion calibration in iot air pollution platforms. *IEEE Internet of Things Journal*, 7(4): 3124–3132, 2020.

Andrew Y. K. Foong, Wessel P. Bruinsma, Jonathan Gordon, Yann Dubois, James Requeima, and Richard E. Turner. Meta-learning stationary stochastic process prediction with convolutional neural processes. In *Advances in Neural Information Processing Systems 33*. Curran Associates, Inc., 2020.

Vincent Fortuin, Dmitry Baranchuk, Gunnar Rätsch, and Stephan Mandt. Gp-vae: Deep probabilistic time series imputation. In *International conference on artificial intelligence and statistics*, pp. 1651–1661. PMLR, 2020.

M. Garnelo, D. Rosenbaum, C. J. Maddison, T. Ramalho, D. Saxton, M. Shanahan, Y. Whye Teh, D. J. Rezende, and S. M. A. Eslami. Conditional neural processes. In *Proceedings of 35th International Conference on Machine Learning*, volume 80 of *Proceedings of Machine Learning Research*. PMLR, 2018a.

M. Garnelo, J. Schwarz, D. Rosenbaum, F. Viola, D. J. Rezende, S. M. A. Eslami, and Y. Whye Teh. Neural processes. In *Proceedings of 35th International Conference on Machine Learning*, 2018b.

Mathieu Germain, Karol Gregor, Iain Murray, and Hugo Larochelle. Made: Masked autoencoder for distribution estimation. In *International conference on machine learning*, pp. 881–889. PMLR, 2015.

Andrew Gettelman, Alan J Geer, Richard M Forbes, Greg R Carmichael, Graham Feingold, Derek J Posselt, Graeme L Stephens, Susan C van den Heever, Adam C Varble, and Paquita Zuidema. The future of earth system prediction: Advances in model-data fusion. *Science Advances*, 8(14): eabn3488, 2022.

I. J. Goodfellow, J. Pouget Abadie, M. Mirza, B. Xu, D. Warde Farley, S. Ozair, A. Courville, and Y. Bengio. Generative adversarial networks. *arXiv preprint arXiv:1406.2661*, 2014.

Jonathan Gordon, Wessel P. Bruinsma, Andrew Y. K. Foong, James Requeima, Yann Dubois, and Richard E. Turner. Convolutional conditional neural processes. In *Proceedings of the 8th International Conference on Learning Representations*, 2020. URL `https://openreview.net/forum?id=Skey4eBYPS`.

Will Grathwohl, Ricky TQ Chen, Jesse Bettencourt, Ilya Sutskever, and David Duvenaud. Ffjord: Free-form continuous dynamics for scalable reversible generative models. *arXiv preprint arXiv:1810.01367*, 2018.

Aditya Grover, Manik Dhar, and Stefano Ermon. Flow-gan: Combining maximum likelihood and adversarial learning in generative models. In *Proceedings of the AAAI Conference on Artificial Intelligence*, volume 32, 2018.

Ishaan Gulrajani, Kundan Kumar, Faruk Ahmed, Adrien Ali Taiga, Francesco Visin, David Vazquez, and Aaron Courville. Pixelvae: A latent variable model for natural images. *arXiv preprint arXiv:1611.05013*, 2016.

Kaiming He, Xiangyu Zhang, Shaoqing Ren, and Jian Sun. Deep residual learning for image recognition. In *Proceedings of the IEEE/CVF Conference on Computer Vision and Pattern Recognition*, 2016.

Hans Hersbach, Bill Bell, Paul Berrisford, Shoji Hirahara, András Horányi, Joaquín Muñoz-Sabater, Julien Nicolas, Carole Peubey, Raluca Radu, Dinand Schepers, Adrian Simmons, Cornel Soci, Saleh Abdalla, Xavier Abellan, Gianpaolo Balsamo, Peter Bechtold, Gionata Biavati, Jean Bidlot, Massimo Bonavita, Giovanna De Chiara, Per Dahlgren, Dick Dee, Michail Diamantakis, Rossana Dragani, Johannes Flemming, Richard Forbes, Manuel Fuentes, Alan Geer, Leo Haimberger, Sean Healy, Robin J. Hogan, Elias Holm, Marta Janiskova, Sarah Keeley, Patrick Laloyaux, Philippe Lopez, Cristina Lupu, Gabor Radnoti, Patricia de Rosnay, Iryna Rozum, Freja Vamborg, Sebastien Villaume, and Jean-Noël Thépaut. The ERA5 global reanalysis. 146(730):1999–2049, 2020. ISSN 1477-870X. doi: 10.1002/qj.3803.

Jonathan Ho, Xi Chen, Aravind Srinivas, Yan Duan, and Pieter Abbeel. Flow++: Improving flow-based generative models with variational dequantization and architecture design. In *International Conference on Machine Learning*, pp. 2722–2730. PMLR, 2019.

Jonathan Ho, Ajay Jain, and Pieter Abbeel. Denoising diffusion probabilistic models. *Advances in Neural Information Processing Systems*, 33:6840–6851, 2020.

Emiel Hoogeboom, Alexey A Gritsenko, Jasmijn Bastings, Ben Poole, Rianne van den Berg, and Tim Salimans. Autoregressive diffusion models. *arXiv preprint arXiv:2110.02037*, 2021.

Marjan Hosseini and Reza Kerachian. A data fusion-based methodology for optimal redesign of groundwater monitoring networks. *Journal of Hydrology*, 552:267–282, 2017.

Chin-Wei Huang, David Krueger, Alexandre Lacoste, and Aaron Courville. Neural autoregressive flows. In *International Conference on Machine Learning*, pp. 2078–2087. PMLR, 2018.

Douglas R. Hundley. Introduction to mathematical modelling. URL http://people.whitman.edu/~hundledr/courses/M250F03/M250.html.

Nikolay Jetchev, Urs Bergmann, and Roland Vollgraf. Texture synthesis with spatial generative adversarial networks. *arXiv preprint arXiv:1611.08207*, 2016.

Tero Karras, Samuli Laine, and Timo Aila. A style-based generator architecture for generative adversarial networks. In *Proceedings of the IEEE/CVF conference on computer vision and pattern recognition*, pp. 4401–4410, 2019.

H. Kim, A. Mnih, J. Schwarz, M. Garnelo, A. Eslami, D. Rosenbaum, O. Vinyals, and Y. Whye Teh. Attentive neural processes. In *Proceedings of the 7th International Conference on Learning Representations*, 2019.

D. P. Kingma and J. Ba. ADAM: A method for stochastic optimization. In *Proceedings of the 3rd International Conference on Learning Representations*, 2015.

D. P. Kingma and M. Welling. Auto-encoding variational Bayes. *arXiv preprint arXiv:1312.6114*, 2013.

D. P. Kingma, T. Salimans, R. Jozefowicz, X. Chen, I. Sutskever, and M. Welling. Improving variational inference with inverse autoregressive flow. *arXiv preprint arXiv:1606.04934*, 2016.

Durk P Kingma and Prafulla Dhariwal. Glow: Generative flow with invertible 1x1 convolutions. *Advances in neural information processing systems*, 31, 2018.

Iryna Korshunova, Yarin Gal, Arthur Gretton, and Joni Dambre. Conditional bruno: A neural process for exchangeable labelled data. *Neurocomputing*, 416:305–309, 2020.

Dana Lahat, Tülay Adali, and Christian Jutten. Multimodal data fusion: an overview of methods, challenges, and prospects. *Proceedings of the IEEE*, 103(9):1449–1477, 2015.

Alfred J. Lotka. Contribution to the theory of periodic reactions. *The Journal of Physical Chemistry*, 14(3):271–274, 1910. ISSN 0092-7325. doi: 10.1021/j150111a004. URL https://doi.org/10.1021/j150111a004.

Chaochao Lu, Richard E. Turner, Yingzhen Li, and Nate Kushman. Interpreting spatially infinite generative models, 2020. URL https://arxiv.org/abs/2007.12411.

Zhenyu Lu, Jungho Im, Lindi Quackenbush, and Kerry Halligan. Population estimation based on multi-sensor data fusion. *International Journal of Remote Sensing*, 31(21):5587–5604, 2010.

D. A. MacLulich. *Fluctuations in the Numbers of the Varying Hare (Lepus Americanus)*. University of Toronto Press, 1937. doi: doi:10.3138/9781487583064.

Douglas Maraun and Martin Widmann. *Statistical Downscaling and Bias Correction for Climate Research*. Cambridge Uiversity Press, 2018. doi: 10.1017/9781107588783.

Douglas Maraun, Martin Widmann, José M. Gutiérrez, Sven Kotlarski, Richard E. Chandler, Elke Hertig, Joanna Wibig, Radan Huth, and Renate A. I. Wilcke. VALUE: A framework to validate downscaling approaches for climate change studies. *Earth's Future*, 3(1):1–14, 2015. doi: 10.1002/2014EF000259. URL https://agupubs.onlinelibrary.wiley.com/doi/abs/10.1002/2014EF000259.

Douglas Maraun, Theodore G. Shepherd, Martin Widmann, Giuseppe Zappa, Daniel Walton, José M. Gutiérrez, Stefan Hagemann, Ingo Richter, Pedro M. M. Soares, Alex Hall, and Linda O. Mearns. Towards process-informed bias correction of climate change simulations. *Nature Climate Change*, 7(11):764–773, 2017. ISSN 1758-6798. doi: 10.1038/nclimate3418.

Stratis Markou, James Requeima, Wessel P. Bruinsma, and Richard E. Turner. Efficient Gaussian neural processes for regression. In *Proceedings of 39th International Conference on Machine Learning*, 2021.

Stratis Markou, James Requeima, Wessel P. Bruinsma, Anna Vaughan, and Richard E. Turner. Practical conditional neural processes via tractable dependent predictions. In *Proceedings of the 10th International Conference on Learning Representations*, 2022.

Juan Maroñas, Oliver Hamelijnck, Jeremias Knoblauch, and Theodoros Damoulas. Transforming gaussian processes with normalizing flows. In *International Conference on Artificial Intelligence and Statistics*, pp. 1081–1089. PMLR, 2021.

Jacob Menick and Nal Kalchbrenner. Generating high fidelity images with subscale pixel networks and multidimensional upscaling. *arXiv preprint arXiv:1812.01608*, 2018.

Thomas P. Minka. Expectation propagation for approximate Bayesian inference. volume 17, pp. 362–369. Morgan Kaufmann Publishers Inc., 2001.

Takeru Miyato, Toshiki Kataoka, Masanori Koyama, and Yuichi Yoshida. Spectral normalization for generative adversarial networks. *arXiv preprint arXiv:1802.05957*, 2018.

M. Morlighem. Measures bedmachine antarctica, version 2, 2020. URL `https://nsidc.org/data/NSIDC-0756/versions/2`.

Tung Nguyen and Aditya Grover. Transformer neural processes: Uncertainty-aware meta learning via sequence modeling. In *International Conference on Machine Learning*, pp. 16569–16594. PMLR, 2022.

Augustus Odena, Vincent Dumoulin, and Chris Olah. Deconvolution and Checkerboard Artifacts. *Distill*, 1(10):e3, October 2016. ISSN 2476-0757. doi: 10.23915/distill.00003. URL `http://distill.pub/2016/deconv-checkerboard`.

Bernt Oksendal. *Stochastic differential equations: an introduction with applications*. Springer Science & Business Media, 2013.

Aaron van den Oord, Sander Dieleman, Heiga Zen, Karen Simonyan, Oriol Vinyals, Alex Graves, Nal Kalchbrenner, Andrew Senior, and Koray Kavukcuoglu. Wavenet: A generative model for raw audio. *arXiv preprint arXiv:1609.03499*, 2016a.

Aaron van den Oord, Nal Kalchbrenner, Lasse Espeholt, Oriol Vinyals, Alex Graves, et al. Conditional image generation with pixelcnn decoders. *Advances in neural information processing systems*, 29, 2016b.

Aaron van den Oord, Oriol Vinyals, et al. Neural discrete representation learning. *Advances in neural information processing systems*, 30, 2017.

Alec Radford, Luke Metz, and Soumith Chintala. Unsupervised representation learning with deep convolutional generative adversarial networks. *arXiv preprint arXiv:1511.06434*, 2015.

Prajit Ramachandran, Tom Le Paine, Pooya Khorrami, Mohammad Babaeizadeh, Shiyu Chang, Yang Zhang, Mark A. Hasegawa-Johnson, Roy H. Campbell, and Thomas S. Huang. Fast generation for convolutional autoregressive models. In *International Conference on Learning Representations*, 2017a.

Prajit Ramachandran, Tom Le Paine, Pooya Khorrami, Mohammad Babaeizadeh, Shiyu Chang, Yang Zhang, Mark A Hasegawa-Johnson, Roy H Campbell, and Thomas S Huang. Fast generation for convolutional autoregressive models. *arXiv preprint arXiv:1704.06001*, 2017b.

Suman Ravuri, Karel Lenc, Matthew Willson, Dmitry Kangin, Remi Lam, Piotr Mirowski, Megan Fitzsimons, Maria Athanassiadou, Sheleem Kashem, Sam Madge, Rachel Prudden, Amol Mandhane, Aidan Clark, Andrew Brock, Karen Simonyan, Raia Hadsell, Niall Robinson, Ellen Clancy, Alberto Arribas, and Shakir Mohamed. Skilful precipitation nowcasting using deep generative models of radar. *Nature*, 597(7878):672–677, September 2021. ISSN 1476-4687. doi: 10.1038/s41586-021-03854-z. URL `https://www.nature.com/articles/s41586-021-03854-z`. Number: 7878 Publisher: Nature Publishing Group.

Caleb Robinson, Kolya Malkin, Nebojsa Jojic, Huijun Chen, Rongjun Qin, Changlin Xiao, Michael Schmitt, Pedram Ghamisi, Ronny Hänsch, and Naoto Yokoya. Global land-cover mapping with weak supervision: Outcome of the 2020 ieee grss data fusion contest. *IEEE Journal of Selected Topics in Applied Earth Observations and Remote Sensing*, 14:3185–3199, 2021.

Olaf Ronneberger, Philipp Fischer, and Thomas Brox. U-net: Convolutional networks for biomedical image segmentation. In *International Conference on Medical image computing and computer-assisted intervention*, pp. 234–241. Springer, 2015.

Tim Salimans, Diederik Kingma, and Max Welling. Markov chain monte carlo and variational inference: Bridging the gap. In *International Conference on Machine Learning*, pp. 1218–1226. PMLR, 2015.

Tim Salimans, Andrej Karpathy, Xi Chen, and Diederik P Kingma. Pixelcnn++: Improving the pixelcnn with discretized logistic mixture likelihood and other modifications. *arXiv preprint arXiv:1701.05517*, 2017.

Jascha Sohl-Dickstein, Eric Weiss, Niru Maheswaranathan, and Surya Ganguli. Deep unsupervised learning using nonequilibrium thermodynamics. In *International Conference on Machine Learning*, pp. 2256–2265. PMLR, 2015.

Thomas F. Stocker, Dahe Qin, Gian-Kasper Plattner, Melinda M.B. Tignor, Simon K. Allen, Judith Boschung, Alexander Nauels, Yu Xia, Vincent Bex, and Pauline M. Midgley. Climate change 2013: The physical science basis. Technical report, Cambridge University Press, 2013.

A. M. G. Klein Tank, J. B. Wijngaard, G. P. Können, R. Böhm, G. Demarée, A. Gocheva, M. Mileta, S. Pashiardis, L. Hejkrlik, C. Kern-Hansen, R. Heino, P. Bessemoulin, G. Müller-Westermeier, M. Tzanakou, S. Szalai, T. Pálsdóttir, D. Fitzgerald, S. Rubin, M. Capaldo, M. Maugeri, A. Leitass, A. Bukantis, R. Aberfeld, A. F. V. van Engelen, E. Forland, M. Mietus, F. Coelho, C. Mares, V. Razuvaev, E. Nieplova, T. Cegnar, J. Antonio López, B. Dahlström, A. Moberg, W. Kirchhofer, A. Ceylan, O. Pachaliuk, L. V. Alexander, and P. Petrovic. Daily dataset of 20th-century surface air temperature and precipitation series for the european climate assessment. *International Journal of Climatology*, 22(12):1441–1453, 2002. doi: 10.1002/joc.773. URL https://rmets.onlinelibrary.wiley.com/doi/abs/10.1002/joc.773.

Benigno Uria, Iain Murray, and Hugo Larochelle. Rnade: The real-valued neural autoregressive density-estimator. *Advances in Neural Information Processing Systems*, 26, 2013.

Benigno Uria, Iain Murray, and Hugo Larochelle. A deep and tractable density estimator. In *International Conference on Machine Learning*, pp. 467–475. PMLR, 2014.

Benigno Uria, Marc-Alexandre Côté, Karol Gregor, Iain Murray, and Hugo Larochelle. Neural autoregressive distribution estimation. *Journal of Machine Learning Research*, 17(205):1–37, 2016. URL http://jmlr.org/papers/v17/16-272.html.

A. Vaswani, N. Shazeer, N. Parmar, J. Uszkoreit, L. Jones, A. N. Gomez, L. Kaiser, and I. Polosukhin. Attention Is all you need. *arXiv preprint arXiv:1706.03762*, 2017.

A. Vaughan, W. Tebbutt, J. S. Hosking, and R. E. Turner. Convolutional conditional neural processes for local climate downscaling. *Geoscientific Model Development*, 15(1):251–268, 2022. doi: 10.5194/gmd-15-251-2022. URL https://gmd.copernicus.org/articles/15/251/2022/.

Oriol Vinyals, Charles Blundell, Timothy Lillicrap, Koray Kavukcuoglu, and Daan Wierstra. Matching networks for one shot learning. In *Advances in Neural Information Processing Systems 29*. Curran Associates, Inc., 2016.

Michael Volpp, Fabian Flürenbrock, Lukas Grossberger, Christian Daniel, and Gerhard Neumann. Bayesian context aggregation for neural processes. In *International Conference on Learning Representations*, 2021. URL https://openreview.net/forum?id=ufZN2-aehFa.

V. Volterra. Variazioni e fluttuazioni del bumero d'ondividui in specie animali conviventi. *Memoria della Reale Accademia Nazionale dei Lincei*, 2:31–113, 1926.

Zhilin Yang, Zihang Dai, Yiming Yang, Jaime Carbonell, Russ R Salakhutdinov, and Quoc V Le. Xlnet: Generalized autoregressive pretraining for language understanding. *Advances in neural information processing systems*, 32, 2019.

Han Zhang, Ian Goodfellow, Dimitris Metaxas, and Augustus Odena. Self-attention generative adversarial networks. In *International conference on machine learning*, pp. 7354–7363. PMLR, 2019.

X. L. Zhang, H. Begleiter, B. Porjesz, W. Wang, and A. Litke. Event related potentials during object recognition tasks. *Brain Research Bulletin*, 38(6):531–538, 1995a.

Xiao Lei Zhang, Henri Begleiter, Bernice Porjesz, Wenyu Wang, and Ann Litke. Event related potentials during object recognition tasks. *Brain research bulletin*, 38(6):531–538, 1995b.

A PROOF OF PROPOSITION 2.1

Additional notation. If $\mathbf{y}_1 \oplus \mathbf{y}_2 \sim P_{\mathbf{x}_1 \oplus \mathbf{x}_2}\pi(D)$, then denote the distribution of $\mathbf{y}_1 \,|\, \mathbf{y}_2$ by $P_{\mathbf{x}_1 \,|\, \mathbf{x}_2}\pi(D)$. Note that $P_{\mathbf{x}_1 \,|\, \mathbf{x}_2}\pi(D)$ depends on $\mathbf{y}_2$, because it is the distribution of $\mathbf{y}_1 \,|\, \mathbf{y}_2$, even though the notation does not make this dependence explicit.

The "appropriate regularity conditions". Let $\mathcal{P}_\lambda^N$ be the collection of distributions on $\mathbb{R}^N$ that (a) have a density with respect to the Lebesgue measure and (b) have a covariance matrix which is strictly positive definite. Let $\mathcal{P}_{\lambda,\mathrm{G}}^N \subseteq \mathcal{P}_\lambda^N$ be the subcollection of distributions which are Gaussian. Then, by Corollary B.1 by Bruinsma et al. (2021), for all $\mu \in \mathcal{P}_\lambda^N$ such that $\inf_{\nu \in \mathcal{P}_{\lambda,\mathrm{G}}^N} \mathrm{KL}(\mu, \nu) < \infty$,

$$\arg\min_{\nu \in \mathcal{P}_{\lambda,\mathrm{G}}^N} \mathrm{KL}(\mu, \nu) = \mathcal{N}(\mu) \tag{10}$$

where $\mathcal{N}(\mu)$ denotes the Gaussian distribution with mean vector and covariance matrix equal to those of μ.

In the proposition, by appropriate regularity conditions on y, we mean the assumption that, for all inputs $\mathbf{x}$ and $D \in \mathcal{D}$, $P_{\mathbf{x}}\pi_y(D)$ is in $\mathcal{P}_\lambda^{|\mathbf{x}|}$ and such that $\inf_{\nu \in \mathcal{P}_{\lambda,\mathrm{G}}^{|\mathbf{x}|}} \mathrm{KL}(P_{\mathbf{x}}\pi_y(D), \nu) < \infty$.

Assume the appropriate regularity conditions on y. We now list three technical observations.

(1) Note that $P_{\mathbf{x}_1 \,|\, \mathbf{x}_2}\pi_y(D)$ is the distribution of $y(\mathbf{x}_1) \,|\, D, (\mathbf{x}_2, \mathbf{y}_2)$, so we have the identity $P_{\mathbf{x}_1 \,|\, \mathbf{x}_2}\pi_y(D) = P_{\mathbf{x}_1}\pi_y(D \oplus (\mathbf{x}_2, \mathbf{y}_2))$. Therefore, for all inputs $\mathbf{x}_1$, inputs $\mathbf{x}_2$, and $D \in \mathcal{D}$, $P_{\mathbf{x}_1 \,|\, \mathbf{x}_2}\pi_y(D)$ is in $\mathcal{P}_\lambda^{|\mathbf{x}_1|}$ and such that $\inf_\nu \mathrm{KL}(P_{\mathbf{x}_1 \,|\, \mathbf{x}_2}\pi_y(D), \nu) < \infty$.

(2) The ideal CNP π_{C} matches the means and marginal variances of the true posterior predictives (Section 2). Hence, for all $x \in \mathcal{X}$ and $D \in \mathcal{D}$, $P_x\pi_{\mathrm{C}}(D)$ is in $\mathcal{P}_{\lambda,\mathrm{G}}^1$.

(3) The ideal GNP π_{G} matches the mean vectors and covariance matrices of the true posterior predictives (Section 2). Hence, for all inputs $\mathbf{x}$ and $D \in \mathcal{D}$, $P_{\mathbf{x}}\pi_{\mathrm{G}}(D)$ is in $\mathcal{P}_{\lambda,\mathrm{G}}^{|\mathbf{x}|}$; which means that, for all $x_1 \in \mathcal{X}$, inputs $\mathbf{x}_2$, and $D \in \mathcal{D}$, $P_{x_1 \,|\, \mathbf{x}_2}\pi_{\mathrm{G}}(D)$ is in $\mathcal{P}_{\lambda,\mathrm{G}}^1$.

In the proof, to apply and use (10), we implicitly use these observations.

Proposition 2.1 (Advantage of AR CNPs over GNPs)**.** Assume appropriate regularity conditions on y. Let π_{C} be the ideal CNP and let π_{G} be the ideal GNP. Then, for all inputs $\mathbf{x}$ and data sets $D \in \mathcal{D}$,

$$\mathrm{KL}(P_{\mathbf{x}}\pi_y(D), \mathrm{AR}_{\mathbf{x}}(\pi_{\mathrm{C}}, D)) \leq \mathrm{KL}(P_{\mathbf{x}}\pi_y(D), P_{\mathbf{x}}\pi_{\mathrm{G}}(D)). \tag{7}$$

Proof of Proposition 2.1. Let $\mathbf{x}$ be some inputs and let $D \in \mathcal{D}$ be some data set. We will argue that, for all $n = 1, \ldots, |\mathbf{x}|$,

$$\begin{aligned} &\mathrm{KL}(P_{x_n \,|\, \mathbf{x}_{1:(n-1)}}\pi_y(D), P_{x_n}\pi_{\mathrm{C}}(D \oplus (\mathbf{x}_{1:(n-1)}, \mathbf{y}_{1:(n-1)}))) \\ &\qquad \leq \mathrm{KL}(P_{x_n \,|\, \mathbf{x}_{1:(n-1)}}\pi_y(D), P_{x_n \,|\, \mathbf{x}_{1:(n-1)}}\pi_{\mathrm{G}}(D)). \end{aligned} \tag{11}$$

Assuming this inequality, the result follows directly from the chain rule for the KL divergence in combination with the definition of $\mathrm{AR}_{\mathbf{x}}$ (Procedure 2.1):

$$\begin{aligned} &\mathrm{KL}(P_{\mathbf{x}}\pi_y(D), \mathrm{AR}_{\mathbf{x}}(\pi_{\mathrm{C}}, D)) \\ &\quad = \textstyle\sum_{n=1}^{|\mathbf{x}|} \mathbb{E}_{\mathbf{y}_{1:(n-1)}}[\mathrm{KL}(P_{x_n \,|\, \mathbf{x}_{1:(n-1)}}\pi_y(D), P_{x_n}\pi_{\mathrm{C}}(D \oplus (\mathbf{x}_{1:(n-1)}, \mathbf{y}_{1:(n-1)})))] && (12) \\ &\quad \leq \textstyle\sum_{n=1}^{|\mathbf{x}|} \mathbb{E}_{\mathbf{y}_{1:(n-1)}}[\mathrm{KL}(P_{x_n \,|\, \mathbf{x}_{1:(n-1)}}\pi_y(D), P_{x_n \,|\, \mathbf{x}_{1:(n-1)}}\pi_{\mathrm{G}}(D))] && (13) \\ &\quad = \mathrm{KL}(P_{\mathbf{x}}\pi_y(D), P_{\mathbf{x}}\pi_{\mathrm{G}}(D)) && (14) \end{aligned}$$

where the expectations are over $\mathbf{y}_{1:(n-1)} \sim P_{\mathbf{x}_{1:(n-1)}}\pi_y(D)$. To prove the inequality, note that, conditional on $\mathbf{y}_{1:(n-1)}$, using (10),

$$\arg\min_{\nu \in \mathcal{P}_{\lambda,\mathrm{G}}^1} \mathrm{KL}(P_{x_n \,|\, \mathbf{x}_{1:(n-1)}}\pi_y(D), \nu) = \mathcal{N}(P_{x_n \,|\, \mathbf{x}_{1:(n-1)}}\pi_y(D)). \tag{15}$$

By the property of π_{C} that it matches the mean and marginal variance of the true posterior (Section 2),

$$\begin{aligned} \mathcal{N}(P_{x_n \,|\, \mathbf{x}_{1:(n-1)}}\pi_y(D)) &= \mathcal{N}(P_{x_n}\pi_y(D \oplus (\mathbf{x}_{1:(n-1)}, \mathbf{y}_{1:(n-1)}))) && (16) \\ &= P_{x_n}\pi_{\mathrm{C}}(D \oplus (\mathbf{x}_{1:(n-1)}, \mathbf{y}_{1:(n-1)})). && (17) \end{aligned}$$

Therefore,

$$\operatorname*{arg\,min}_{\nu \in \mathcal{P}_{\lambda,\mathrm{G}}^1} \mathrm{KL}(P_{x_n \,|\, \mathbf{x}_{1:(n-1)}}\pi_y(D), \nu) = P_{x_n}\pi_{\mathrm{C}}(D \oplus (\mathbf{x}_{1:(n-1)}, \mathbf{y}_{1:(n-1)})). \tag{18}$$

Noting that $P_{x_n \,|\, \mathbf{x}_{1:(n-1)}}\pi_{\mathrm{G}}(D) \in \mathcal{P}_{\lambda,\mathrm{G}}^1$, we obtain the desired inequality. □

B PROOF OF PROPOSITION 2.2

Proposition 2.2 (Recovery of smooth samples)**.** Let $\mathcal{X} \subseteq \mathbb{R}$ be compact, and let f be a stochastic process with surely continuous sample paths and $\sup_{x\in\mathcal{X}} \|f(x)\|_{L^2} < \infty$. Let $(\varepsilon_n)_{n\geq 0}$ be i.i.d. (potentially non-Gaussian) random variables such that $\mathbb{E}[\varepsilon_0] = 0$ and $\mathbb{V}[\varepsilon_0] < \infty$. Consider any sequence $(x_n)_{n\geq 1} \subseteq \mathcal{X}$, and let $x^* \in \mathcal{X}$ be a limit point of $(x_n)_{n\geq 1}$. If $y(x^*) = f(x^*) + \varepsilon_0$ and $y_n = f(x_n) + \varepsilon_n$ are noisy observations of f, then

$$\lim_{n\to\infty} \mathbb{E}[y(x^*) \,|\, y_1, \ldots, y_n] = f(x^*) \quad \text{almost surely.} \tag{8}$$

Proof of Proposition 2.2. Consider the increasing filtration $\mathcal{F}_n = \sigma(y_1, \ldots, y_n)$ with limit $\mathcal{F}_\infty = \sigma(\bigcup_{n=1}^\infty \mathcal{F}_n)$. Also let $\mathcal{T}_n = \sigma(\varepsilon_{n+1}, \varepsilon_{n+2}, \ldots)$ and consider the tail σ-algebra $\mathcal{T} = \bigcap_{n=1}^\infty \mathcal{T}_n$. Let $(x_{n_i})_{i=1}^\infty$ be a subsequence of $(x_n)_{n=1}^\infty$ such that $x_{n_i} \to x^*$. Let $g_n = \frac{1}{n}\sum_{i=1}^n y_i$. Since g_n is a function of $y_1, \ldots, y_n$, it is $\mathcal{F}_n$–measurable and therefore $\mathcal{F}_\infty$–measurable. Note that

$$g_n = \frac{1}{n}\sum_{i=1}^n f(x_{n_i}) + \frac{1}{n}\sum_{i=1}^n \varepsilon_i. \tag{19}$$

By sure continuity of f, the first term converges to $f(x^*)$ surely. By the strong law of large numbers (Example 5.6.1; Durrett, 2010), the second term converges to zero on a tail event $A \in \mathcal{T}$ of probability one. We conclude that $\mathbb{1}_A f(x^*)$ is $\sigma(\mathcal{F}_\infty, \mathcal{T})$–measurable. Therefore, by almost sure convergence of L^2–bounded martingales (Theorem 5.4.5; Durrett, 2010),

$$\begin{aligned}
\lim_{n\to\infty} \mathbb{E}[y(x^*) \,|\, y_1, \ldots, y_n] &= \lim_{n\to\infty} \mathbb{E}[f(x^*) \,|\, y_1, \ldots, y_n] && (\mathbb{E}[\varepsilon_0] = 0) && (20)\\
&= \lim_{n\to\infty} \mathbb{E}[f(x^*) \,|\, \mathcal{F}_n] && (\text{definition of } \mathcal{F}_n) && (21)\\
&= \lim_{n\to\infty} \mathbb{E}[f(x^*) \,|\, \mathcal{F}_n, \mathcal{T}] && (\sigma(f(x^*), \mathcal{F}_n) \perp \mathcal{T}) && (22)\\
&= \lim_{n\to\infty} \mathbb{E}[\mathbb{1}_A f(x^*) \,|\, \mathcal{F}_n, \mathcal{T}] && (\mathbb{P}(A) = 1) && (23)\\
&= \mathbb{E}[\mathbb{1}_A f(x^*) \,|\, \mathcal{F}_\infty, \mathcal{T}] && (L^2\text{–mart. convergence}) && (24)\\
&= \mathbb{1}_A f(x^*) && (\mathbb{1}_A f(x^*) \in \sigma(\mathcal{F}_\infty, \mathcal{T})) && (25)\\
&= f(x^*), && (\mathbb{P}(A) = 1) && (26)
\end{aligned}$$

where all equalities hold almost surely. □

C ILLUSTRATION OF THE AR PROCEDURE

Figure 7 depicts the AR sampling procedure (Procedure 2.1) and procedure to produce smooth samples (Proposition 2.2) using the ConvCNP trained on the EQ data process from Section 4.1.

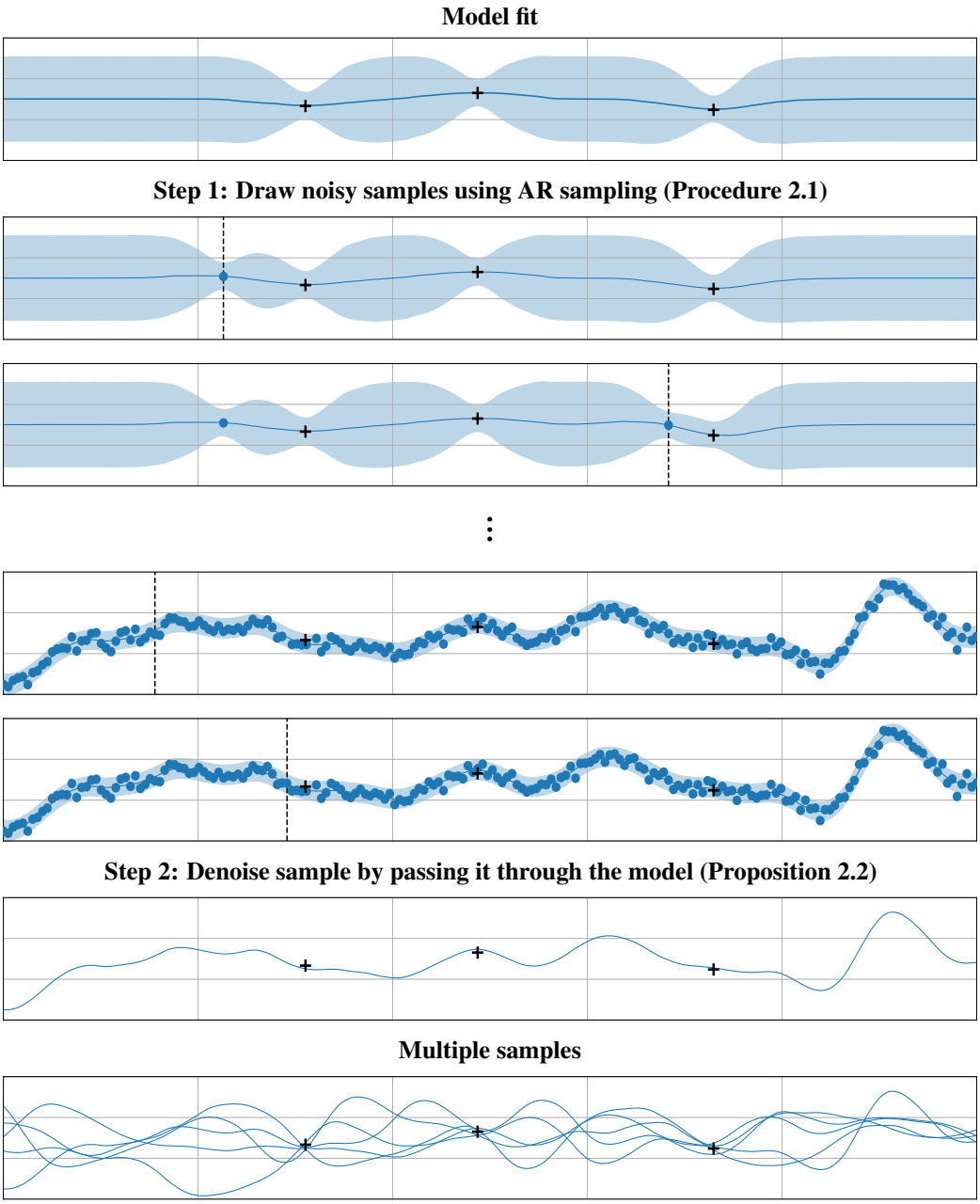

Figure 7: Illustration of the AR procedure with a random AR ordering and the de-noising step (Procedure 2.1 and Proposition 2.2), to produce smooth samples. Given a context set (black crosses), we can use the CNP to get marginal predictions at arbitrary input locations (first figure). We choose a randomly sampled input location, draw a corresponding output sample from the model's predictive (blue dot in the second plot), append this to the context set, and pass the augmented context set through the model again. We repeat this step a number of times (third and fourth figures), until all function (epistemic) uncertainty has been removed and all that remains is irreducible noise (aleatoric) uncertainty (fifth figure). This procedure yields noisy function samples (blue dots in the sixth plot), which we pass one last time through the model to obtained a denoised sample, treating the mean prediction as an approximate noiseless sample (seventh figure). Repeating this procedure yields high-quality samples from the model predictive (eighth figure).

D Number and Order of Target Points

When deploying a conditional neural process (CNP) autoregressively (AR; Procedure 2.1), the number and ordering of the target points matters. In this appendix, we describe our observations of the effects of the number and ordering of the target points on the quality of the predictions. In short, our recommendation is to choose a different random ordering for every sample, and to not let the number/density of target points exceed that at training time.

D.1 Effects of the Number of Target Points

During the AR sampling procedure, the AR CNP is evaluated at context sets of increasing size. Our experience is that, as long as the sizes of these context sets do not exceed the sizes seen at training time, the predictions should not be significantly affected by changes in the number of target points. However, if the AR sampling procedure evaluates the model at context sets of larger sizes than seen during training time, then that presents the model with an out-of-distribution situation. What happens then comes down to how well the neural networks generalise. Our experience is that the predictions quickly start to break down.

A notable exception of this rule of thumb are convolutional-deep-set–based models, such as the Convolutional Conditional Neural Process (ConvCNP; Gordon et al., 2020). For these models, the *magnitude of the density channel* is what determines whether the models generalises or not. This means that it is not the total number of points that matters, but rather the *density* of the points. Therefore, the AR ConvCNP can be evaluated at arbitrarily many target points, as long as the density of these points does not significantly exceed the density of context points seen at training time. Once the density exceeds the density of the training data, the model is presented with an out-of-distribution situation, and what happens then again comes down to how well neural networks generalise.

Figure Appendix D.1 illustrates this observation. When the density target points does not exceed the training data (50 and 100 points), the predictions look calibrated. However, once the density of target points comes close or exceed the training data (200, 500, and 1000 points), bias starts to creep into the predictions.

Although the number/density of points in the AR sampling procedure should not exceed that at training time, AR CNPs can still produce high-quality samples at arbitrarily many target points by following the trick outlined at the end of the two-step procedure below Proposition 2.2.

D.2 Effects of the Ordering of Target Points

Our experience is that, as long as the number of target points (or density) does not exceed that at training time, the ordering of the target point does not really matter. Appendix D.1 also demonstrates this. When the density of the target points does not exceed the training data (50 and 100 points), sampling randomly or left to right does not really matter. However, once the density of the target points comes close to or exceeds the training data (200, 500, and 1000 points), we observe a difference in performance between sampling randomly and sampling left to right. Across all numbers of target points, a random ordering seems to perform most robustly. Our recommendation is therefore to choose a different random ordering of the target points for every sample.

D.3 Analysis of AR CNPs for CNPs with Gaussian Marginals

In this subsection, we argue that, for CNPs with Gaussian marginals, predictions in the first few AR steps might be poor, but predictions in later AR steps tend to be more accurate. Choosing a different random ordering for every sample therefore "averages out" the effects from these first few AR steps.

When evaluating a CNP with Gaussian marginals in AR mode, every conditional prediction in the AR process is Gaussian. Let us consider the process of producing an AR sample. For the first target input x_1, we run the CNP forward to obtain a distribution for the corresponding target output y_1. In reality, the true posterior most likely is non-Gaussian, which means that the prediction for the first target point may be poor. Nevertheless, we sample this Gaussian, append the sample (x_1, y_1) to the context set, and run the CNP forward again. Because we now feed the earlier sample y_1 through the non-linear network, the marginal predictive for the next target output y_2 (having integrated out y_1)

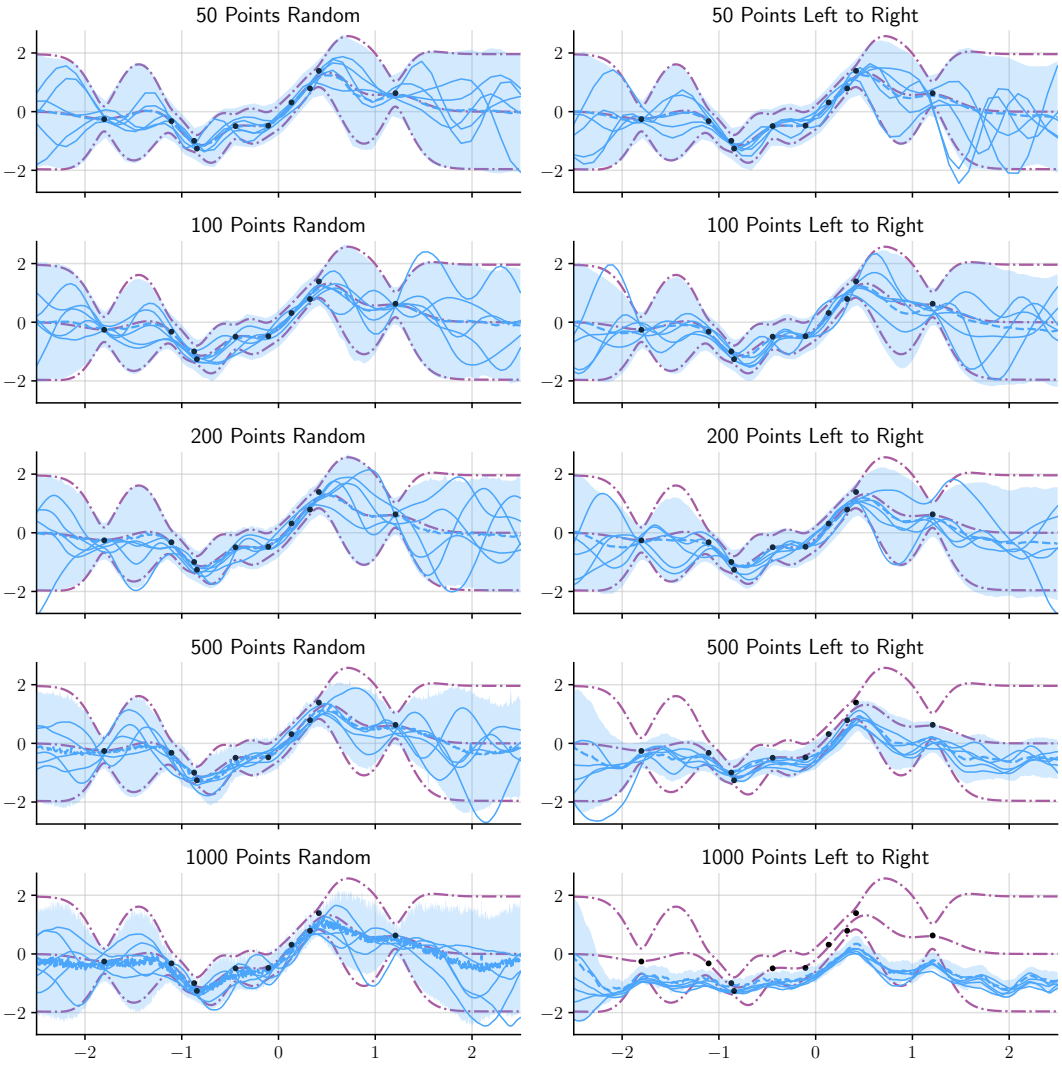

Figure 8: Samples and predictions for an AR ConvCNP with various numbers of target points ordered randomly (*left column*) and ordered left to right (*right column*). When the density of the target points does not exceed the training data (50 and 100 points), ordering the target points randomly or left to right does not matter. When the density of the target points comes close to the training data or exceeds it (200, 500, and 1000 points), bias creeps into the predictions. The random ordering appears to perform more robustly than left to right. The data is sampled from the EQ data process from the synthetic experiments (Section 4.1), and the trained model is also taken from the synthetic experiments. The predictions by the model are shown in solid blue and the marginals by the ground-truth EQ process are shown in dot-dashed purple.

is non-Gaussian. As we perform more AR steps, the marginal predictions of later points become increasingly non-Gaussian, increasing the model's flexibility.

We see that, for a given ordering of the target inputs, the prediction for the first target input is likely poor (because it is Gaussian), and (in the best case) the predictions become more and more accurate as we take more AR steps (because they become more and more non-Gaussian). This is exactly what is happening in Figure 3: the left prediction is Gaussian and therefore a poor approximation, and, as we go to the right and take more and more AR steps, the prediction becomes more and more non-Gaussian and therefore more accurate. If we were to feed the target inputs in right to left, then the same phenomenon would happen. The right prediction would be a Gaussian and a very poor

approximation, and, as we go to the left and take more AR steps, the prediction would become more non-Gaussian and therefore more accurate.

More generally, for a given ordering of the target points, the ordering will produce high quality predictions if the conditional distributions of the AR factorisation match the corresponding conditional distributions of the true posterior. Since the conditionals of the AR CNP are typically Gaussian by design, this means that the ordering is "good" if the corresponding conditionals of the true posterior are close to Gaussian.

So when is a conditional of the posterior close to Gaussian? Let us assume that the true underlying process is a sum of a non-Gaussian process (constituting epistemic uncertainty) and independent Gaussian noise (constituting aleatoric uncertainty). Generally, a conditional will have both epistemic and aleatoric uncertainty, so a Gaussian will be a bad fit. *However*, as we condition the conditionals of the true generative process on more and more data, the underlying function will be pinned down more and more accurately, meaning that the conditional will consist mostly of aleatoric uncertainty, which is Gaussian. Therefore, as we condition on more and more data, we expect the conditionals to become more and more Gaussian. This again suggests that the samples in the first few AR steps might be a poor fit (because the corresponding conditionals of the true posterior are not yet Gaussian), but that samples in later AR steps should be a better fit (because the corresponding conditionals are then close to Gaussian).

To summarise, an ordering of the target points is "good" if the corresponding conditionals of the true posterior are also close to Gaussian. Under the assumption that the ground-truth process is a non-Gaussian process with additive Gaussian noise, conditionals tend to be close to Gaussian if they are conditioned on many data points. As a consequence, the earlier conditionals in the AR factorisation tend to be poor fits to the ground-truth posterior, whereas later conditionals tend to produce better fits. Choosing a different random ordering for every sample therefore "averages out" the effects from the first few AR steps.

E DETAILS FOR FIGURE 3

The generative process visualised in the top panel of figure 3 is defined by the following mixture distribution:

$$p_{\text{true}}(y \mid x) = a_1 \cdot \mathcal{N}(f_1(x), 1) + a_2 \cdot \mathcal{N}(f_2(x), 1) + a_3 \cdot \mathcal{N}(f_3(x), 1). \tag{27}$$

Given this mixture distribution, the (Gaussian) ideal CNP can be computed in closed form by computing the first two moments of p_{true}:

$$p_{\text{CNP}}(y \mid x) = \mathcal{N}(\mu(x), \sigma(x)^2) \tag{28}$$

where

$$\mu(x) = \sum_{i=1}^{3} a_i f_i(x) \tag{29}$$

$$\sigma(x)^2 = \sum_{i=1}^{3} a_i \left(1 + f_i(x)^2\right) - \left(\sum_{i=1}^{3} a_i f_i(x)\right)^2. \tag{30}$$

The updated mixture weights for the posterior distribution $p_{\text{true}}(y \mid x, D^{(c)})$ given a context set $D^{(c)}$ can be computed via Bayes rule and $p_{\text{CNP}}(y \mid x, D^{(c)})$ can be computed given the updated mixture weights. Note that in figure 3 the prior mixture weights are $a_1 = a_3 = 0.25$ and $a_2 = 0.5$, means are given by

$$f_1(x) = x^2 + 1, \tag{31}$$

$$f_2(x) = x, \tag{32}$$

$$f_3(x) = -x, \tag{33}$$

and the target locations are $x = 1, 2, 4$, and 6. The bottom four panels of figure 3 show squared exponential kernel density estimates of 30 000 samples drawn from the generative distribution $p_{\text{true}}(y_1, y_2, y_4, y_6)$, the ideal CNP $p_{\text{CNP}}(y_1, y_2, y_4, y_6)$, and the ideal CNP applied in AR mode from left to right

$$p_{\text{AR CNP}}(y_1, y_2, y_4, y_6) = p_{\text{CNP}}(y_1) \cdot p_{\text{CNP}}(y_2 \mid y_1) \cdot p_{\text{CNP}}(y_4 \mid y_1, y_2) \cdot p_{\text{CNP}}(y_6 \mid y_1, y_2, y_4). \tag{34}$$

F Description of Models

The architectures follow the descriptions from the respective papers they are introduced. Although these descriptions are for one-dimensional inputs and outputs, the architectures are readily generalised to multidimensional inputs and outputs; we will explicitly mention wherever that generalisation requires extra care. All architectures use ReLU activation functions. All GNPs, in addition to a covariance matrix over the target points, also output heterogeneous observation noise along the marginal means; the total covariance over the target points is thus the sum of the covariance by the model and a diagonal matrix formed from these observation noises.

Conditional neural process (CNP; Garnelo et al., 2018a). Set the dimensionality of the encoding to $K = 256$. Parametrise the encoder with a three-hidden-layer multi-layer perceptron (MLP) of width 256; and parametrise the decoder with a six-hidden-layer MLP of width 256. For multidimensional outputs, let the decoder have width 512. For multidimensional outputs where outputs can have context points at different inputs, produce a separate encoding for every output and concatenate these into one big encoding. These encoders may or may not share parameters. In our experiments, for two-dimensional outputs, parametrise separate encoders; for higher-dimensional outputs, apply the same encoder.

Gaussian neural process (GNP; Markou et al., 2022). Use the same choices for K, the encoder, and the decoder as the CNP. Set the rank of the kernel map to $R = 64$. As mentioned in the introduction, let the decoder produce one extra dimension which forms heterogeneous observation noise. For multidimensional outputs, the same caveats as for the CNP apply.

Latent neural process (LNP; Garnelo et al., 2018b). The LNP builds off the CNP. Call the existing encoder the *deterministic encoder*. The NP adds one more encoder called the *stochastic encoder*. The stochastic encoder mimics the deterministic encoder, but outputs a K-dimensional vector of means and a K-dimensional vector of marginal variances. These are used to sample a K-dimensional Gaussian latent variable (the *stochastic encoding*). The decoder now additionally takes in the stochastic encoding. For multidimensional outputs, the same caveats as for the CNP apply.

Attentive conditional neural process (ACNP; Kim et al., 2019). The ACNP builds off the CNP. It replaces the deterministic encoder $\mathrm{enc}_\theta \colon \mathcal{D} \to \mathbb{R}^K$ with an eight-head attentive encoder $\mathrm{enc}_\theta^{(\mathrm{att})} \colon \mathcal{D} \times \mathcal{X} \to \mathbb{R}^K$ (Vaswani et al., 2017). Unlike the original deterministic encoder enc_θ, the new attentive encoder $\mathrm{enc}_\theta^{(\mathrm{att})}$ also takes in the target input. Let $D^{(\mathrm{c})} = (\mathbf{x}^{(\mathrm{c})}, \mathbf{y}^{(\mathrm{c})}) \in \mathcal{D}$ be a context set of size N and let $x^{(\mathrm{t})} \in \mathcal{X}$ be a target input. We now descibe the computation of $\mathrm{enc}_\theta^{(\mathrm{att})}(D^{(\mathrm{c})}, x^{(\mathrm{t})})$. Parametrise $\phi_x \colon \mathcal{X} \to (\mathbb{R}^{32})^8$ and $\phi_{xy} \colon \mathcal{X} \times \mathcal{Y} \to (\mathbb{R}^{32})^8$ both with three-hidden-layer MLPs of width 256. Compute

$$\text{the } \textit{keys}\text{:} \quad (\mathbf{k}_{h,n})_{h=1}^8 = \phi_x(x_n^{(\mathrm{c})}) \qquad \text{for } n = 1, \ldots, N, \tag{35}$$

$$\text{the } \textit{values}\text{:} \quad (\mathbf{v}_{h,n})_{h=1}^8 = \phi_{xy}(x_n^{(\mathrm{c})}, y_n^{(\mathrm{c})}) \quad \text{for } n = 1, \ldots, N, \tag{36}$$

$$\text{the } \textit{query}\text{:} \quad (\mathbf{q}_h)_{h=1}^8 = \phi_x(x^{(\mathrm{t})}). \tag{37}$$

Then compute

$$\mathbf{v}_h^{(\mathrm{q})} = \sum_{n=1}^N \frac{e^{\langle \mathbf{q}_h, \mathbf{k}_{h,n} \rangle}}{\sum_{n'=1}^N e^{\langle \mathbf{q}_h, \mathbf{k}_{h,n'} \rangle}} \mathbf{v}_{h,n} \in \mathbb{R}^{256} \tag{38}$$

Concatenate $\mathbf{v}^{(\mathrm{q})} = (\mathbf{v}_1^{(\mathrm{q})}, \ldots, \mathbf{v}_8^{(\mathrm{q})}) \in \mathbb{R}^{256}$ and $\mathbf{q} = (\mathbf{q}_1, \ldots, \mathbf{q}_8) \in \mathbb{R}^{256}$. Let $\mathbf{L} \colon \mathbb{R}^{256} \to \mathbb{R}^{256}$ be a linear layer; let $\phi^{(\mathrm{res})} \colon \mathbb{R}^{256} \to \mathbb{R}^{256}$ be a one-hidden-layer MLP of width 256; and let norm_1 and norm_2 be two layer normalisation layers with learned pointwise transformations (Ba et al., 2016). Then

$$\mathrm{enc}_\theta^{(\mathrm{att})}(D^{(\mathrm{c})}, x^{(\mathrm{t})}) = \mathrm{norm}_2(\mathbf{z} + \phi^{(\mathrm{res})}(\mathbf{z})) \quad \text{where} \quad \mathbf{z} = \mathrm{norm}_1(\mathbf{v}^{(\mathrm{q})} + \mathbf{L}\mathbf{q}). \tag{39}$$

For multidimensional outputs, the same caveats as for the CNP apply.

Attentive Gaussian neural process (AGNP). The AGNP build off the GNP. It replaces the deterministic encoder with the same eight-head attentive deterministic encoder of the ACNP.

Attentive neural process (ALNP; Kim et al., 2019). The ALNP build off the LNP. It replaces the deterministic encoder with the same eight-head attentive deterministic encoder of the ACNP.

Convolutional Conditional Neural Process (ConvCNP; Gordon et al., 2020). Set the discretisation to an evenly spaced grid at a certain density (the *points per unit*) spanning a bit more (the *margin*) than the most extremal context and target inputs. The points per unit and margin are specified separately for every experiment. Initialise the length scales of all Gaussian kernels to twice the interpoint spacing of the discretisation. Divide the data channel by the density channel. Parametrise dec_θ with a U-Net (Ronneberger et al., 2015). Before the U-turn, let the U-Net have six convolutional layers with kernel size five, stride two, and 64 output channels; and six more such layers, but using transposed convolutions, after the U-turn. The layers after the U-turn additionally take in the outputs of the layers before the U-turn in reversed order; this is the U-net structure (Figure 1; Ronneberger et al., 2015). For multidimensional outputs where outputs can have context points at different inputs, produce a separate data and density channel for every output and concatenate these into one big encoding; use separate length scales for every application of enc_θ.

Convolutional Gaussian neural process (ConvGNP; Markou et al., 2022). Use the same choices for the discretisation, length scales, and CNN architecture as for the ConvCNP. Set the rank of the kernel map to $R = 64$. As mentioned in the introduction, let the decoder produce one extra channel which forms heterogeneous observation noise. For multidimensional outputs, the same caveat as for the ConvCNP applies.

Fully convolutional Gaussian neural process (FullConvGNP; Bruinsma et al., 2021). For the mean architecture and the kernel architecture, use the same choices for the discretisation, length scales, and CNN architecture as for the ConvCNP. Implement the source channel with the identity matrix and apply the matrix transform $\mathbf{Z} \mapsto \mathbf{Z}\mathbf{Z}^\intercal$ to ensure positive definiteness. Let the decoder produce one extra channel which forms heterogeneous observation noise. For multidimensional outputs, in addition to the caveat for the ConvCNP, two additional caveats apply. First, for D_{o}-dimensional outputs, let the decoder produce D_{o}^2 channels rather than just one. These channels should be interpreted as all covariance and cross-covariance matrices between all outputs. Second, when applying the matrix transform $\mathbf{Z} \mapsto \mathbf{Z}\mathbf{Z}^\intercal$, these channels should first be assembled into one total covariance matrix.

Convolutional latent neural process (ConvLNP; Foong et al., 2020). The ConvLNP builds off the ConvCNP. The ConvLNP replaces the CNN architecture by two copies of this architecture placed in sequence. In between the two architectures, there is a sampling step: the first architecture outputs 32 channels, comprising 16 means and 16 marginal variances, which are used to sample a 16-dimensional Gaussian latent variable; and the second architecture then takes in this sample.

Autoregressive Conditional Neural Processes (AR CNPs). The AR CNP, AR ACNP, and AR ConvCNP use the architectures described above. Rolling out an AR CNP according to Procedure 2.1 requires an ordering of the target points. In all experiments, we choose a random ordering of the target points.

G Training, Cross-Validation, and Evaluation Protocols

The following description applies to the synthetic experiments (Section 4.1), the predator–prey experiments (Section 4.2), the EEG experiments (Section 4.3), and the environmental downscaling experiments (Section 4.4). For the environmental data assimilation experiments, a different protocol was used; we refer the reader to Appendix K for full details of the environmental data assimilation experiments.

A *task* consists of a context set and target set. How precisely the context and target sets are generated is specific to an experiment. To train a model, we consider batches of 16 tasks at a time, compute an objective function value, and update the model parameters using ADAM (Kingma & Ba, 2015). The learning rate is specified separately for every experiment. We define an epoch to consist of $2^{14} \approx 16\,\mathrm{k}$ tasks. We typically train a model for between 100 and 1000 epochs.

For an experiment, we split up the meta–data set into a *training set*, a *cross-validation set*, and an *evaluation set*. The model is trained on the training set. During training, after every epoch, the model is cross-validated on the cross-validation set. Cross-validation uses 2^{12} fixed tasks. These 2^{12} are fixed, which means that cross-validation always happens with exactly the same data. The cross-validation objective is a confidence bound computed from the model objective. Suppose that model objective over all 2^{12} cross-validation tasks has empirical mean $\hat{\mu}$ and empirical variance $\hat{\sigma}^2$. If a higher model objective is better, then the cross-validation objective is given by $\hat{\mu} - 1.96 \cdot \hat{\sigma}/\sqrt{2^{12}}$. The model with the best cross-validation objective is selected and used for evaluation. Evaluation is performed with the evaluation set and also uses 2^{12} tasks.

Conditional neural processes and Gaussian neural processes are trained, cross-validated, and evaluated with the neural process ELBO objective proposed by Garnelo et al. (2018a). We normalise the terms in the neural process objective by the target set sizes. Latent-variable neural processes (LNPs) are trained, cross-validated, and evaluated with the ELBO objective proposed by Garnelo et al. (2018b) using five samples, also normalised by the target set size. When training LNPs with the ELBO objective, but not when cross-validating and evaluating, the context set is subsumed in the target set. Additionally, LNPs are trained, cross-validated, and evaluated with the ML objective proposed by Foong et al. (2020), again normalised by the target set size. When training and cross-validating LNPs with the ML objective, we use twenty samples; and when evaluating, we use 512 samples. For completeness, LNPs trained with the ELBO objective are also evaluated with the ML objective using 512 samples.

To stabilise the numerics for GNPs, we increase the regularisation of covariance matrices for one epoch. To encourage LNPs to fit, we fix the variance of the observation noise of the decoder to 10^{-4} for the first three epochs.

H Details of Synthetic Experiments

H.1 Description of Experiments

We synthetically generate data sets by randomly sampling from five different choices for the ground-truth stochastic process f. Let the inputs be d_x-dimensional. Then define the following stochastic processes:

EQ: a Gaussian process with an exponentiated quadratic (EQ) kernel:

$$f \sim \mathcal{GP}(0, \exp(-\tfrac{1}{2\ell^2}\|\mathbf{x}-\mathbf{x}'\|_2^2)) \tag{40}$$

where $\ell > 0$ is a length scale;

Matérn–$\frac{5}{2}$: a Gaussian process with a Matérn–$\frac{5}{2}$ kernel:

$$f \sim \mathcal{GP}(0, k(\tfrac{1}{\ell}\|\mathbf{x}-\mathbf{x}'\|_2)) \tag{41}$$

where $k(r) = (1 + \sqrt{5}r + \frac{5}{3}r^2)e^{-r}$ and $\ell > 0$ is a length scale;

weakly periodic: a Gaussian process with a weakly periodic kernel:

$$f \sim \mathcal{GP}(0, \exp(-\tfrac{1}{2\ell_\mathrm{d}^2}\|\mathbf{x}-\mathbf{x}'\|_2^2 - \tfrac{2}{\ell_\mathrm{p}^2}\|\sin(\tfrac{\pi}{p}(\mathbf{x}-\mathbf{x}'))\|_2^2)) \tag{42}$$

where $\ell_\mathrm{d} > 0$ is a length scale specifying how quickly the periodic pattern changes, $\ell_\mathrm{p} > 0$ a length scale of the periodic pattern, and $p > 0$ the period; and where the application of $\sin$ is elementwise;

sawtooth: a sawtooth process with a random frequency, direction, and phase:

$$f = \omega\langle \mathbf{x}, \mathbf{u}\rangle_2 + \phi \mod 1 \tag{43}$$

where $\omega \sim \mathrm{Unif}(\Omega)$ is the frequency of the sawtooth wave, $\mathbf{u} \sim \mathrm{Unif}(\{\mathbf{x} \in \mathbb{R}^{d_x} : \|\mathbf{x}\|_2 = 1\})$ the direction, and $\phi \sim \mathrm{Unif}([0, 1])$ the phase;

mixture: with equal probability, sample f from the EQ process, Matérn–$\frac{5}{2}$ process, weakly periodic process, or sawtooth process.

We will call these stochastic processes the *data processes*. The data processes are stochastic processes with d_x-dimensional inputs and one-dimensional outputs. We will turn them into processes with d_y-dimensional outputs according to the following procedure: sample from the one-dimensional-output prior d_y times; and, for these d_y samples, take d_y different linear combinations.

We choose the parameters of the data processes based on the input dimensionality d_x:

$$\ell = c \cdot \tfrac{1}{4}, \qquad \ell_\mathrm{d} = c \cdot \tfrac{1}{2}, \qquad \ell_\mathrm{s} = c, \qquad p = c \cdot \tfrac{1}{4}, \qquad \Omega = [c^{-1} \cdot 2, c^{-1} \cdot 4] \tag{44}$$

with $c = \sqrt{d_x}$. Scaling with the input dimensionality aims to roughly ensure that data with one-dimensional inputs and data with two-dimensional inputs are equally difficult. Figure 9 illustrates the sawtooth data process in all four configurations.

We will construct data sets by sampling inputs uniformly at random from $\mathcal{X} = [-2, 2]^{d_x}$ and then sampling outputs from one of the data processes. We will colloquially call $\mathcal{X}$ the *training range*. For the EQ, Matérn–$\frac{5}{2}$, and weakly periodic process, but not for the sawtooth process[6], we also add independent Gaussian noise with variance 0.05. The numbers of context and target points are as follows. For the EQ, Matérn–$\frac{5}{2}$, and weakly periodic process, the number of context points is chosen uniformly at random from $\{0, \ldots, 30 \cdot d_x\}$ and the number of targets points is fixed to $50 \cdot d_x$. For the sawtooth and mixture process, the number of context points is chosen uniformly at random from $\{0, \ldots, 30\}$ if $d_x = 1$ and $\{0, \ldots, 75 \cdot d_x\}$ otherwise; and the number of targets points is fixed to $100 \cdot d_x$. In the case of a multidimensional-output data process, we separately sample the number and positions of the context and target inputs for every output dimension.

For every data process and each of the four configurations, we evaluate every model in three different ways. First, we evaluate the model on data generated exactly like the training data. This task is called *interpolation* and abbreviated "int." in the tables of results. The interpolation task measures how well a model fits the data and is the primary measure of performance. Second, we evaluate the model on data with inputs sampled from $[2, 6]^{d_x}$. This task is called *out-of-input-distribution (OOID)*

[6] The sawtooth process is already challenging enough.

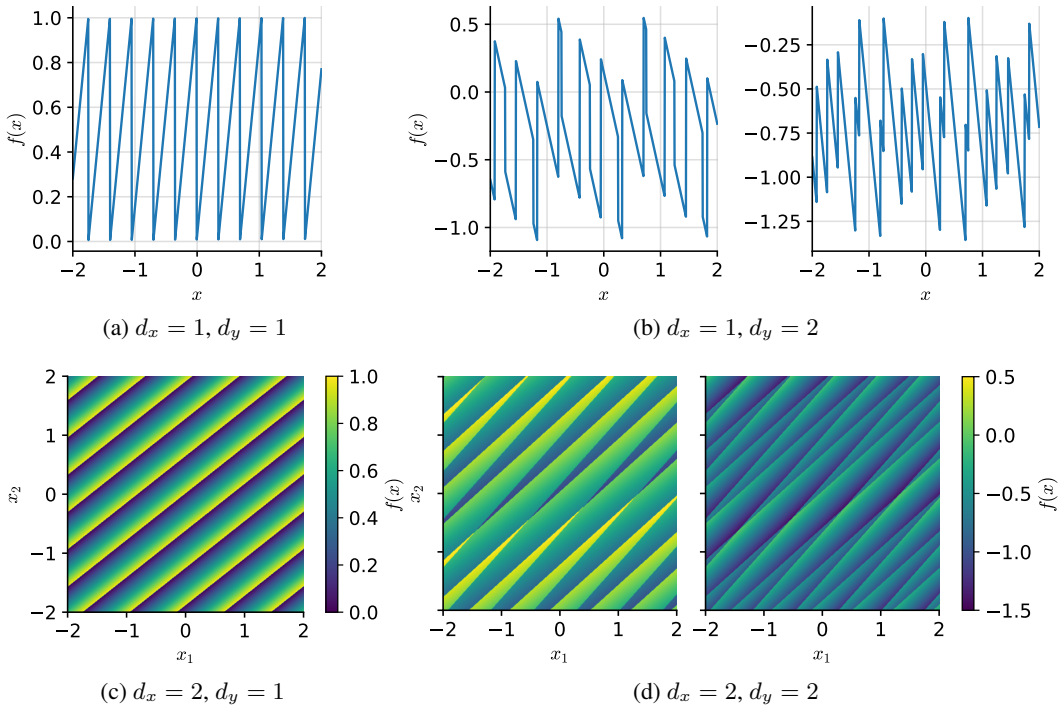

(a) $d_x = 1$, $d_y = 1$ (b) $d_x = 1$, $d_y = 2$

(c) $d_x = 2$, $d_y = 1$ (d) $d_x = 2$, $d_y = 2$

Figure 9: Samples from the sawtooth data process with one and two-dimensional inputs ($d_x = 1$ and $d_x = 2$) and one and two-dimensional outputs ($d_y = 1$ and $d_y = 2$)

interpolation and abbreviated "OOID" in the tables of results. OOID interpolation measures how well a model generalises to data sampled from other regions of the input space. Third, we evaluate the model on data with context inputs sampled from $[-2, 2]^{d_x}$ and target inputs sampled from $[2, 6]^{d_x}$. This task is called *extrapolation* and abbreviated "ext." in the tables of results. The extrapolation task measures how well predictions based on data in the training range generalise to other regions of the input space.

For this experiment, the learning rate is $3 \cdot 10^{-4}$, the margin is 0.1, and the points per unit is 64. We trained the models for 100 epochs. Due to an error in the cross-validation procedure, we did not use cross-validation, but used the model at epoch 100.

For the kernel architecture of the FullConvGNP, we reduce the points per unit and the number of channels in the U-Net by a factor two. For the ConvLNP with two-dimensional inputs, we reduce the number of outputs channels in the U-Net by a factor $\sqrt{2}$; and, for training and cross-validation, we reduce the number of samples of the ELBO objective to one and the number of samples for the ML objective to five.

H.2 Multi-Modality of Predictions by AR ConvCNP

Figure 10 demonstrates multi-modality of predictions by the AR ConvCNP trained on the sawtooth process. Note that the prediction is bimodal for one and two observations, and collapses to a single mode upon observing the third observation.

H.3 Full Results

We the show the full results for all data sets and tasks in Tables 7 to 18. The AR ConvCNP consistently shows very strong performance compared to other NP models. Note that the FullConvGNP takes much longer to train than the ConvCNP (Figure 2), and cannot be applied to tasks with 2-dimensional input spaces.

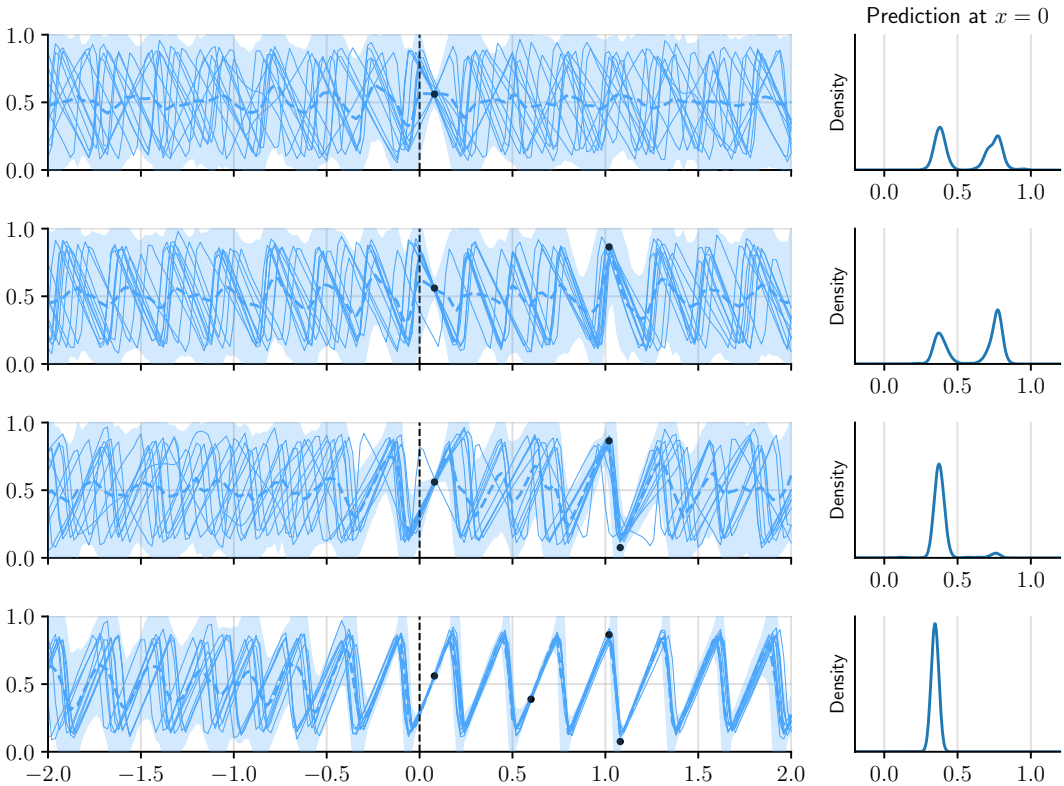

Figure 10: Multi-modality of predictions by the AR ConvCNP. Shows four observations sampled from the sawtooth process. In the four rows, these four observations are revealed one data point at a time. Every row also shows a kernel density estimate of the prediction at $x = 0$. Filled regions are central 95%-credible regions.

Table 7: For the Gaussian experiments, average Kullback–Leibler divergences of the posterior prediction map π_y with respect to the model normalised by the number of target points. Shows for one-dimensional inputs (1D; $d_x = 1$) and two-dimensional inputs (2D; $d_y = 2$) the performance for interpolation within the range $[-2, 2]^{d_x}$ where the models were trained ("Int."); interpolation within the range $[2, 6]^{d_x}$ which the models have never seen before ("OOID"); and extrapolation from the range $[-2, 2]^{d_x}$ to the range $[2, 6]^{d_x}$ ("Ext."). Models are ordered by interpolation performance for one-dimensional inputs. The latent variable models are trained and evaluated with the ELBO objective (E); trained and evaluated with the ML objective (M); and trained with the ELBO objective and evaluated with the ML objective (E–M). Diagonal GP refers to predictions by the ground-truth Gaussian processes without correlations. Trivial refers to predicting the empirical means and standard deviation of the test data. Errors indicate the central 95%-confidence interval. Numbers which are significantly best ($p < 0.05$) are boldfaced. Numbers which are very large are marked as failed with "F". Numbers which are missing could not be run.

Model	Int. (1D)	OOID (1D)	Ext. (1D)	Int. (2D)	OOID (2D)	Ext. (2D)
FullConvGNP	**0.01** ±0.00	**0.01** ±0.00	**0.00** ±0.00			
ConvCNP (AR)	0.03 ±0.00	0.03 ±0.00	0.02 ±0.00	**0.03** ±0.00	**0.03** ±0.00	**0.02** ±0.00
ConvGNP	0.04 ±0.00	0.04 ±0.00	1.75 ±0.12	0.12 ±0.00	0.12 ±0.00	0.71 ±0.03
AGNP	0.10 ±0.00	4.34 ±0.17	5.45 ±0.23	0.17 ±0.00	0.62 ±0.01	0.39 ±0.01
ConvLNP (E)	0.19 ±0.01	0.19 ±0.01	0.29 ±0.03	0.39 ±0.01	0.39 ±0.01	0.36 ±0.01
ACNP (AR)	0.24 ±0.01	1.08 ±0.02	0.86 ±0.01	0.13 ±0.00	0.57 ±0.01	0.40 ±0.01
GNP	0.25 ±0.01	F	F	0.25 ±0.01	0.75 ±0.01	0.57 ±0.00
ConvLNP (M)	0.31 ±0.01	0.31 ±0.01	0.64 ±0.01	0.28 ±0.01	0.28 ±0.01	0.36 ±0.01
Diagonal GP	0.42 ±0.02	0.42 ±0.02	0.84 ±0.01	0.29 ±0.01	0.29 ±0.01	0.40 ±0.01
ALNP (M)	0.43 ±0.01	1.03 ±0.02	0.78 ±0.01	0.31 ±0.01	0.55 ±0.01	0.39 ±0.01
ConvCNP	0.43 ±0.02	0.43 ±0.02	0.84 ±0.01	0.30 ±0.01	0.30 ±0.01	0.40 ±0.01
CNP (AR)	0.46 ±0.01	F	F	0.36 ±0.01	F	F
LNP (E)	0.51 ±0.01	F	4.34 ±0.76	0.40 ±0.01	3.03 ±1.68	0.60 ±0.01
LNP (E–M)	0.52 ±0.02	F	2.39 ±0.33	0.39 ±0.01	2.35 ±1.06	0.57 ±0.01
ALNP (E–M)	0.53 ±0.01	1.12 ±0.03	0.85 ±0.02	0.42 ±0.01	0.78 ±1.72	0.41 ±0.01
ACNP	0.54 ±0.02	1.11 ±0.02	0.84 ±0.01	0.34 ±0.01	0.57 ±0.01	0.40 ±0.01
ALNP (E)	0.54 ±0.01	1.60 ±0.06	1.25 ±0.03	0.43 ±0.01	1.06 ±3.04	0.42 ±0.01
LNP (M)	0.59 ±0.01	F	1.13 ±0.01	0.41 ±0.01	0.88 ±0.03	0.52 ±0.01
CNP	0.63 ±0.01	F	1.08 ±0.02	0.43 ±0.01	1.16 ±0.45	0.52 ±0.01
Trivial	1.08 ±0.01	1.08 ±0.01	0.85 ±0.01	0.57 ±0.01	0.57 ±0.01	0.40 ±0.00
ConvLNP (E–M)	2.01 ±0.11	2.01 ±0.11	5.95 ±0.16	0.44 ±0.01	0.44 ±0.01	0.47 ±0.01

Table 8: For the non-Gaussian experiments, average log-likelihoods normalised by the number of target points. Shows for one-dimensional inputs (1D; $d_x = 1$) and two-dimensional inputs (2D; $d_y = 2$) the performance for interpolation within the range $[-2, 2]^{d_x}$ where the models were trained ("Int."); interpolation within the range $[2, 6]^{d_x}$ which the models have never seen before ("OOID"); and extrapolation from the range $[-2, 2]^{d_x}$ to the range $[2, 6]^{d_x}$ ("Ext."). Models are ordered by interpolation performance for one-dimensional inputs. The latent variable models are trained and evaluated with the ELBO objective (E); trained and evaluated with the ML objective (M); and trained with the ELBO objective and evaluated with the ML objective (E–M). Trivial refers to predicting the empirical means and standard deviation of the test data. Errors indicate the central 95%-confidence interval. Numbers which are significantly best ($p < 0.05$) are boldfaced. Numbers which are very large are marked as failed with "F". Numbers which are missing could not be run.

Model	Int. (1D)	OOID (1D)	Ext. (1D)	Int. (2D)	OOID (2D)	Ext. (2D)
ConvCNP (AR)	**1.52** ±0.04	**1.53** ±0.04	**1.32** ±0.04	**0.56** ±0.03	**0.56** ±0.03	**0.29** ±0.03
ConvLNP (E)	1.40 ±0.05	1.40 ±0.05	0.82 ±0.05	0.06 ±0.03	0.06 ±0.03	−0.62 ±0.04
ConvLNP (M)	1.08 ±0.06	1.08 ±0.06	−0.36 ±0.03	0.26 ±0.04	0.26 ±0.04	−0.70 ±0.02
ConvGNP	0.79 ±0.06	0.79 ±0.06	−1.03 ±0.07	0.23 ±0.04	0.23 ±0.04	−0.79 ±0.02
FullConvGNP	0.71 ±0.08	0.72 ±0.06	−0.20 ±0.02			
ConvCNP	0.57 ±0.07	0.57 ±0.07	−0.73 ±0.02	0.18 ±0.05	0.18 ±0.05	−0.86 ±0.03
ACNP (AR)	0.07 ±0.03	−0.85 ±0.03	−0.84 ±0.02	−0.53 ±0.02	−1.52 ±0.10	−1.51 ±0.09
AGNP	−0.31 ±0.03	−1.22 ±0.07	−1.58 ±0.11	−0.55 ±0.02	−0.79 ±0.02	−0.76 ±0.03
ALNP (E–M)	−0.33 ±0.03	−0.91 ±0.03	−0.80 ±0.04	−0.67 ±0.03	−1.06 ±0.62	−0.70 ±0.03
ALNP (E)	−0.35 ±0.03	−5.00 ±0.17	−3.37 ±0.06	−0.68 ±0.03	−2.59 ±7.64	−0.75 ±0.03
ALNP (M)	−0.36 ±0.02	−0.68 ±0.02	−0.68 ±0.02	−0.53 ±0.02	−0.74 ±0.04	−0.69 ±0.02
GNP	−0.38 ±0.02	F	F	−0.69 ±0.02	−0.74 ±0.04	−0.70 ±0.03
LNP (E–M)	−0.43 ±0.02	F	−3.34 ±0.53	−0.66 ±0.02	F	−0.96 ±0.03
LNP (E)	−0.44 ±0.02	F	F	−0.66 ±0.02	F	F
ACNP	−0.50 ±0.03	−0.83 ±0.03	−0.85 ±0.03	−0.60 ±0.02	−1.50 ±0.10	−0.73 ±0.03
LNP (M)	−0.53 ±0.02	−1.28 ±0.05	−0.80 ±0.03	−0.62 ±0.02	−1.50 ±0.11	−0.75 ±0.03
CNP (AR)	−0.65 ±0.02	−1.14 ±0.19	−0.98 ±0.06	−0.69 ±0.02	−1.05 ±0.07	−0.72 ±0.03
CNP	−0.68 ±0.02	−0.79 ±0.04	−0.73 ±0.03	−0.69 ±0.02	−1.05 ±0.08	−0.71 ±0.03
Trivial	−0.82 ±0.00	−0.82 ±0.00	−0.82 ±0.00	−0.82 ±0.00	−0.82 ±0.00	−0.82 ±0.00
ConvLNP (E–M)	F	F	F	−0.04 ±0.05	−0.04 ±0.05	−1.47 ±0.87

Table 9: For the EQ synthetic experiments with one-dimensional inputs, average Kullback–Leibler divergences of the posterior prediction map π_y with respect to the model normalised by the number of target points. Shows for one-dimensional outputs ($d_y = 1$) and two-dimensional outputs ($d_y = 2$) the performance for interpolation within the range $[-2, 2]$ where the models where trained ("Int."); interpolation within the range $[2, 6]$ which the models have never seen before ("OOID"); and extrapolation from the range $[-2, 2]$ to the range $[2, 6]$ ("Ext."). Models are ordered by interpolation performance. The latent variable models are trained and evaluated with the ELBO objective (E); trained and evaluated with the ML objective (M); and trained with the ELBO objective and evaluated with the ML objective (E–M). Diagonal GP refers to predictions by the ground-truth Gaussian processes without correlations. Trivial refers to predicting the empirical means and standard deviation of the test data. Errors indicate the central 95%-confidence interval. Numbers which are significantly best ($p < 0.05$) are boldfaced. Numbers which are very large are marked as failed with "F". Numbers which are missing could not be run.

EQ $d_x = 1,\ d_y = 1$	Int.	OOID	Ext.
FullConvGNP	**0.00** ±0.00	**0.00** ±0.00	**0.00** ±0.00
ConvGNP	0.01 ±0.00	0.01 ±0.00	3.46 ±0.08
ConvCNP (AR)	0.01 ±0.00	0.01 ±0.00	0.01 ±0.00
AGNP	0.03 ±0.00	4.28 ±0.08	7.38 ±0.13
ConvLNP (E)	0.06 ±0.00	0.06 ±0.00	0.11 ±0.01
ACNP (AR)	0.07 ±0.00	1.19 ±0.01	0.98 ±0.01
GNP	0.08 ±0.00	F	F
ConvLNP (M)	0.25 ±0.01	0.25 ±0.01	0.67 ±0.01
CNP (AR)	0.28 ±0.00	F	F
ALNP (M)	0.31 ±0.01	1.04 ±0.01	0.84 ±0.01
LNP (E)	0.34 ±0.01	F	1.34 ±0.01
LNP (E–M)	0.37 ±0.01	F	1.27 ±0.01
Diagonal GP	0.40 ±0.01	0.40 ±0.01	0.95 ±0.01
ConvCNP	0.41 ±0.01	0.41 ±0.01	0.95 ±0.01
ANP (E–M)	0.42 ±0.01	1.18 ±0.01	0.94 ±0.01
ANP (E)	0.44 ±0.01	1.32 ±0.01	1.25 ±0.01
ACNP	0.45 ±0.01	1.22 ±0.01	0.95 ±0.01
LNP (M)	0.49 ±0.01	1.54 ±0.01	1.45 ±0.01
CNP	0.54 ±0.01	F	1.41 ±0.01
ConvLNP (E–M)	0.90 ±0.04	0.90 ±0.04	4.05 ±0.06
Trivial	1.19 ±0.00	1.19 ±0.00	0.96 ±0.00

EQ $d_x = 1,\ d_y = 2$	Int.	OOID	Ext.
FullConvGNP	**0.00** ±0.00	**0.00** ±0.00	**0.00** ±0.00
ConvGNP	0.01 ±0.00	0.01 ±0.00	1.73 ±0.05
ConvCNP (AR)	0.01 ±0.00	0.01 ±0.00	0.01 ±0.00
AGNP	0.04 ±0.00	7.71 ±0.10	7.87 ±0.10
ACNP (AR)	0.07 ±0.00	1.31 ±0.01	1.09 ±0.01
ConvLNP (E)	0.08 ±0.00	0.08 ±0.00	0.13 ±0.00
GNP	0.13 ±0.00	F	F
ConvLNP (M)	0.36 ±0.01	0.36 ±0.01	0.88 ±0.00
ALNP (M)	0.41 ±0.01	1.23 ±0.01	0.99 ±0.00
CNP (AR)	0.42 ±0.00	F	F
Diagonal GP	0.47 ±0.01	0.47 ±0.01	1.06 ±0.00
ConvCNP	0.48 ±0.01	0.48 ±0.01	1.06 ±0.00
ACNP	0.51 ±0.01	1.38 ±0.01	1.06 ±0.01
ALNP (E–M)	0.52 ±0.01	1.47 ±0.02	1.07 ±0.01
ALNP (E)	0.53 ±0.01	3.79 ±0.05	2.84 ±0.02
LNP (E)	0.54 ±0.01	F	1.47 ±0.01
LNP (E–M)	0.56 ±0.01	F	1.42 ±0.01
LNP (M)	0.64 ±0.00	F	1.52 ±0.00
CNP	0.66 ±0.01	F	1.28 ±0.00
Trivial	1.31 ±0.00	1.31 ±0.00	1.07 ±0.00
ConvLNP (E–M)	2.14 ±0.06	2.14 ±0.06	9.30 ±0.08

Table 10: For the EQ synthetic experiments with two-dimensional inputs, average Kullback–Leibler divergences of the posterior prediction map π_y with respect to the model normalised by the number of target points. Shows for one-dimensional outputs ($d_y = 1$) and two-dimensional outputs ($d_y = 2$) the performance for interpolation within the range $[-2, 2]^2$ where the models where trained ("Int."); interpolation within the range $[2, 6]^2$ which the models have never seen before ("OOID"); and extrapolation from the range $[-2, 2]^2$ to the range $[2, 6]^2$ ("Ext."). Models are ordered by interpolation performance. The latent variable models are trained and evaluated with the ELBO objective (E); trained and evaluated with the ML objective (M); and trained with the ELBO objective and evaluated with the ML objective (E–M). Diagonal GP refers to predictions by the ground-truth Gaussian processes without correlations. Trivial refers to predicting the empirical means and standard deviation of the test data. Errors indicate the central 95%-confidence interval. Numbers which are significantly best ($p < 0.05$) are boldfaced. Numbers which are very large are marked as failed with "F". Numbers which are missing could not be run.

EQ $d_x = 2,\ d_y = 1$	Int.	OOID	Ext.
ConvCNP (AR)	**0.01** ±0.00	**0.01** ±0.00	**0.01** ±0.00
ConvGNP	0.08 ±0.00	0.08 ±0.00	1.92 ±0.02
AGNP	0.09 ±0.00	0.70 ±0.00	0.50 ±0.00
ACNP (AR)	0.09 ±0.00	0.72 ±0.00	0.51 ±0.00
GNP	0.19 ±0.00	1.01 ±0.00	0.80 ±0.00
ConvLNP (M)	0.34 ±0.00	0.34 ±0.00	0.47 ±0.00
ALNP (M)	0.34 ±0.00	0.70 ±0.00	0.51 ±0.00
Diagonal GP	0.36 ±0.00	0.36 ±0.00	0.51 ±0.00
ConvCNP	0.37 ±0.00	0.37 ±0.00	0.51 ±0.00
ACNP	0.40 ±0.00	0.72 ±0.00	0.51 ±0.00
ConvLNP (E)	0.41 ±0.00	0.41 ±0.00	0.46 ±0.00
CNP (AR)	0.41 ±0.00	0.90 ±0.00	0.71 ±0.00
LNP (E–M)	0.46 ±0.00	0.99 ±0.01	0.65 ±0.00
LNP (E)	0.48 ±0.00	1.04 ±0.01	0.67 ±0.00
ConvLNP (E–M)	0.48 ±0.00	0.48 ±0.00	0.59 ±0.01
ALNP (E–M)	0.49 ±0.01	0.72 ±0.00	0.51 ±0.00
ALNP (E)	0.50 ±0.01	0.73 ±0.00	0.52 ±0.00
LNP (M)	0.51 ±0.00	0.92 ±0.00	0.72 ±0.00
CNP	0.52 ±0.00	0.92 ±0.00	0.72 ±0.00
Trivial	0.72 ±0.00	0.72 ±0.00	0.51 ±0.00
FullConvGNP			

EQ $d_x = 2,\ d_y = 2$	Int.	OOID	Ext.
ConvCNP (AR)	**0.03** ±0.00	**0.03** ±0.00	**0.02** ±0.00
ACNP (AR)	0.11 ±0.00	0.79 ±0.00	0.56 ±0.00
ConvGNP	0.19 ±0.00	0.19 ±0.00	0.74 ±0.01
AGNP	0.22 ±0.00	0.87 ±0.01	0.57 ±0.00
GNP	0.38 ±0.00	1.06 ±0.00	0.75 ±0.00
ConvNP (M)	0.39 ±0.00	0.39 ±0.00	0.52 ±0.00
Diagonal GP	0.40 ±0.00	0.40 ±0.00	0.56 ±0.00
ConvCNP	0.41 ±0.00	0.41 ±0.00	0.56 ±0.00
ANP (M)	0.42 ±0.00	0.79 ±0.00	0.54 ±0.00
ACNP	0.44 ±0.00	0.79 ±0.00	0.56 ±0.00
CNP (AR)	0.52 ±0.00	F	F
NP (E–M)	0.56 ±0.00	1.95 ±0.03	0.72 ±0.00
ANP (E–M)	0.56 ±0.00	1.90 ±1.72	0.55 ±0.00
NP (E)	0.57 ±0.00	1.99 ±0.03	0.72 ±0.00
ANP (E)	0.57 ±0.00	3.51 ±3.04	0.56 ±0.00
NP (M)	0.59 ±0.00	1.17 ±0.01	0.75 ±0.00
CNP	0.60 ±0.00	3.08 ±0.42	0.66 ±0.00
Trivial	0.79 ±0.00	0.79 ±0.00	0.56 ±0.00
ConvNP (E–M)	0.79 ±0.00	0.79 ±0.00	0.56 ±0.00
ConvNP (E)	0.79 ±0.00	0.79 ±0.00	0.56 ±0.00
FullConvGNP			

Table 11: For the Matérn–$\frac{5}{2}$ synthetic experiments with one-dimensional inputs, average Kullback–Leibler divergences of the posterior prediction map π_y with respect to the model normalised by the number of target points. Shows for one-dimensional outputs ($d_y = 1$) and two-dimensional outputs ($d_y = 2$) the performance for interpolation within the range $[-2, 2]$ where the models where trained ("Int."); interpolation within the range $[2, 6]$ which the models have never seen before ("OOID"); and extrapolation from the range $[-2, 2]$ to the range $[2, 6]$ ("Ext."). Models are ordered by interpolation performance. The latent variable models are trained and evaluated with the ELBO objective (E); trained and evaluated with the ML objective (M); and trained with the ELBO objective and evaluated with the ML objective (E–M). Diagonal GP refers to predictions by the ground-truth Gaussian processes without correlations. Trivial refers to predicting the empirical means and standard deviation of the test data. Errors indicate the central 95%-confidence interval. Numbers which are significantly best ($p < 0.05$) are boldfaced. Numbers which are very large are marked as failed with "F". Numbers which are missing could not be run.

Matérn–$\frac{5}{2}$ $d_x = 1,\ d_y = 1$	Int.	OOID	Ext.
FullConvGNP	**0.00** ±0.00	**0.00** ±0.00	**0.00** ±0.00
ConvCNP (AR)	0.00 ±0.00	0.00 ±0.00	0.00 ±0.00
ConvGNP	0.01 ±0.00	0.01 ±0.00	2.32 ±0.06
AGNP	0.03 ±0.00	4.53 ±0.08	7.22 ±0.12
ACNP (AR)	0.04 ±0.00	1.08 ±0.01	0.87 ±0.01
GNP	0.09 ±0.00	F	F
ConvLNP (E)	0.13 ±0.00	0.13 ±0.00	0.31 ±0.02
ConvLNP (M)	0.26 ±0.01	0.26 ±0.01	0.58 ±0.00
ALNP (M)	0.30 ±0.00	0.98 ±0.01	0.78 ±0.01
CNP (AR)	0.34 ±0.01	1.81 ±0.04	1.32 ±0.02
LNP (E)	0.36 ±0.00	F	1.31 ±0.01
LNP (E–M)	0.37 ±0.01	F	1.14 ±0.00
Diagonal GP	0.40 ±0.01	0.40 ±0.01	0.84 ±0.01
ConvCNP	0.40 ±0.01	0.40 ±0.01	0.84 ±0.01
ALNP (E–M)	0.41 ±0.01	1.13 ±0.01	0.84 ±0.01
ACNP	0.42 ±0.01	1.10 ±0.01	0.84 ±0.01
ALNP (E)	0.43 ±0.01	1.15 ±0.01	0.87 ±0.01
LNP (M)	0.51 ±0.00	1.87 ±0.02	1.30 ±0.01
CNP	0.54 ±0.01	1.47 ±0.02	1.11 ±0.01
Trivial	1.08 ±0.00	1.08 ±0.00	0.85 ±0.00
ConvLNP (E–M)	1.37 ±0.04	1.36 ±0.04	4.30 ±0.06

Matérn–$\frac{5}{2}$ $d_x = 1,\ d_y = 2$	Int.	OOID	Ext.
FullConvGNP	**0.00** ±0.00	**0.00** ±0.00	**0.00** ±0.00
ConvCNP (AR)	0.01 ±0.00	0.01 ±0.00	0.01 ±0.00
ConvGNP	0.02 ±0.00	0.02 ±0.00	1.71 ±0.04
AGNP	0.04 ±0.00	6.14 ±0.08	7.03 ±0.09
ACNP (AR)	0.05 ±0.00	1.18 ±0.01	0.96 ±0.01
GNP	0.13 ±0.00	F	F
ConvLNP (E)	0.16 ±0.00	0.16 ±0.00	0.29 ±0.00
ConvLNP (M)	0.36 ±0.00	0.36 ±0.00	0.76 ±0.00
ALNP (M)	0.40 ±0.00	1.10 ±0.01	0.88 ±0.00
CNP (AR)	0.45 ±0.00	F	F
Diagonal GP	0.46 ±0.01	0.46 ±0.01	0.93 ±0.00
ConvCNP	0.46 ±0.01	0.46 ±0.01	0.93 ±0.00
ACNP	0.49 ±0.01	1.23 ±0.01	0.93 ±0.00
ALNP (E–M)	0.51 ±0.01	1.28 ±0.01	0.99 ±0.01
ALNP (E)	0.51 ±0.01	1.43 ±0.02	1.10 ±0.01
LNP (E–M)	0.54 ±0.00	F	1.24 ±0.00
LNP (E)	0.54 ±0.00	F	1.79 ±0.01
LNP (M)	0.63 ±0.00	2.33 ±0.02	1.23 ±0.00
CNP	0.65 ±0.00	7.72 ±0.69	1.23 ±0.00
Trivial	1.18 ±0.00	1.18 ±0.00	0.94 ±0.00
ConvLNP (E–M)	3.07 ±0.06	3.06 ±0.06	9.83 ±0.09

Table 12: For the Matérn–$\frac{5}{2}$ synthetic experiments with two-dimensional inputs, average Kullback–Leibler divergences of the posterior prediction map π_y with respect to the model normalised by the number of target points. Shows for one-dimensional outputs ($d_y = 1$) and two-dimensional outputs ($d_y = 2$) the performance for interpolation within the range $[-2, 2]^2$ where the models where trained ("Int."); interpolation within the range $[2, 6]^2$ which the models have never seen before ("OOID"); and extrapolation from the range $[-2, 2]^2$ to the range $[2, 6]^2$ ("Ext."). Models are ordered by interpolation performance. Diagonal GP refers to predictions by the ground-truth Gaussian processes without correlations. Trivial refers to predicting the empirical means and standard deviation of the test data. Errors indicate the central 95%-confidence interval. Numbers which are significantly best ($p < 0.05$) are boldfaced. Numbers which are very large are marked as failed with "F". Numbers which are missing could not be run.

Matérn–$\frac{5}{2}$ $d_x = 2,\ d_y = 1$	Int.	OOID	Ext.
ConvCNP (AR)	**0.01** ±0.00	**0.01** ±0.00	**0.00** ±0.00
ACNP (AR)	0.05 ±0.00	0.54 ±0.00	0.38 ±0.00
AGNP	0.08 ±0.00	0.83 ±0.01	0.37 ±0.00
ConvGNP	0.08 ±0.00	0.08 ±0.00	0.60 ±0.01
GNP	0.16 ±0.00	0.90 ±0.00	0.75 ±0.00
ConvLNP (M)	0.25 ±0.00	0.25 ±0.00	0.34 ±0.00
ALNP (M)	0.26 ±0.00	0.51 ±0.00	0.37 ±0.00
Diagonal GP	0.28 ±0.00	0.28 ±0.00	0.39 ±0.00
ConvCNP	0.28 ±0.00	0.28 ±0.00	0.39 ±0.00
ACNP	0.29 ±0.00	0.54 ±0.00	0.39 ±0.00
CNP (AR)	0.31 ±0.00	0.69 ±0.00	0.52 ±0.00
ConvLNP (E)	0.32 ±0.00	0.32 ±0.00	0.30 ±0.00
LNP (E–M)	0.34 ±0.00	1.07 ±0.01	0.69 ±0.00
LNP (E)	0.35 ±0.00	1.25 ±0.01	0.72 ±0.00
ConvLNP (E–M)	0.36 ±0.00	0.36 ±0.00	0.43 ±0.00
LNP (M)	0.37 ±0.00	0.75 ±0.01	0.51 ±0.00
ALNP (E–M)	0.39 ±0.00	0.65 ±0.01	0.43 ±0.00
CNP	0.39 ±0.00	0.67 ±0.00	0.54 ±0.00
ALNP (E)	0.41 ±0.01	0.67 ±0.01	0.44 ±0.00
Trivial	0.55 ±0.00	0.55 ±0.00	0.39 ±0.00
FullConvGNP			

Matérn–$\frac{5}{2}$ $d_x = 2,\ d_y = 2$	Int.	OOID	Ext.
ConvCNP (AR)	**0.01** ±0.00	**0.01** ±0.00	**0.01** ±0.00
ACNP (AR)	0.06 ±0.00	0.58 ±0.00	0.41 ±0.00
ConvGNP	0.14 ±0.00	0.14 ±0.00	0.64 ±0.01
AGNP	0.17 ±0.00	0.58 ±0.00	0.40 ±0.00
GNP	0.28 ±0.00	0.78 ±0.00	0.60 ±0.00
ConvLNP (M)	0.29 ±0.00	0.29 ±0.00	0.38 ±0.00
ALNP (M)	0.29 ±0.00	0.56 ±0.00	0.40 ±0.00
Diagonal GP	0.30 ±0.00	0.30 ±0.00	0.41 ±0.00
ConvCNP	0.30 ±0.00	0.30 ±0.00	0.41 ±0.00
ACNP	0.32 ±0.00	0.58 ±0.00	0.41 ±0.00
ConvLNP (E)	0.36 ±0.00	0.36 ±0.00	0.37 ±0.00
CNP (AR)	0.37 ±0.00	F	0.88 ±0.17
LNP (E–M)	0.41 ±0.00	2.29 ±0.05	0.59 ±0.00
LNP (E)	0.41 ±0.00	2.36 ±0.05	0.60 ±0.00
ALNP (E–M)	0.42 ±0.00	0.61 ±0.00	0.41 ±0.00
ALNP (E)	0.42 ±0.00	0.61 ±0.00	0.41 ±0.00
LNP (M)	0.43 ±0.00	0.68 ±0.00	0.53 ±0.00
CNP	0.44 ±0.00	0.86 ±0.17	0.59 ±0.00
ConvLNP (E–M)	0.49 ±0.00	0.49 ±0.00	0.61 ±0.00
Trivial	0.58 ±0.00	0.58 ±0.00	0.41 ±0.00
FullConvGNP			

Table 13: For the weakly periodic synthetic experiments with one-dimensional inputs, average Kullback–Leibler divergences of the posterior prediction map π_y with respect to the model normalised by the number of target points. Shows for one-dimensional outputs ($d_y = 1$) and two-dimensional outputs ($d_y = 2$) the performance for interpolation within the range $[-2, 2]$ where the models where trained ("Int."); interpolation within the range $[2, 6]$ which the models have never seen before ("OOID"); and extrapolation from the range $[-2, 2]$ to the range $[2, 6]$ ("Ext."). Models are ordered by interpolation performance. The latent variable models are trained and evaluated with the ELBO objective (E); trained and evaluated with the ML objective (M); and trained with the ELBO objective and evaluated with the ML objective (E–M). Diagonal GP refers to predictions by the ground-truth Gaussian processes without correlations. Trivial refers to predicting the empirical means and standard deviation of the test data. Errors indicate the central 95%-confidence interval. Numbers which are significantly best ($p < 0.05$) are boldfaced. Numbers which are very large are marked as failed with "F". Numbers which are missing could not be run.

Weakly Periodic $d_x = 1,\ d_y = 1$	Int.	OOID	Ext.
FullConvGNP	**0.02** ±0.00	**0.02** ±0.00	**0.00** ±0.00
ConvCNP (AR)	0.05 ±0.00	0.05 ±0.00	0.04 ±0.00
ConvGNP	0.05 ±0.00	0.05 ±0.00	0.56 ±0.02
AGNP	0.22 ±0.00	1.25 ±0.02	1.25 ±0.02
ConvLNP (M)	0.28 ±0.00	0.28 ±0.00	0.43 ±0.00
ConvLNP (E)	0.34 ±0.00	0.33 ±0.00	0.45 ±0.02
Diagonal GP	0.38 ±0.01	0.38 ±0.01	0.59 ±0.01
ConvCNP	0.40 ±0.01	0.40 ±0.01	0.60 ±0.01
ALNP (M)	0.53 ±0.00	0.77 ±0.01	0.57 ±0.01
ACNP (AR)	0.57 ±0.01	0.82 ±0.01	0.61 ±0.01
GNP	0.59 ±0.01	1.31 ±0.02	0.62 ±0.01
CNP (AR)	0.59 ±0.01	2.33 ±0.27	1.46 ±0.05
LNP (E–M)	0.60 ±0.01	F	4.09 ±0.28
ALNP (E–M)	0.60 ±0.01	0.78 ±0.01	0.59 ±0.01
LNP (M)	0.60 ±0.01	0.80 ±0.01	0.62 ±0.01
LNP (E)	0.61 ±0.01	F	9.91 ±0.70
ALNP (E)	0.62 ±0.01	1.01 ±0.01	0.71 ±0.01
ACNP	0.65 ±0.01	0.82 ±0.01	0.61 ±0.01
CNP	0.67 ±0.01	1.45 ±0.03	0.68 ±0.01
Trivial	0.82 ±0.00	0.82 ±0.00	0.61 ±0.00
ConvLNP (E–M)	1.58 ±0.03	1.57 ±0.03	2.85 ±0.04

Weakly Periodic $d_x = 1,\ d_y = 2$	Int.	OOID	Ext.
FullConvGNP	**0.03** ±0.00	**0.03** ±0.00	**0.00** ±0.00
ConvCNP (AR)	0.09 ±0.00	0.09 ±0.00	0.06 ±0.00
ConvGNP	0.12 ±0.00	0.12 ±0.00	0.72 ±0.01
AGNP	0.25 ±0.00	2.17 ±0.02	1.95 ±0.02
ConvLNP (M)	0.38 ±0.00	0.38 ±0.00	0.54 ±0.00
ConvLNP (E)	0.39 ±0.00	0.39 ±0.00	0.44 ±0.00
Diagonal GP	0.42 ±0.00	0.42 ±0.00	0.65 ±0.00
ConvCNP	0.46 ±0.00	0.46 ±0.00	0.65 ±0.00
GNP	0.50 ±0.00	1.02 ±0.01	0.76 ±0.00
ALNP (M)	0.62 ±0.00	1.04 ±0.01	0.64 ±0.00
ACNP (AR)	0.63 ±0.00	0.89 ±0.01	0.66 ±0.00
CNP (AR)	0.67 ±0.00	2.52 ±0.07	1.21 ±0.01
LNP (E–M)	0.68 ±0.00	F	5.18 ±0.18
LNP (M)	0.69 ±0.00	1.26 ±0.01	0.68 ±0.01
LNP (E)	0.69 ±0.00	F	F
ALNP (E–M)	0.70 ±0.00	0.85 ±0.01	0.64 ±0.00
ACNP	0.71 ±0.00	0.89 ±0.01	0.66 ±0.00
ALNP (E)	0.72 ±0.00	0.93 ±0.01	0.72 ±0.00
CNP	0.74 ±0.00	1.27 ±0.01	0.77 ±0.01
Trivial	0.89 ±0.00	0.89 ±0.00	0.67 ±0.00
ConvLNP (E–M)	3.02 ±0.03	3.02 ±0.03	5.40 ±0.04

Table 14: For the weakly periodic synthetic experiments with two-dimensional inputs, average Kullback–Leibler divergences of the posterior prediction map π_y with respect to the model normalised by the number of target points. Shows for one-dimensional outputs ($d_y = 1$) and two-dimensional outputs ($d_y = 2$) the performance for interpolation within the range $[-2, 2]^2$ where the models where trained ("Int."); interpolation within the range $[2, 6]^2$ which the models have never seen before ("OOID"); and extrapolation from the range $[-2, 2]^2$ to the range $[2, 6]^2$ ("Ext."). Models are ordered by interpolation performance. The latent variable models are trained and evaluated with the ELBO objective (E); trained and evaluated with the ML objective (M); and trained with the ELBO objective and evaluated with the ML objective (E–M). Diagonal GP refers to predictions by the ground-truth Gaussian processes without correlations. Trivial refers to predicting the empirical means and standard deviation of the test data. Errors indicate the central 95%-confidence interval. Numbers which are significantly best ($p < 0.05$) are boldfaced. Numbers which are very large are marked as failed with "F". Numbers which are missing could not be run.

Weakly Periodic $d_x = 2,\ d_y = 1$	Int.	OOID	Ext.
ConvCNP (AR)	**0.05** ±0.00	**0.05** ±0.00	**0.03** ±0.00
ConvGNP	0.10 ±0.00	0.10 ±0.00	0.19 ±0.00
ConvLNP (M)	0.18 ±0.00	0.18 ±0.00	0.21 ±0.00
Diagonal GP	0.19 ±0.00	0.19 ±0.00	0.27 ±0.00
ConvCNP	0.20 ±0.00	0.20 ±0.00	0.27 ±0.00
ConvLNP (E)	0.22 ±0.00	0.22 ±0.00	0.22 ±0.00
AGNP	0.23 ±0.00	0.35 ±0.00	0.26 ±0.00
ACNP (AR)	0.23 ±0.00	0.37 ±0.00	0.26 ±0.00
ConvLNP (E–M)	0.23 ±0.00	0.23 ±0.00	0.29 ±0.00
GNP	0.23 ±0.00	0.35 ±0.00	0.24 ±0.00
CNP (AR)	0.25 ±0.00	0.82 ±0.01	0.72 ±0.01
ALNP (M)	0.25 ±0.00	0.36 ±0.00	0.25 ±0.00
LNP (M)	0.26 ±0.00	1.32 ±0.03	0.33 ±0.00
LNP (E–M)	0.26 ±0.00	6.28 ±1.06	0.44 ±0.01
LNP (E)	0.27 ±0.00	9.91 ±1.68	0.52 ±0.01
ACNP	0.28 ±0.00	0.37 ±0.00	0.27 ±0.00
CNP	0.29 ±0.00	0.81 ±0.01	0.29 ±0.00
ALNP (E–M)	0.31 ±0.00	0.39 ±0.00	0.26 ±0.00
ALNP (E)	0.32 ±0.00	0.42 ±0.00	0.29 ±0.00
Trivial	0.38 ±0.00	0.38 ±0.00	0.27 ±0.00
FullConvGNP			

Weakly Periodic $d_x = 2,\ d_y = 2$	Int.	OOID	Ext.
ConvCNP (AR)	**0.08** ±0.00	**0.08** ±0.00	**0.05** ±0.00
ConvGNP	0.13 ±0.00	0.13 ±0.00	0.18 ±0.00
Diagonal GP	0.20 ±0.00	0.20 ±0.00	0.28 ±0.00
ConvLNP (M)	0.21 ±0.00	0.21 ±0.00	0.25 ±0.00
ConvCNP	0.23 ±0.00	0.23 ±0.00	0.28 ±0.00
AGNP	0.24 ±0.00	0.39 ±0.00	0.27 ±0.00
ACNP (AR)	0.25 ±0.00	0.40 ±0.00	0.28 ±0.00
GNP	0.25 ±0.00	0.38 ±0.00	0.25 ±0.00
ConvLNP (E)	0.26 ±0.00	0.26 ±0.00	0.27 ±0.00
CNP (AR)	0.27 ±0.00	3.21 ±0.14	0.77 ±0.02
ALNP (M)	0.28 ±0.00	0.39 ±0.00	0.28 ±0.00
LNP (M)	0.29 ±0.00	0.42 ±0.00	0.31 ±0.00
LNP (E–M)	0.29 ±0.00	1.52 ±0.04	0.36 ±0.00
LNP (E)	0.30 ±0.00	1.60 ±0.05	0.39 ±0.00
ConvLNP (E–M)	0.30 ±0.00	0.30 ±0.00	0.34 ±0.00
ACNP	0.30 ±0.00	0.40 ±0.00	0.29 ±0.00
CNP	0.31 ±0.00	0.63 ±0.01	0.33 ±0.00
ALNP (E–M)	0.36 ±0.00	0.43 ±0.00	0.28 ±0.00
ALNP (E)	0.36 ±0.00	0.44 ±0.00	0.29 ±0.00
Trivial	0.40 ±0.00	0.40 ±0.00	0.28 ±0.00
FullConvGNP			

Table 15: For the sawtooth synthetic experiments with one-dimensional inputs, average log-likelihoods normalised by the number of target points. Shows for one-dimensional outputs ($d_y = 1$) and two-dimensional outputs ($d_y = 2$) the performance for interpolation within the range $[-2, 2]$ where the models where trained ("Int."); interpolation within the range $[2, 6]$ which the models have never seen before ("OOID"); and extrapolation from the range $[-2, 2]$ to the range $[2, 6]$ ("Ext."). Models are ordered by interpolation performance. The latent variable models are trained and evaluated with the ELBO objective (E); trained and evaluated with the ML objective (M); and trained with the ELBO objective and evaluated with the ML objective (E–M). Trivial refers to predicting the empirical means and standard deviation of the test data. Errors indicate the central 95%-confidence interval. Numbers which are significantly best ($p < 0.05$) are boldfaced. Numbers which are very large are marked as failed with "F". Numbers which are missing could not be run.

Sawtooth $d_x = 1,\ d_y = 1$	Int.	OOID	Ext.
ConvCNP (AR)	**3.60**±0.01	**3.60**±0.01	**3.34**±0.01
ConvLNP (E)	3.51±0.02	3.52±0.02	2.68±0.02
ConvLNP	3.06±0.04	3.06±0.04	0.64±0.01
ConvGNP	2.62±0.05	2.61±0.08	−0.04±0.01
ConvCNP	2.38±0.04	2.37±0.04	−0.00±0.01
FullConvGNP	2.16±0.04	2.15±0.04	0.18±0.01
ALNP (E–M)	0.27±0.01	−0.18±0.00	−0.31±0.02
ALNP (E)	0.27±0.01	−15.96±0.17	−9.14±0.04
ALNP	0.20±0.00	−0.18±0.00	−0.18±0.00
LNP (E–M)	0.07±0.01	F	−8.67±0.53
LNP (E)	0.06±0.01	F	F
Trivial	−0.18±0.00	−0.18±0.00	−0.18±0.00
LNP	−0.18±0.00	−0.18±0.00	−0.18±0.00
CNP (AR)	−0.18±0.00	−0.18±0.00	−0.18±0.00
CNP	−0.18±0.00	−0.18±0.00	−0.18±0.00
GNP	−0.18±0.00	−0.18±0.00	−0.18±0.00
AGNP	−0.18±0.00	−0.18±0.00	−0.18±0.00
ACNP	−0.18±0.00	−0.18±0.00	−0.18±0.00
ACNP (AR)	−0.18±0.00	−0.18±0.00	−0.18±0.00
ConvLNP (E–M)	F	F	F

Sawtooth $d_x = 1,\ d_y = 2$	Int.	OOID	Ext.
ConvCNP (AR)	**2.22**±0.01	**2.22**±0.01	**1.91**±0.01
ConvLNP (E)	2.01±0.01	2.01±0.01	1.47±0.01
ConvLNP	1.73±0.03	1.73±0.03	−0.12±0.01
ACNP (AR)	1.01±0.01	−0.47±0.01	−0.45±0.01
FullConvGNP	0.99±0.06	1.04±0.03	0.11±0.00
ConvCNP	0.83±0.03	0.84±0.02	−0.29±0.00
ConvGNP	0.82±0.03	0.82±0.03	−0.29±0.00
GNP	−0.03±0.00	F	F
ALNP (E–M)	−0.06±0.01	−0.75±0.01	−0.35±0.00
ALNP (E)	−0.07±0.01	−0.78±0.02	−0.35±0.00
AGNP	−0.07±0.01	−0.37±0.00	−0.48±0.07
ACNP	−0.08±0.01	−0.41±0.01	−0.42±0.01
LNP (E–M)	−0.20±0.00	F	−1.33±0.00
LNP (E)	−0.20±0.00	F	−1.33±0.00
ALNP	−0.28±0.00	−0.33±0.00	−0.33±0.00
CNP (AR)	−0.29±0.00	−1.96±0.19	−1.43±0.06
CNP	−0.30±0.00	−0.51±0.01	−0.34±0.00
LNP	−0.32±0.00	−0.32±0.00	−0.32±0.00
Trivial	−0.33±0.00	−0.33±0.00	−0.33±0.00
ConvLNP (E–M)	−2.98±0.10	−2.98±0.10	−6.74±0.04

Table 16: For the sawtooth synthetic experiments with two-dimensional inputs, average log-likelihoods normalised by the number of target points. Shows for one-dimensional outputs ($d_y = 1$) and two-dimensional outputs ($d_y = 2$) the performance for interpolation within the range $[-2, 2]^2$ where the models where trained ("Int."); interpolation within the range $[2, 6]^2$ which the models have never seen before ("OOID"); and extrapolation from the range $[-2, 2]^2$ to the range $[2, 6]^2$ ("Ext."). Models are ordered by interpolation performance. The latent variable models are trained and evaluated with the ELBO objective (E); trained and evaluated with the ML objective (M); and trained with the ELBO objective and evaluated with the ML objective (E–M). Trivial refers to predicting the empirical means and standard deviation of the test data. Errors indicate the central 95%-confidence interval. Numbers which are significantly best ($p < 0.05$) are boldfaced. Numbers which are very large are marked as failed with "F". Numbers which are missing could not be run.

Sawtooth $d_x = 2,\ d_y = 1$	Int.	OOID	Ext.
ConvCNP (AR)	**2.59** ±0.01	**2.59** ±0.01	**2.10** ±0.01
ConvLNP (M)	2.07 ±0.02	2.08 ±0.02	−0.17 ±0.00
ConvCNP	1.93 ±0.04	1.94 ±0.03	−0.18 ±0.00
ConvGNP	1.90 ±0.04	1.91 ±0.03	−0.18 ±0.00
ConvLNP (E)	1.77 ±0.02	1.77 ±0.02	0.33 ±0.02
ConvLNP (E–M)	1.71 ±0.04	1.72 ±0.04	−2.30 ±0.87
Trivial	−0.18 ±0.00	−0.18 ±0.00	−0.18 ±0.00
CNP (AR)	−0.18 ±0.00	−0.18 ±0.00	−0.18 ±0.00
CNP	−0.18 ±0.00	−0.18 ±0.00	−0.18 ±0.00
GNP	−0.18 ±0.00	−0.18 ±0.00	−0.18 ±0.00
LNP (M)	−0.18 ±0.00	−0.18 ±0.00	−0.18 ±0.00
AGNP	−0.18 ±0.00	−0.18 ±0.00	−0.18 ±0.00
ALNP (M)	−0.18 ±0.00	−0.18 ±0.00	−0.18 ±0.00
ACNP (AR)	−0.18 ±0.00	−0.18 ±0.00	−0.18 ±0.00
ACNP	−0.18 ±0.00	−0.18 ±0.00	−0.18 ±0.00
LNP (E–M)	−0.19 ±0.00	F	−0.86 ±0.02
LNP (E)	−0.19 ±0.00	F	F
ALNP (E–M)	−0.20 ±0.01	−0.18 ±0.00	−0.18 ±0.00
ALNP (E)	−0.20 ±0.01	−0.71 ±0.00	−0.33 ±0.00
FullConvGNP			

Sawtooth $d_x = 2,\ d_y = 2$	Int.	OOID	Ext.
ConvCNP (AR)	**0.38** ±0.00	**0.38** ±0.00	**0.18** ±0.00
ConvLNP (M)	0.31 ±0.01	0.31 ±0.01	−0.32 ±0.00
ConvGNP	0.26 ±0.01	0.26 ±0.01	−0.33 ±0.00
ConvCNP	0.12 ±0.01	0.12 ±0.01	−0.32 ±0.00
ConvLNP (E)	0.04 ±0.00	0.04 ±0.00	−0.30 ±0.00
ConvLNP (E–M)	−0.07 ±0.01	−0.07 ±0.01	−0.48 ±0.00
Trivial	−0.32 ±0.00	−0.32 ±0.00	−0.32 ±0.00
ALNP (M)	−0.32 ±0.00	−0.32 ±0.00	−0.32 ±0.00
CNP (AR)	−0.32 ±0.00	−0.32 ±0.00	−0.32 ±0.00
CNP	−0.32 ±0.00	−0.32 ±0.00	−0.32 ±0.00
LNP (M)	−0.32 ±0.00	−0.32 ±0.00	−0.32 ±0.00
ACNP	−0.32 ±0.00	−0.32 ±0.00	−0.32 ±0.00
ACNP (AR)	−0.32 ±0.00	−0.32 ±0.00	−0.32 ±0.00
GNP	−0.32 ±0.00	−0.32 ±0.00	−0.32 ±0.00
AGNP	−0.32 ±0.00	−0.32 ±0.00	−0.32 ±0.00
LNP (E–M)	−0.33 ±0.00	−0.54 ±0.00	−0.34 ±0.00
LNP (E)	−0.33 ±0.00	−0.54 ±0.00	−0.34 ±0.00
ALNP (E–M)	−0.36 ±0.00	−0.33 ±0.00	−0.33 ±0.00
ALNP (E)	−0.36 ±0.00	−0.33 ±0.00	−0.33 ±0.00
FullConvGNP			

Table 17: For the mixture synthetic experiments with one-dimensional inputs, average log-likelihoods normalised by the number of target points. Shows for one-dimensional outputs ($d_y = 1$) and two-dimensional outputs ($d_y = 2$) the performance for interpolation within the range $[-2, 2]$ where the models where trained ("Int."); interpolation within the range $[2, 6]$ which the models have never seen before ("OOID"); and extrapolation from the range $[-2, 2]$ to the range $[2, 6]$ ("Ext."). Models are ordered by interpolation performance. The latent variable models are trained and evaluated with the ELBO objective (E); trained and evaluated with the ML objective (M); and trained with the ELBO objective and evaluated with the ML objective (E–M). Trivial refers to predicting the empirical means and standard deviation of the test data. Errors indicate the central 95%-confidence interval. Numbers which are significantly best ($p < 0.05$) are boldfaced. Numbers which are very large are marked as failed with "F". Numbers which are missing could not be run.

Mixture $d_x = 1,\ d_y = 1$	Int.	OOID	Ext.
ConvCNP (AR)	**0.45**±0.04	**0.45**±0.04	**0.30**±0.04
ConvLNP (E)	0.12±0.04	0.12±0.04	−0.37±0.03
FullConvGNP	−0.05±0.03	−0.05±0.03	−0.49±0.01
ConvLNP	−0.06±0.03	−0.06±0.03	−0.88±0.02
ACNP (AR)	−0.19±0.02	−1.32±0.01	−1.32±0.01
ConvCNP	−0.23±0.04	−0.24±0.04	−1.23±0.01
ConvGNP	−0.24±0.02	−0.23±0.02	−1.00±0.02
AGNP	−0.41±0.02	−1.03±0.03	−2.61±0.06
ALNP	−0.61±0.02	−1.01±0.02	−1.03±0.02
ALNP (E–M)	−0.63±0.02	−1.24±0.01	−1.10±0.02
ALNP (E)	−0.67±0.02	−1.52±0.02	−2.25±0.03
LNP (E–M)	−0.68±0.01	−3.05±0.04	−1.75±0.01
GNP	−0.70±0.02	−2.22±0.05	−1.62±0.04
LNP (E)	−0.71±0.01	−3.71±0.05	−2.08±0.01
LNP	−0.72±0.01	−1.46±0.01	−1.29±0.02
ACNP	−0.79±0.02	−1.31±0.01	−1.25±0.01
CNP (AR)	−1.00±0.02	−1.15±0.02	−1.09±0.02
CNP	−1.05±0.02	−1.14±0.02	−1.15±0.02
ConvLNP (E–M)	−1.41±0.15	−1.43±0.13	−3.40±0.06
Trivial	−1.32±0.00	−1.32±0.00	−1.32±0.00

Mixture $d_x = 1,\ d_y = 2$	Int.	OOID	Ext.
ConvLNP (E)	**−0.05**±0.03	**−0.05**±0.03	**−0.50**±0.02
ConvCNP (AR)	−0.17±0.02	−0.17±0.02	−0.29±0.02
FullConvGNP	−0.27±0.01	−0.27±0.01	−0.63±0.01
ConvGNP	−0.29±0.02	−0.29±0.02	−2.59±0.06
ACNP (AR)	−0.35±0.02	−1.43±0.02	−1.43±0.02
ConvLNP	−0.39±0.03	−0.40±0.03	−1.10±0.02
AGNP	−0.57±0.02	−3.29±0.07	−3.05±0.06
GNP	−0.60±0.01	−1.70±0.03	−1.67±0.03
ConvCNP	−0.68±0.02	−0.68±0.02	−1.39±0.01
ALNP	−0.76±0.02	−1.19±0.02	−1.19±0.02
LNP	−0.89±0.01	−3.18±0.05	−1.40±0.02
LNP (E–M)	−0.89±0.01	−4.43±0.07	−1.62±0.02
ALNP (E–M)	−0.92±0.02	−1.47±0.03	−1.46±0.03
LNP (E)	−0.92±0.01	−4.71±0.07	−1.86±0.01
ACNP	−0.93±0.02	−1.42±0.02	−1.53±0.03
ALNP (E)	−0.95±0.02	−1.75±0.04	−1.73±0.04
CNP (AR)	−1.15±0.02	−1.27±0.02	−1.21±0.02
CNP	−1.18±0.02	−1.32±0.03	−1.27±0.02
ConvLNP (E–M)	−3.45±0.07	−3.40±0.07	−5.30±0.07
Trivial	−1.46±0.00	−1.46±0.00	−1.46±0.00

Table 18: For the mixture synthetic experiments with two-dimensional inputs, average log-likelihoods normalised by the number of target points. Shows for one-dimensional outputs ($d_y = 1$) and two-dimensional outputs ($d_y = 2$) the performance for interpolation within the range $[-2, 2]^2$ where the models where trained ("Int."); interpolation within the range $[2, 6]^2$ which the models have never seen before ("OOID"); and extrapolation from the range $[-2, 2]^2$ to the range $[2, 6]^2$ ("Ext."). Models are ordered by interpolation performance. The latent variable models are trained and evaluated with the ELBO objective (E); trained and evaluated with the ML objective (M); and trained with the ELBO objective and evaluated with the ML objective (E–M). Trivial refers to predicting the empirical means and standard deviation of the test data. Errors indicate the central 95%-confidence interval. Numbers which are significantly best ($p < 0.05$) are boldfaced. Numbers which are very large are marked as failed with "F". Numbers which are missing could not be run.

Mixture $d_x = 2,\ d_y = 1$	Int.	OOID	Ext.
ConvCNP (AR)	**−0.10** ±0.03	**−0.10** ±0.03	**−0.34** ±0.03
ConvCNP	−0.49 ±0.03	−0.49 ±0.03	−1.45 ±0.02
ConvGNP	−0.50 ±0.02	−0.50 ±0.02	−1.24 ±0.02
ConvLNP (M)	−0.57 ±0.02	−0.57 ±0.02	−1.07 ±0.02
ConvLNP (E)	−0.63 ±0.02	−0.63 ±0.02	−1.08 ±0.02
ALNP (M)	−0.73 ±0.02	−1.04 ±0.02	−1.05 ±0.02
ConvLNP (E–M)	−0.76 ±0.02	−0.76 ±0.02	−1.37 ±0.02
ACNP (AR)	−0.77 ±0.01	−1.28 ±0.01	−1.30 ±0.01
AGNP	−0.78 ±0.01	−1.32 ±0.02	−1.32 ±0.02
ACNP	−0.91 ±0.02	−1.29 ±0.01	−1.17 ±0.02
LNP (M)	−0.91 ±0.02	−1.44 ±0.04	−1.19 ±0.02
LNP (E–M)	−0.92 ±0.02	−1.51 ±0.02	−1.38 ±0.02
LNP (E)	−0.93 ±0.02	−1.74 ±0.03	−1.44 ±0.02
ALNP (E–M)	−1.00 ±0.02	−1.07 ±0.02	−1.08 ±0.02
ALNP (E)	−1.03 ±0.02	−1.08 ±0.02	−1.09 ±0.02
CNP (AR)	−1.06 ±0.02	−1.07 ±0.02	−1.08 ±0.02
GNP	−1.06 ±0.02	−1.09 ±0.02	−1.08 ±0.02
CNP	−1.07 ±0.02	−1.09 ±0.02	−1.10 ±0.02
Trivial	−1.32 ±0.00	−1.32 ±0.00	−1.32 ±0.00
FullConvGNP			

Mixture $d_x = 2,\ d_y = 2$	Int.	OOID	Ext.
ConvCNP (AR)	**−0.62** ±0.01	**−0.62** ±0.01	**−0.79** ±0.01
ConvGNP	−0.74 ±0.01	−0.74 ±0.01	−1.43 ±0.02
ConvLNP (M)	−0.78 ±0.02	−0.79 ±0.02	−1.25 ±0.02
ConvCNP	−0.85 ±0.01	−0.85 ±0.01	−1.50 ±0.02
ACNP (AR)	−0.85 ±0.01	−4.30 ±0.09	−4.24 ±0.09
ALNP (M)	−0.88 ±0.01	−1.41 ±0.03	−1.21 ±0.02
ConvLNP (E)	−0.92 ±0.01	−0.92 ±0.01	−1.41 ±0.02
AGNP	−0.93 ±0.01	−1.34 ±0.01	−1.21 ±0.02
ACNP	−0.99 ±0.02	−4.19 ±0.10	−1.27 ±0.02
ConvLNP (E–M)	−1.05 ±0.01	−1.05 ±0.01	−1.73 ±0.03
LNP (M)	−1.07 ±0.01	−4.04 ±0.11	−1.31 ±0.02
ALNP (E–M)	−1.11 ±0.02	−2.65 ±0.62	−1.23 ±0.02
ALNP (E)	−1.12 ±0.02	−8.22 ±7.64	−1.26 ±0.02
GNP	−1.20 ±0.02	−1.39 ±0.03	−1.21 ±0.02
CNP (AR)	−1.20 ±0.02	−2.61 ±0.07	−1.32 ±0.02
CNP	−1.20 ±0.02	−2.60 ±0.08	−1.23 ±0.02
LNP (E–M)	−1.20 ±0.02	−3.23 ±0.10	−1.24 ±0.02
LNP (E)	−1.20 ±0.02	−3.25 ±0.10	−1.24 ±0.02
Trivial	−1.46 ±0.00	−1.46 ±0.00	−1.46 ±0.00
FullConvGNP			

I Details of Sim-to-Real Transfer Experiments

I.1 Description of Experiment

Our goal will be to make predictions for the famous hare–lynx data set. The hare–lynx data set is a time series from 1845 to 1935 recording yearly population counts of a population of Snowshoe hares and a population of Canadian lynx (MacLulich, 1937). A digital version extracted from the original graph by MacLulich (1937) is available by Hundley.[7] Hundley, the author of this digital source, says that other authors caution that the hare–lynx data is actually a composition of multiple time series, and presents the data with that caution. We, therefore, also present the data with this caution. Figure 11a visualises the hare–lynx data set.

To make predictions for the hare–lynx data set, we use the Lotka–Volterra equations (Lotka, 1910; Volterra, 1926), also called the predator–prey equations. The Lotka–Volterra equations are an idealised mathematical model for the population counts of a prey population and a predator population:

$$\text{prey population:} \qquad x'(t) = \alpha x(t) - \beta x(t) y(t), \tag{45}$$

$$\text{predator population:} \qquad y'(t) = -\delta y(t) + \gamma x(t) y(t). \tag{46}$$

These differential equations say that the prey population naturally grows exponentially with rate α, and that the predator population naturally decays exponentially with rate δ. In addition, the predators hunt the prey. The resulting additional growth in the predator population and the resulting additional decrease in the prey population are both proportional to the product of the densities. In this idealised mathematical form, the population counts converge to a smooth, noiseless limit cycle and then perfectly track this limit cycle ever after. This is unlike real-world predator–prey population counts, which exhibit noisy behaviour and imperfect cycles. We therefore consider a stochastic version of the Lotka–Volterra equations, given by the following two coupled stochastic differential equations:

$$\mathrm{d}X_t = \alpha X_t \,\mathrm{d}t - \beta Y_t X_t \,\mathrm{d}t + \sigma X_t^\nu \,\mathrm{d}W_t^{(1)}, \tag{47}$$

$$\mathrm{d}Y_t = -\gamma X_t \,\mathrm{d}t + \delta Y_t X_t \,\mathrm{d}t + \sigma Y_t^\nu \,\mathrm{d}W_t^{(2)} \tag{48}$$

where $W^{(1)}$ and $W^{(2)}$ are two independent Brownian motions. Compared to the Lotka–Volterra equations, (47) and (48) have two additional terms, $\sigma X_t^\nu \,\mathrm{d}W_t^{(1)}$ and $\sigma Y_t^\nu \,\mathrm{d}W_t^{(2)}$, which introduce noisy behaviour. In these terms, multiplying by X_t^ν and Y_t^ν makes the noise go to zero when X_t and Y_t become small, ensuring that X_t and Y_t remain positive. In addition, we multiply by a parameter $\sigma > 0$ to control the magnitude of the noise, and we raise X_t and Y_t to a power $\nu > 0$ to control how quickly the noise grows as X_t and Y_t grow. Namely, X_t naturally grows exponentially, so, by adding noise of magnitude proportional to X_t, we risk large spikes in the prey population. To moderate this behaviour, we choose ν to be strictly less than one. Finally, to obtain a variety of magnitudes of population counts, we multiply the realisation with a scale η.

After simulating from (47) and (48) a few times, we settle on $\nu = \frac{1}{6}$. For the remainder of the parameters, we simply manually play around with (47) and (48), settle on parameter ranges that look reasonable, and randomly sample parameters from those intervals. Table 19 summarises the sampling distributions for all parameters of (47) and (48). Figure 11b shows four samples from the proposed stochastic model.

To generate a meta–data set, we simulate (47) and (48) on a dense grid spanning 110 years, throw away the first 10 years, and retain between 150 and 250 data points for X_t and Y_t. The numbers of data points and the locations of the data points are sampled separately for X_t and Y_t. Hence, whereas the hare–lynx data is regularly spaced and the populations are always simultaneously observed, our simulator generates data at arbitrary and nonsimultaneous points in time. We split these data sets into context and target sets in three different ways. To train the models, for every batch, we randomly choose one of the interpolation, forecasting or reconstruction tasks by rolling a three-sided die. We will also perform these tasks on the real hare–lynx data; in that case, for interpolation, we let the number of target points per output be between one and fifteen. The tasks on simulated and real data are similar, but slightly differ in the number of context and target points.

To deal with the positivity of population counts, we transform the marginals of all models to distributions on $(0, \infty)$ by pushing the marginals through $x \mapsto \log(1 + x)$.

[7] See `http://people.whitman.edu/~hundledr/courses/M250F03/LynxHare.txt`.

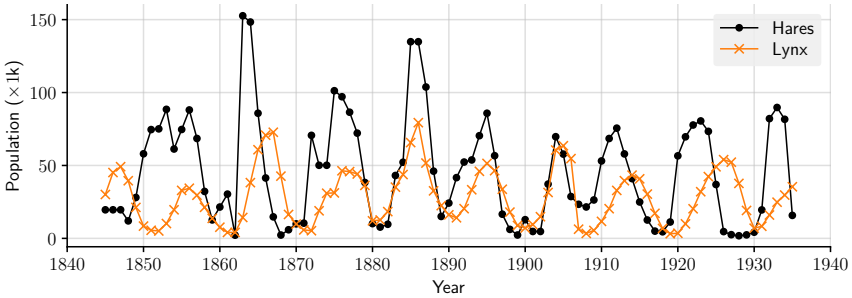

(a) Illustration of the hare–lynx data set

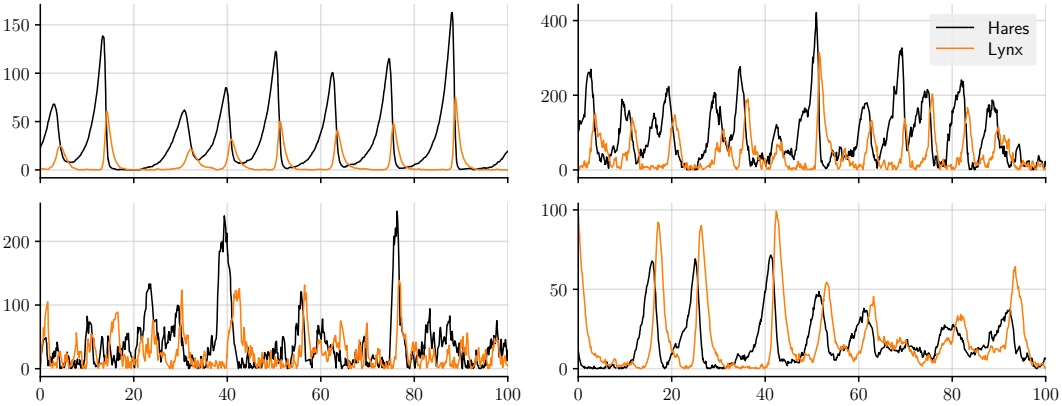

(b) Four samples from the proposed stochastic version of the Lotka–Volterra equations (47) and (48). The parameters of (47) and (48) are sampled according to Table 19.

Figure 11: Hare–lynx data set and proposed stochastic simulator

Parameter	Distribution
Initial condition X_{-10}	$\mathrm{Unif}([5, 100])$
Initial condition Y_{-10}	$\mathrm{Unif}([5, 100])$
α	$\mathrm{Unif}([0.2, 0.8])$
β	$\mathrm{Unif}([0.04, 0.08])$
γ	$\mathrm{Unif}([0.8, 1.2])$
δ	$\mathrm{Unif}([0.04, 0.08])$
ν	Fixed to $1/6$
σ	$\mathrm{Unif}([0.5, 10])$
η	$\mathrm{Unif}([1, 5])$

Table 19: Sampling distributions for the parameters of the stochastic version of the Lotka–Volterra equations (47) and (48). These equations are simulated on a dense grid spanning $[-10, 100]$. The table also shows the distribution for the initial conditions at $t = -10$. To not depend too heavily on these initial conditions, the simulation results on $[-10, 0]$ are discarded.

For this experiment, the learning rate is $1 \cdot 10^{-4}$, the margin is 1, and the points per unit is 4. We trained the models for 200 epochs.

The convolutional models use a U-Net architecture with seven layers instead of six where, in the first layer, the stride is one instead of two. For the kernel architecture of the FullConvGNP, we reduce the points per unit and the number of channels in the U-Net by a factor two.

Model	Int. (S)	For. (S)	Rec. (S)	Int. (R)	For. (R)	Rec. (R)
FullConvGNP	$\mathbf{-3.29}$ ± 0.02	$\mathbf{-3.46}$ ± 0.02	-3.79 ± 0.02	-4.16 ± 0.04	$\mathbf{-4.28}$ ± 0.04	-4.45 ± 0.00
ConvCNP (AR)	$\mathbf{-3.30}$ ± 0.02	$\mathbf{-3.47}$ ± 0.02	$\mathbf{-3.60}$ ± 0.02	$\mathbf{-4.10}$ ± 0.03	$\mathbf{-4.27}$ ± 0.03	$\mathbf{-4.32}$ ± 0.01
ConvNP (ML)	-3.41 ± 0.02	-3.84 ± 0.02	-4.44 ± 0.02	$\mathbf{-4.13}$ ± 0.04	-4.45 ± 0.05	-4.54 ± 0.01
ConvGNP	-3.47 ± 0.02	-3.65 ± 0.02	-4.15 ± 0.02	-4.21 ± 0.05	-4.82 ± 0.13	-4.61 ± 0.01
ConvCNP	-3.47 ± 0.02	-4.06 ± 0.02	-4.85 ± 0.02	-4.17 ± 0.04	-4.70 ± 0.06	-4.97 ± 0.01
ConvNP (ELBO)	-3.77 ± 0.02	-3.83 ± 0.02	-4.12 ± 0.02	-5.45 ± 0.05	-5.47 ± 0.07	-6.39 ± 0.05
ANP (ML)	-4.09 ± 0.02	-4.32 ± 0.02	-4.55 ± 0.02	-4.31 ± 0.03	-4.43 ± 0.04	-4.49 ± 0.01
ANP (ELBO–ML)	-4.22 ± 0.02	-4.54 ± 0.02	-4.80 ± 0.02	-4.58 ± 0.11	-4.58 ± 0.04	-4.68 ± 0.01
ACNP (AR)	-4.23 ± 0.02	-4.44 ± 0.02	-4.58 ± 0.02	-4.40 ± 0.03	-4.55 ± 0.04	-4.59 ± 0.02
ANP (ELBO)	-4.32 ± 0.03	-4.58 ± 0.02	-4.82 ± 0.02	-4.71 ± 0.15	-4.63 ± 0.05	-4.70 ± 0.01
ACNP	-4.34 ± 0.02	-4.65 ± 0.02	-4.88 ± 0.02	-4.43 ± 0.04	-4.58 ± 0.04	-4.74 ± 0.00
ConvNP (E.–M.)	-6.71 ± 0.05	-8.44 ± 0.11	F	-7.20 ± 0.31	F	F

Table 20: Normalised log-likelihoods in the predator–prey experiments. Shows the performance for interpolation ("Int."), forecasting ("For."), and reconstruction ("Rec.") on simulated ("S") and real ("R") data. Models are ordered by interpolation performance on simulated data. The latent variable models are trained and evaluated with the ELBO objective (E); trained and evaluated with the ML objective (M); and trained with the ELBO objective and evaluated with the ML objective (E–M). Errors indicate the central 95%-confidence interval. Numbers which are significantly best ($p < 0.05$) are boldfaced. Numbers which are very large are marked as failed with "F". Numbers which are missing could not be run.

I.2 Full Results

In Table 20, we present the full results for the sim-to-real experiments.

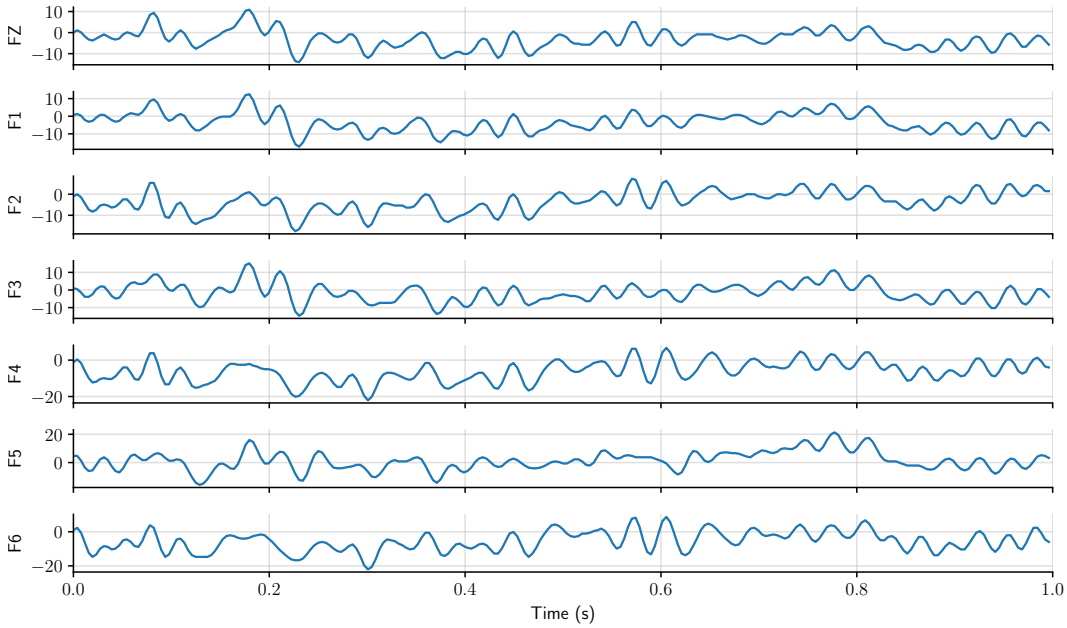

Figure 12: Example of trial in the EEG data set. Note that the signals for all electrodes appear correlated, but are subtly different.

J Details of Electroencephalography Experiments

We explore an electroencephalography data set collected from 122 subjects (Begleiter, 2022). There are two groups of subjects: alcoholic and control. Every subject was subjected to a single stimulus or two stimuli, and their response was measured with 64 electrodes placed on a subject's scalp. These measurements are in terms of *trials*, where a trial consists of 256 samples of the electrodes spanning one second. The data sets contains up to 120 trials for each subject. The data is available at `https://archive.ics.uci.edu/ml/datasets/eeg+database` and the collection is described in detail by Zhang et al. (1995a). In this experiment, we focus only on seven frontal electrodes: FZ, F1, F2, F3, F4, F5, and F6. Figure 12 illustrates a trial of a subject, showing the samples for these seven electrodes.

We randomly split all subjects into three sets: an evaluation set consisting of ten subjects, a cross-validation set consisting of ten other subjects, and a training set consisting of all remaining subjects. For each of these sets, we create a meta–data set by aggregating the trials for all subjects. We split every trial into a context and target set in the same three ways as for the predator–prey experiment. First, for all seven electrodes separately, randomly designate between 50 and 256 points to be the target points and let the remainder (between 0 and 206) be the context points. This task is called *interpolation* and is the primary measure of performance. Additionally, randomly choose one of the seven electrodes and, for that choice, split the data in two exactly like for forecasting. For all other electrodes, append all data to the context set. This task is called *reconstruction* and measures the model's ability to infer a signal for one electrode from the others. We train all models on the interpolation task, and evaluate the models on the interpolation and reconstruction task.

For this experiment, the learning rate is $5 \cdot 10^{-5}$, the margin is 0.1, and the points per unit is 256. We trained the models for 1000 epochs. For the FullConvGNP, the learning rate is $2 \cdot 10^{-4}$. The training run for the FullConvGNP was terminated after 84 hours, reaching epoch 127.

The convolutional models use a U-Net architecture where, in the first layer, the stride is one instead of two. In addition, the number of channels are adjusted as follows: the ConvCNP and ConvGNP use 128 channels, the ConvLNP uses 96 channels, and the FullConvGNP uses 64 channels. The length scales of the Gaussian kernels of the convolutional model is initialised to $0.77/256$. To scale to seven outputs, the deep set–based and attentive models reuse the same encoder for every output dimension.

K DETAILS OF ENVIRONMENTAL DATA ASSIMILATION EXPERIMENT

In this section we provide further details on the Antarctic cloud cover data assimilation experiment described in Section 4.4.

K.1 DATA CONSIDERATIONS

Data sources. Daily-averaged cloud cover reanalysis data was obtained from ERA5 (Hersbach et al., 2020). An Antarctic land mask and elevation field was obtained from the BedMachine dataset (Morlighem, 2020).

Figure 13 shows an empircal density of the ERA5 cloud cover values calculated over the models' training period of 2000-2013. The spikes at 0 and 1 correspond largely to values of exactly 0 and exactly 1. This motivates the beta-categorical likelihood described in Section 4.4.

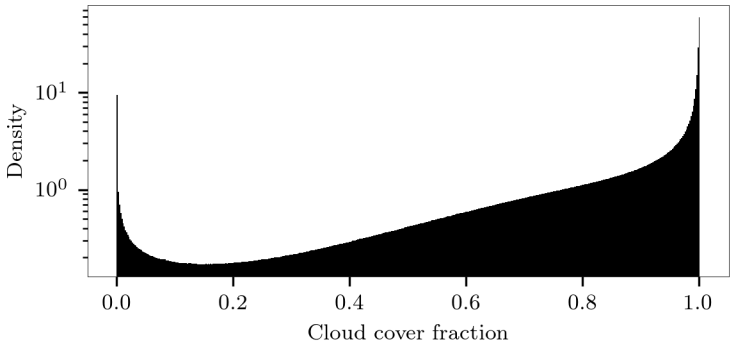

Figure 13: Empirical density of ERA5 cloud cover fraction computed over the period 2000-2013.

Data preprocessing. The cloud cover data and land/elevation auxiliary data were regridded from lat/lon to a Southern Hemisphere Equal Area Scalable Earth 2 (EASE2) grid at 25 km resolution and cropping to a size of 280 $\times$ 280. This centres the data on the South Pole.

Data normalisation. We normalised the data before passing it to the convolutional NP models. The cloud cover and land mask data already took appropriate normalised values in $[0, 1]$. The elevation field was normalised from metres to values in $[0, 1]$.

The input coordinates x were normalised from metres to take values in $[-1, 1]$.

K.2 MODEL CONSIDERATIONS

Here we provide details on the training procedure and architectures for each of the convolutional NP models in the Antarctic data assimilation experiment.

Generating the training, validation, and test tasks. Following meta-learning principles, we collect data from day τ into a task D_τ. Each task D_τ was generated by first drawing the integer number of simulated cloud cover context points $N^{(\mathrm{c})} \sim \mathrm{Unif}\{1, 2, \ldots 500\}$. Letting $N^{(\mathrm{c})}$ vary encourages the model to learn to deal with both data-sparse and data-rich scenarios. The number of target points $N^{(\mathrm{t})}$ was fixed to a value of 2,000.

Next, the input locations $\mathbf{x}_\tau^{(\mathrm{c})}$ and $\mathbf{x}_\tau^{(\mathrm{t})}$ were sampled uniformly at random across the entire 280×280 input space and the corresponding $\mathbf{y}_\tau$ values were sampled without observation noise.

For the training dates, the random seed used for generating D_τ is updated every epoch, allowing for an infinitely growing simulated training data set. In contrast, for the validation and test dates,

the random seeds were held fixed so that metrics computed over the validation and test sets are not stochastic.

Training procedure. Each model was trained for 150 epochs on 14 years of data from 2000–2013. An Adam optimiser was used with a learning rate of 5×10^{-5} and a batch size of 2. For the loss functions we use a negative log-likelihood loss function for the ConvCNP and ConvGNP. For the ConvLNP we use the ELBO objective and fix the variance of the observation noise to 0.01 for the first four epochs. Validation data from 2014–2017 was used for checkpointing the model weights using the per-datapoint predictive log-likelihood. The two year period of 2018–2019 data was reserved for the test set.

The time taken to train each model on a Tesla V100 GPU is as follows:

- ConvCNP: 25.0 hours,
- ConvGNP: 27.5 hours,
- ConvLNP: 43.6 hours.

Architectures. For each model, the U-Net component of the encoder uses 5×5 convolutional kernels with the following sequence of channel numbers (d.s. = 2×2 downsample layer, u.s. = 2×2 upsample layer): $16 \xrightarrow{\text{d.s.}} 32 \xrightarrow{\text{d.s.}} 64 \xrightarrow{\text{d.s.}} 128 \xrightarrow{\text{u.s.}} 64 \xrightarrow{\text{u.s.}} 32 \xrightarrow{\text{u.s.}} 16$. We use bilinear resize operators for the upsampling layers to fix checkerboard artifacts that we encountered when using standard zero-padding upsampling (Odena et al., 2016). We use a margin of 0.1 and 150 points per unit for the encoder's internal discretisation. The length scales of the Gaussian kernels for both the encoder and decoder SetConv layers are set to $1/150$ and held fixed during training. These architecture choices result in a receptive field of 0.433 in normalised input space, or roughly $1.500\,\mathrm{km}$ in raw input space, spanning around 20% of the region in Figure 6 in either dimension.

For the ConvGNP we use 128 basis functions for the low-rank covariance parameterisation described in Markou et al. 2021.

For the ConvLNP we use an 8-dimensional latent variable and evaluate the ML objective (Foong et al., 2020) using 8 latent samples.

The number of learnable parameters for each model is as follows:

- ConvCNP: $618\,\mathrm{k}$,
- ConvGNP: $621\,\mathrm{k}$,
- ConvLNP: $1.234\,\mathrm{k}$ (increase due to second UNet architecture after the latent variable).

The difference in parameters from switching to a beta-categorical likelihood from a Gaussian likelihood is negligible.

Input data. Each model receives two context sets as input. The first contains observations of the simulated ERA5 daily-average cloud cover. The second contains a set of 6 gridded auxiliary variables. These are elevation, land mask, $\cos(2\pi \times \text{day of year}/365)$, $\sin(2\pi \times \text{day of year}/365)$, x_1, and x_2. The elevation and land mask auxiliary fields allow the models to predict spatial non-stationarity. For example, the convolutional filters of the model's encoder could learn how cloud cover around the Antarctic coastline behaves differently to the centre of the continent. The $\cos$ and $\sin$ variables inform the model at what time of year D_τ corresponds to, helping with learning seasonal variations in the data. The x_1 and x_2 inputs again help with breaking translation equivariance in the convolutional filters by informing the model where in input space the data corresponds to.

K.3 Antarctic cloud cover model samples

Figure 14 gives a detailed breakdown of sample extrapolation ability, showing seven samples from the four Antarctic cloud cover models. The AR ConvCNP samples display remarkable structure and variation while still closely interpolating the context points. The samples also provide interesting scenarios in the gaps between the context points on the left hand side.

In contrast, the ConvCNP samples are incoherent, underestimating the probability of joint events.

The ConvLNP samples were generated by sampling from the latent variable and then computing the mean of the marginal distributions. As is visible in Figure 14, the ConvLNP displays low sample variance with respect to the latent variable. However, to the best of our knowledge we used a

faithful reproduction of the original ConvLNP model, so we leave a more rigorous treatment of this undesirable behaviour to future work.

For all the non-AR models, the limited receptive field size leads to samples on the right hand side becoming independent of the context observations on the left hand side after roughly $750\,\mathrm{km}$ of distance from them. This results in the models defaulting to some mean representation of the data. It is interesting to see that all the non-AR models display similar marginal mean structure, with greater cloud cover towards the centre of the continent and lower cloud cover towards the coastline, followed by increased cloud levels over the Southern Ocean.

The AR samples were drawn on a sparse 70x70 grid spanning the entire input space to save compute time. The ConvCNP model was then conditioned on these AR samples and the predictive mean was computed over the dense 280x280 target space. It took 14 minutes to generate these AR ConvCNP samples on a Tesla V100 GPU.

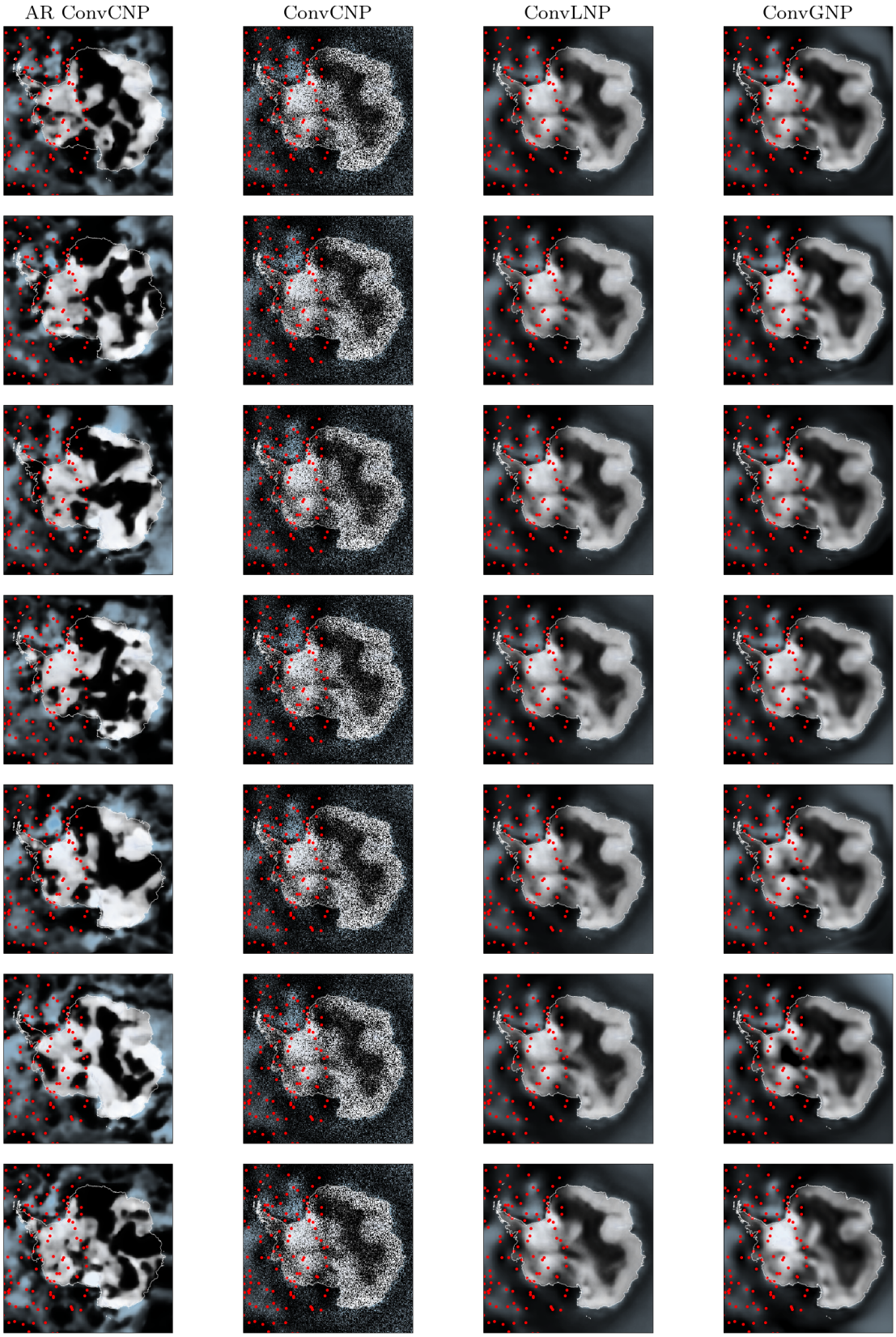

Figure 14: Seven samples from each model in the Antarctic cloud cover sample extrapolation task for 25/06/2018.

L DETAILS OF CLIMATE DOWNSCALING EXPERIMENTS

L.1 DESCRIPTION OF EXPERIMENT

The MLP ConvGNP (Markou et al., 2022) can be used to successfully model dependencies between outputs in a statistical downscaling task, improving log-likelihoods over the MLP ConvCNP (Vaughan et al., 2022) and enabling coherent samples. In this experiment, we demonstrate that the AR ConvCNP can also be used for this purpose.

The goal of this experiment is to estimate the maximum daily temperature at 589 weather stations around Germany. To estimate these temperatures, we follow Vaughan et al. (2022) and use 25 coarse-grained ERA-Interim reanalysis variables (Dee et al., 2011) in combination with $1\,\mathrm{km}$–resolution elevation data (Earth Resources Observation and Science Center, U.S. Geological Survey, U.S. Department of the Interior, 1997). We also consider a second setup where we reveal some of the weather station observations. These revealed weather station observations can be used by the models to aid downscaling performance.

The ERA-Interim reanalysis variables considered are tabulated in Table 21. In contrast to previous downscaling work, which degrade reanalysis data to between 2° and 2.5°, we opt to use the ERA-Reanalysis data at the native 0.75° resolution, consistent with the latest high-resolution climate models with horizontal resolution ranging from 0.5° to 1.0°. All variables are spatially subset to between 6° to 16° longitude and 47° to 55° latitude, covering Germany. The weather station data are a subselection from of the European Climate Assessment & Dataset (Tank et al., 2002) and are available at `https://www.ecad.eu`; we use the blended data. Like for the ERA-Reanaysis variables, we take the weather stations located within the aforementioned square. The locations of the weather stations around Germany are visualised in Figure 15. The $1\,\mathrm{km}$–resolution elevation data is taken from the United States Geological Survey GTOPO30 elevation data set available at `https://doi.org/10.5066/F7DF6PQS`. This provides global elevation data at 30-arc second resolution, which is approximately $1\,\mathrm{km}$.

Following the VALUE framework (Maraun et al., 2015), we consider all days of the years 1979–2008 and split these years into five folds. We use the first four folds (spanning 1979–2003) for training, holding out the last 1000 days for cross-validation; and use the fifth fold (spanning 2003–2008) for evaluation.

L.2 MULTISCALE CONVOLUTIONAL ARCHITECTURE

Deploying the AR ConvCNP in this downscaling experiment comes with a significant challenge. Because the elevation data has a fine resolution of $1\,\mathrm{km}$, we expect that predictions by the AR ConvCNP will vary roughly also on this length scale. In the autoregressive sampling procedure (Procedure 2.1), samples from the model will be fed back into the model. Therefore, the AR ConvCNP must handle context data which varies on a $1\,\mathrm{km}$ spatial scale, which means that the discretisation of the AR ConvCNP must roughly be a $1\,\mathrm{km}$–resolution grid. Unfortunately, making the discretisation this fine is prohibitively expensive and imposes prohibitive memory requirements. It is this limitation that prevents us from extending the Vaughan et al. (2022)'s MLP ConvCNP and Markou et al. (2022)'s MLP ConvGNP to include additional weather station observations. We must therefore innovate on the AR ConvCNP design to come up with a convolutional architecture that can handle such a fine discretisation at reasonable computational expense.

The architecture that we propose is a *multiscale architecture* operating on multiple spatial length scales. Let us divide the context set $D = D_{\mathrm{lr}} \cup D_{\mathrm{mr}} \cup D_{\mathrm{hr}}$ into a low-resolution component D_{lr}, a medium-resolution component D_{mr}, and a high-resolution component D_{hr}. Let the low-resolution component D_{lr} consist of features of the context set that vary on a *long* spatial length scale, the medium-resolution component D_{mr} of features that vary on a *medium-range* spatial length scale, and the high-resolution component D_{hr} of features that vary on a *short* spatial length scale. The central assumption of the architecture is that predictions for target points depend on precise short-length-scale details D_{hr} nearby, but that this dependence weakens as we move away from the target point, starting to depend more on broad-stroke long-length-scale components D_{lr}. For example, predictions might depend on detailed orographic information nearby, but more on general orographic shapes farther away.

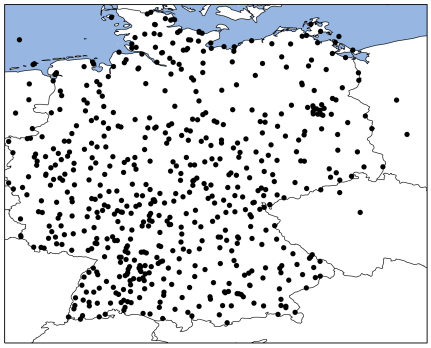

Figure 15: Locations of the 589 weather stations around Germany in the downscaling experiments.

Variable	Level	Units
Surface		
Maximum temperature	2 m	degrees Celsius
Mean temperature	2 m	degrees Celsius
Northward wind	10 m	knots
Eastward wind	10 m	knots
Upper atmosphere		
Specific humidity	850, 700, and 500 hPa	degrees Celsius
Mean temperature	850, 700, and 500 hPa	degrees Celsius
Northward wind	850, 700, and 500 hPa	knots
Eastward wind	850, 700, and 500 hPa	knots
Invariant		
Angle of sub-grid-scale orography	surface	
Anisotropy of sub-grid-scale orography	surface	
Standard deviation of filtered sub-grid-scale orography	surface	
Standard deviation of orography	surface	
Geopotential	surface	metres
Longitude	surface	degrees Celsius
Latitude	surface	degrees Celsius
Temporal		
Fractional position in the year t transformed encoded with $t \mapsto (\cos(2\pi t), \sin(2\pi t))$		

Table 21: ERA-Interim reanalysis predictors.

Figure 16 depicts the multiscale architecture. The architecture is a cascade of three convolutional deep sets, parametrised by three CNNs; please see the caption. The low-resolution CNN handles the context data D_{lr} with a long spatial length scale. Because these features have a long spatial length scale, the CNN can get away with a low-resolution discretisation. The output of the low-resolution CNN then feeds into a medium-resolution CNN. The medium-resolution CNN handles the context data D_{mr} with a medium spatial length scale and has a medium-resolution discretisation. Finally, the output of the medium-resolution CNN feeds into a high-resolution CNN. This CNN handles the context data D_{hr} with a short spatial length scale and has a high-resolution discretisation.

The key to the computational efficiency of this architecture is that we construct the high-resolution discretisation only locally to the target points: a small square covering 0.25° more than the most extremal target points. If the target points are confined to a small region, then the high-resolution grid will also be small, covering only 0.25° more than that region. Crucially, the high-resolution

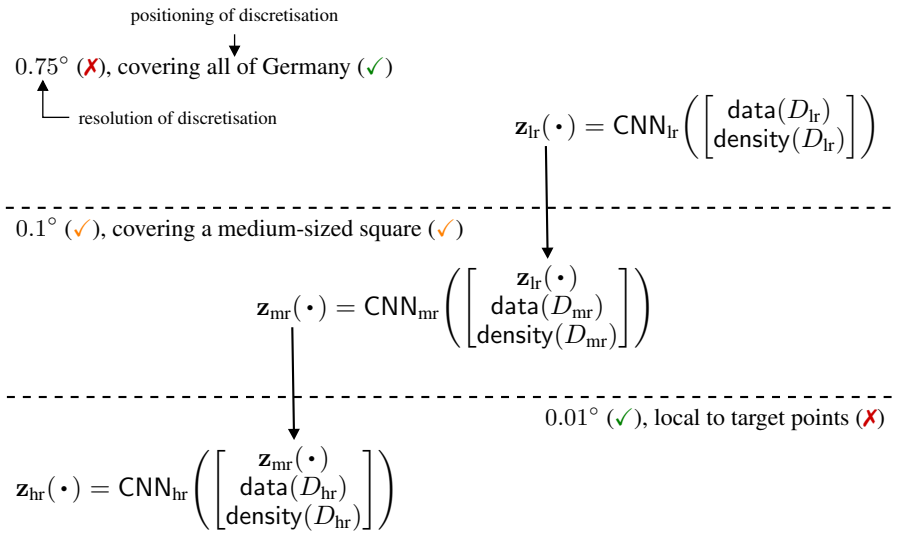

Figure 16: Multiscale architecture for the AR ConvCNP. A cascade of three convolutional deep sets (Gordon et al., 2020) representing a low-resolution, medium-resolution, and high-resolution component. Shows the resolution and positioning of the internal discretisation for every convolutional deep set. The context set $D = D_{\text{lr}} \cup D_{\text{mr}} \cup D_{\text{hr}}$ is also divided into a low-resolution D_{lr}, medium-resolution D_{mr}, and high-resolution component D_{hr}. The low-resolution context data D_{lr} consists of the 25 coarse-grained ERA-Interim reanalysis variables. The medium-resolution D_{mr} and high-resolution context data D_{hr} both consist of the station observations and the $1\,\text{km}$–resolution elevation data. The functions $\text{data}(D)$ and $\text{density}(D)$ produce respectively the data channel and density channel for context data D; see Gordon et al. (2020). The variables $\mathbf{z}_{\text{lr}}(\bullet)$, $\mathbf{z}_{\text{mr}}(\bullet)$, and $\mathbf{z}_{\text{hr}}(\bullet)$ represent intermediate representations as continuous functions, and the maps CNN_{lr}, CNN_{mr}, and CNN_{hr} are translation-equivariant maps between functions on $\mathcal{X}$. Following the construction of the ConvCNP (Gordon et al., 2020), these maps are all implemented with convolutional neural networks (CNN) using a discretisation. For CNN_{lr}, the internal discretisation is the $0.75°$-resolution grid corresponding to the 25 coarse-grained ERA-Interim reanalysis variables. For CNN_{mr}, the internal discretisation is a $0.1°$-resolution grid spanning $5°$ more than the most extremal target inputs; the discretisation does *not* depend on the context set. For CNN_{hr}, the internal discretisation is a $0.01°$-resolution grid spanning $0.25°$ more than the most extremal target inputs; the discretisation also does *not* depend on the context set.

grid will not be constructed over all of Germany, like it would if we were to more naively apply the ConvCNP with a high-resolution discretisation, incurring prohitive computational cost. Even though the high-resolution grid is only constructed locally to the target points, the model can still capture long-range dependencies via the medium-resolution and low-resolution grids. Namely, the medium-resolution grid is a square covering $5°$ more than the most extremal target points, and the low-resolution grid covers all of Germany; see Figure 16. To utilise this computational gain, the target points must be confined to a small region. This perfectly synergises with the autoregressive sampling procedure (Procedure 2.1), because this procedure evaluates the model one target point at a time. The training procedure, however, must be adapted. During training, we subsample the target points to ensure that the target set is always confined to a small square, which is described in Appendix L.4.

During the autoregressive sampling procedure, the AR ConvCNP takes in earlier AR samples from the model. In the architectures of the MLP ConvCNP and MLP ConvGNP, these is no natural context data to which these samples can be appended. Therefore, in addition to the ERA-Interim reanalysis variables and the elevation data, we also let the AR ConvCNP take in observed weather stations as context data. We will append the earlier AR samples to these weather station context data. To have the model make appropriate use of the weather station context set, we must randomly divide the weather stations observations over the context and target set, which we describe in Appendix L.4. We let the low-resolution context data D_{lr} consist of the 25 coarse-grained ERA-Interim reanalysis variables, and let the medium-resolution D_{mr} and high-resolution context data D_{hr} both consist of the weather station observations (and earlier AR samples) and the $1\,\text{km}$–resolution elevation data. When

the $1\,\mathrm{km}$–resolution data is fed to the medium-resolution CNN, the data loses some detail, because the internal discretisation of the medium-resolution CNN is coarser than the data; however, when it is fed to the high-resolution CNN, the data retains its detail. The same holds for the weather station observations (and earlier AR samples).

L.3 Architectures

MLP ConvCNP and MLP ConvGNP (Vaughan et al., 2022; Markou et al., 2022). The MLP ConvCNP and MLP ConvGNP are a respectively a ConvCNP and ConvGNP where the decoder $\mathrm{dec}_\theta = \mathsf{fuse}_\theta \circ \mathrm{dec}'_\theta$ is decomposed into a convolutional architecture dec'_θ followed by a pointwise MLP fuse_θ:

$$\mathsf{fuse}_\theta(\mathbf{z}(\cdot)) = \mathsf{MLP}_\theta(\mathbf{z}(\cdot), \mathsf{elevation}(\cdot)). \tag{49}$$

In this architecture, the ERA-Interim variables are incorporated via the convolutional architecture, producing the encoding $\mathbf{z}(\cdot)$. On the other hand, as (49) shows, the $1\,\mathrm{km}$–resolution elevation data is included via the pointwise MLP fuse_θ.

Parametrise dec'_θ with a seven-layer residual convolutional neural network (He et al., 2016). Every residual layer involves one depthwise-separable convolutional filter (Chollet, 2017) with kernel size three followed by a pointwise MLP. Every layer has 128 channels, and the network also outputs 128 channels. The discretisation for dec'_θ is the grid of the ERA-Interim reanalysis variables. Parametrise fuse_θ with a three-hidden-layer MLP of width 128.

AR ConvCNP. The AR ConvCNP does not use the pointwise MLP fuse_θ to incorporate the $1\,\mathrm{km}$–resolution elevation data. Instead, it is a normal ConvCNP where the convolutional architecture is implemented by the multi-scale architecture described in Figure 16.

Parametrise $\mathsf{CNN}_{\mathrm{lr}}$ with a depthwise-separable residual convolutional neural network like in the MLP ConvCNP and MLP ConvGNP, but use six layers instead of seven. Let $\mathsf{CNN}_{\mathrm{lr}}$ output 64 channels. The discretisation for $\mathsf{CNN}_{\mathrm{lr}}$ is the grid of the ERA-Interim reanalysis variables. Parametrise $\mathsf{CNN}_{\mathrm{mr}}$ with a U-Net (Ronneberger et al., 2015) using an architecture similar to what we have been using. Before the U-turn, let the U-Net have five convolutional layers with kernel size five, stride one for the first layer and stride two afterwards, 64 output channels for the first three layers and 128 output channels afterwards. After the U-turn, instead of using transposed convolutions, use regular convolutions combined with an upsampling layer using bilinear interpolation. Let $\mathsf{CNN}_{\mathrm{mr}}$ output 64 channels. The receptive field of $\mathsf{CNN}_{\mathrm{mr}}$ is approximately 10°. The discretisation for $\mathsf{CNN}_{\mathrm{mr}}$ is centred around the target points with margin 5°. Parametrise $\mathsf{CNN}_{\mathrm{hr}}$ with a U-Net like for $\mathsf{CNN}_{\mathrm{hr}}$, but with four convolutional layers before the U-turn. The receptive field of $\mathsf{CNN}_{\mathrm{hr}}$ is approximately 0.5°. The discretisation for $\mathsf{CNN}_{\mathrm{hr}}$ is centred around the target points with margin 0.25°.

L.4 Training Details

MLP ConvCNP and MLP ConvGNP. The MLP ConvCNP and MLP ConvGNP are trained with learning rate $2.5 \cdot 10^{-5}$ for 500 epochs. For the MLP ConvGNP, to encourage the covariance to fit, we fix the variance of the decoder to $10^{-4}\mathbf{I}$ for the first ten epochs.

AR ConvCNP. The AR ConvCNP is trained with learning rate $1 \cdot 10^{-5}$ for 500 epochs. During training and cross-validation, the target points are subsampled to lie in a $3^\circ \times 3^\circ$ square. For training, the number of target points is ensured to be at least ten; and for cross-validation, at least one. The size of the cross-validation set is increased ten fold.

Sampling of data. For the MLP ConvCNP and MLP ConvGNP, since these architectures cannot take in weather station observations, all weather stations are used as context data. For the AR ConvCNP, a data set is split into a context and target set by randomly selecting n points as context points and letting the remainder be target points. Specifically, the number of context points n is sampled from $p(n) \propto e^{-0.01n}$. This splitting is done after subsampling the $3^\circ \times 3^\circ$ square.

M ALTERNATE AR PROCEDURE WITH AUXILIARY DATA

We propose an additional procedure which uses autoregressive sampling with auxiliary data to generate more expressive marginal predictives. The input points of the auxiliary data are chosen randomly, and then sampled autoregressively before sampling the target points. Finally, we discard the sampled values for the auxiliary data, but retain the samples for the target points. Adding auxiliary points in this way allows the model to roll out autoregressively with more steps, even if the target set is small (or just a single point). We describe the procedure below:

Procedure M.1 (Autoregressive application of neural process with auxiliary data)**.** For a neural process π_θ, context set $D^{(\mathrm{c})} = (\mathbf{x}^{(\mathrm{c})}, \mathbf{y}^{(\mathrm{c})})$, a target input $x^{(\mathrm{t})}$, a distribution r over $\mathcal{X}$, a number of auxiliary data points $R \in \mathbb{N}$, and a number of trajectories $M \in \mathbb{N}$, let $\mathrm{AuxAR}_{\mathbf{x}^{(\mathrm{t})}}(\pi_\theta, D^{(\mathrm{c})}, r, R, M)$ be the distribution defined as follows. We first autoregressively sample the auxiliary data trajectories at random locations sampled from r:

$$\text{for } j = 1, \ldots, M \text{ and } \ell = 1, \ldots, R, \qquad x_\ell^{(\mathrm{aux},j)} \sim r, \tag{50}$$

$$\text{for } j = 1, \ldots, M, \qquad \mathbf{y}^{(\mathrm{aux},j)} \sim \mathrm{AR}_{\mathbf{x}^{(\mathrm{aux},j)}}(\pi_\theta, D^{(\mathrm{c})}). \tag{51}$$

Next, conditioned on the auxiliary data, we sample the target point of interest to make predictions. We then marginalise out the auxiliary data by averaging over the M trajectories:

$$y^{(\mathrm{t})} \sim \tfrac{1}{M} \textstyle\sum_{j=1}^{M} P_{x^{(\mathrm{t})}}(\mathbf{x}^{(\mathrm{c})} \oplus \mathbf{x}^{(\mathrm{aux},j)},\, \mathbf{y}^{(\mathrm{c})} \oplus \mathbf{y}^{(\mathrm{aux},j)}). \tag{52}$$

This procedure introduces three hyperparameters: the distribution from which to draw inputs r, the length of trajectories R, and the number of trajectories to sample M.

In the following experiments, we set the distribution r to be uniform over the training domain with no dependence on the context set or target point of interest: $r = \mathrm{Uniform}([b, h])$, where b and h are the lower and upper bounds of the training domain, respectively. One could experiment with other choices for the distribution r. The trajectory length R is chosen between 0[8] and 8, and the number of trajectories M is chosen between 1 and 128.

M.1 GENERATED DATA

We create three data generating processes for our experiments: a mixture of functions, random sawtooth functions, and random audio-like functions. The first two experiments have multi-modal true marginals, whereas the last has heavy-tailed marginals.

Function mixture. The function mixture data are generated by choosing one of the following three functions, the first with a probability of $\frac{1}{4}$, the second with a probability of $\frac{1}{2}$, and the third with a probability of $\frac{1}{4}$:

$$y = x^2 + \epsilon, \qquad \epsilon \sim \mathcal{N}(0, 0.25), \tag{53}$$

$$y = x + \epsilon, \qquad \epsilon \sim \mathcal{N}(0, 0.0625), \tag{54}$$

$$y = -x + \epsilon, \qquad \epsilon \sim \mathcal{N}(0, 0.25). \tag{55}$$

Sawtooth. The sawtooth data are generated from the following function:

$$y(x) = [\omega(dx - \phi)] \bmod 1 \tag{56}$$

We sample the frequency $\omega \sim \mathrm{Unif}([3, 5])$, the direction d as either -1 or 1 with equal probability, and the shift as $\phi \sim \mathrm{Unif}([\frac{1}{\omega}, 1])$.

Synthetic Audio. Synthetic audio data are generated by convolving a Dirac comb[9] with a truncated decaying sum of sinusoids:

$$s(t) = \begin{cases} e^{-\frac{t}{\tau}} \left[\sin(\omega_1 t) + \sin(\omega_2 t)\right] & \text{for } 0 \le t < T, \\ 0 & \text{otherwise,} \end{cases} \tag{57}$$

$$f(x) = \mathrm{Comb}_T(x) * s(x), \tag{58}$$

$$y = f(x) + \epsilon \quad \text{where} \quad \epsilon \sim \mathcal{N}(0, 0.001) \tag{59}$$

[8] A trajectory length of 0 is equivalent to the standard test-time procedure.

[9] The Dirac comb is defined as $\mathrm{Comb}_T(t) := \sum_{k=-\infty}^{\infty} \delta(t - kT)$ for given period P.

Experiment	ConvCNP	ConvCNP (AuxAR)
Function Mixture	-0.63 ± 0.20	$-\mathbf{0.46} \pm 0.15$
Sawtooth	1.46 ± 0.30	1.64 ± 0.28
Synthetic Audio	0.12 ± 0.14	$\mathbf{0.55} \pm 0.10$

Table 22: Using autoregressive sampling for marginal approximation improves held-out log-likelihoods on all experiments. Values are normalized by the number of target points. Values which are significantly best ($p < 0.05$) are shown in bold.

where

$$\omega_1, \omega_2 \sim \text{Unif}([50, 70]), \quad T \sim \text{Unif}([0.75, 1.25]), \quad \tau \sim \text{Unif}([0.1, 0.3]). \tag{60}$$

We truncate the waves up to the period length, because otherwise the convolution with the Dirac comb would lead to increasing amplitude, resulting in a non-stationary process.

M.2 Training

For the function mixture experiment, no training is required because we use the analytically derived ideal CNP π_∞ as our model. See Section 2.

For the sawtooth and synthetic audio experiments, we train ConvCNP models. We train each model for 100 epochs using 1024 batches per epoch with a batch size of 16. We discretise the encoder by evaluating 64 points per unit. We use a margin of 0.1, and a stride length of 2 for each of the 6 layers of the U-Net. Each layer has 64 channels. The receptive field size from this combination of parameters is 6.953.

During training, we sample a number of context points between uniformly at random from {0,...,75}, and we sample exactly 100 target points. The context points and target points are sampled uniformly from $[-2, 2]$. We use the Adam optimizer with a learning rate of 3×10^{-4}.

M.3 Results

Model	0	1	2	4	8	16
ConvCNP	$-0.47_{\pm 0.07}$	$-0.45_{\pm 0.18}$	$-0.24_{\pm 0.12}$	$-0.12_{\pm 0.12}$	$0.36_{\pm 0.15}$	$1.07_{\pm 0.18}$
ConvCNP (AuxAR)	$\mathbf{0.02}_{\pm 0.11}$	$\mathbf{0.19}_{\pm 0.11}$	$\mathbf{0.24}_{\pm 0.12}$	$\mathbf{0.31}_{\pm 0.11}$	$\mathbf{0.74}_{\pm 0.10}$	$1.27_{\pm 0.12}$

Table 23: Log likelihood values for varying context sizes using ConvCNP and ConvCNP (AuxAR) using the function mixture data generator. Column headers indicate the context set size. Log-likelihoods are shown in bold when they are significantly best ($p < 0.05$). Column headers are context sizes. Errors indicate central 95% confidence interval.

Model	0	1	2	4	8	16	32
ConvCNP	$-\mathbf{0.18}_{\pm 0.00}$	$-0.14_{\pm 0.02}$	$-0.02_{\pm 0.05}$	$0.42_{\pm 0.19}$	$1.89_{\pm 0.23}$	$3.06_{\pm 0.13}$	$3.54_{\pm 0.08}$
ConvCNP (AuxAR)	$-0.21_{\pm 0.02}$	$-0.09_{\pm 0.04}$	$0.08_{\pm 0.08}$	$\mathbf{0.95}_{\pm 0.16}$	$\mathbf{2.37}_{\pm 0.15}$	$3.03_{\pm 0.13}$	$3.51_{\pm 0.08}$

Table 24: Log likelihood values for varying context sizes using ConvCNP and ConvCNP (AuxAR) using the sawtooth data generator. Column headers indicate the context set size.. Log-likelihoods are shown in bold when they are significantly best ($p < 0.05$). Column headers are context sizes. Errors indicate central 95% confidence interval.

In Table 22, we see that using this procedure improves the held-out log-likelihoods for all of the experiments. We can better understand the utility of this method by observing the performance for

Model	0	1	2
ConvCNP	$-1.40_{\pm 0.11}$	$-0.91_{\pm 0.28}$	$-0.36_{\pm 0.20}$
ConvCNP (AuxAR)	$-\mathbf{1.05}_{\pm 0.11}$	$-0.63_{\pm 0.23}$	$-0.29_{\pm 0.17}$

Table 25: Log likelihood values for varying context sizes using ConvCNP and ConvCNP (AuxAR) using the function mixture data generator. Column headers indicate the context set size. Log-likelihoods are shown in bold when they are significantly best ($p < 0.05$). Column headers are context sizes. Errors indicate central 95% confidence interval.

different context sizes in Tables 24 and 23. For example, the sawtooth data results in Table 24 show that, for context set sizes 16, the AR method provides no benefits. The increased flexibility of this AR method is not needed in this case — a Gaussian predictive models the marginal sufficiently well. For context set sizes of 4 and 8, on the other hand, we see significant improvements using the AR method. Similarly, for the synthetic audio data results in Table 23, we see improvements using the ConvCNP (AuxAR) for all context set sizes except 16.

The autoregressive sampling with auxiliary data method shown here shows promise for improving modeling of processes with multi-modal and heavy-tailed marginal distributions — all with no changes to the training procedure. The scenarios where this method are most useful are highly contingent upon the context set size, because of its impact how well the marginals are modeled by Gaussians.